

NASA CR-175025

**Under Distribution Limitation
Until December 31, 1987**



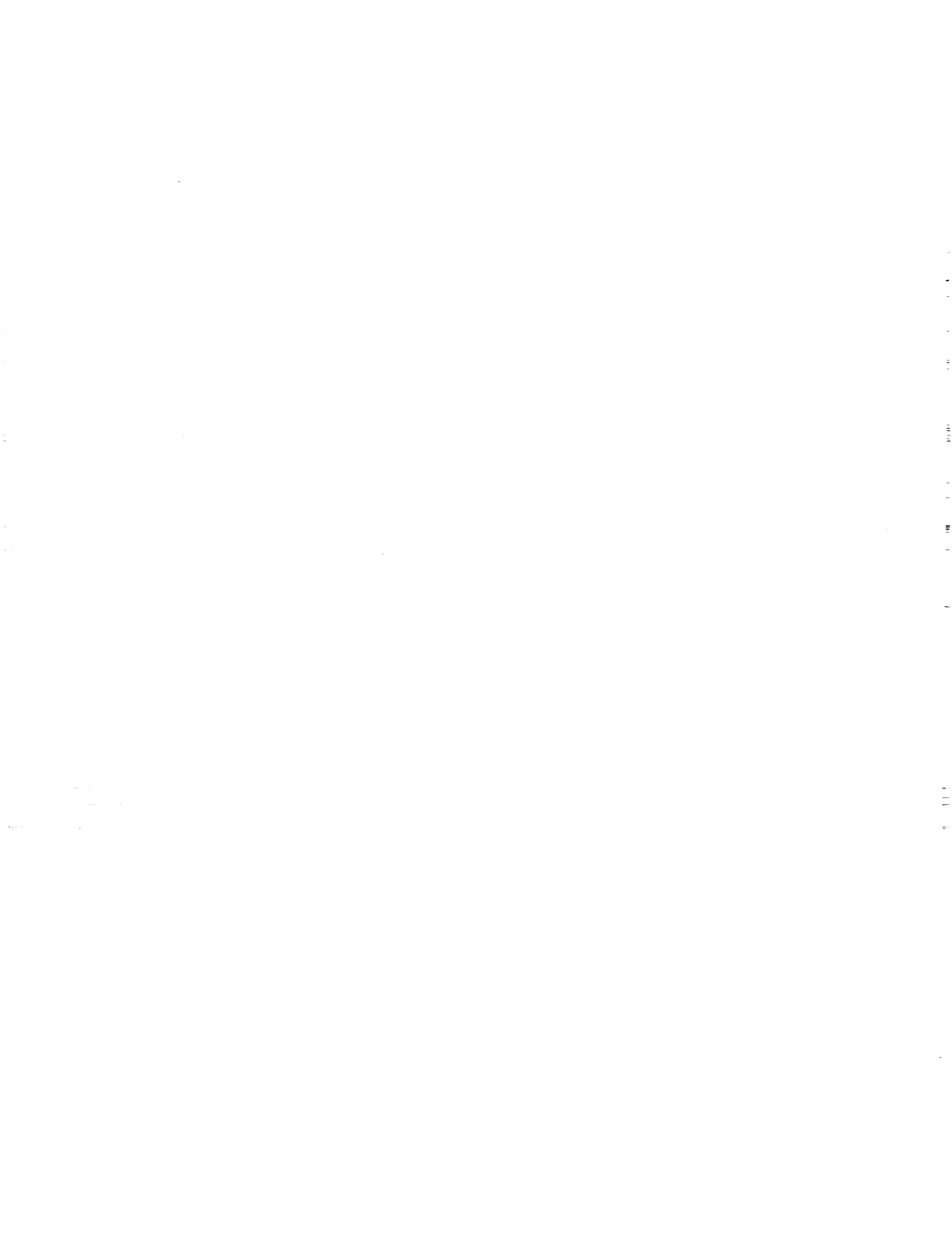
**ANALYSIS AND TEST EVALUATION OF THE DYNAMIC
STABILITY OF THREE ADVANCED TURBOPROP MODELS
AT ZERO FORWARD SPEED**

**By
Arthur F. Smith**

**HAMILTON STANDARD DIVISION
UNITED TECHNOLOGIES CORPORATION
WINDSOR LOCKS, CONNECTICUT 06096**

December, 1985

**National Aeronautics and Space Administration
Lewis Research Center
Cleveland, Ohio 44135
Contract NAS3-22755**



1. Report No. NASA CR-175025		2. Government Accession No.		3. Recipient's Catalog No.	
4. Title and Subtitle Analysis and Test Evaluation of the Dynamic Stability of Three Advanced Turboprop Models at Zero Forward Speed				5. Report Date December, 1985	
				6. Performing Organization Code	
7. Author(s) Arthur F. Smith*				8. Performing Organization Report No. HSER 11054	
9. Performing Organization Name and Address Hamilton Standard Division United Technologies Corporation Windsor Locks, Conn. 06096				10. Work Unit No.	
				11. Contract or Grant No. NAS 3-22755	
12. Sponsoring Agency Name and Address National Aeronautics & Space Administration Washington, D.C. 20546				13. Type of Report and Period Covered Contractor Report	
				14. Sponsoring Agency Code	
15. Supplementary Notes Final Report, Project Technical Monitor, O. Mehmed, NASA Lewis Research Center, Cleveland, Ohio 44135 *Now with: Hirock Corporation, 1 Main Road, Granville, MA 01034					
16. Abstract Results of static stability wind tunnel tests of three 62.2 cm (24.5 in) diameter models of the Prop-Fan are presented. Measurements of blade stresses were made with the Prop-Fans mounted on an isolated nacelle in an open 5.5 meter (18 foot) wind tunnel test section with no tunnel flow. The tests were conducted in the United Technology Research Center Large Subsonic Wind Tunnel. Stall flutter was determined by regions of high stress, which were compared with predictions of boundaries of zero total viscous damping. The structural analysis used beam methods for the model with straight blades and finite element methods for the models with swept blades. Increasing blade sweep tends to suppress stall flutter. Comparisons with similar test data acquired at NASA/Lewis are good. Correlations between measured and predicted critical speeds for all the models are good. The trend of increased stability with increased blade sweep is well predicted. Calculated flutter boundaries generally coincide with tested boundaries. Stall flutter is predicted to occur in the third (torsion) mode. The straight blade test shows third mode response, while the swept blades respond in other modes.					
17. Key Words (Suggested by Author(s)) Advanced Turboprop Propellers Prop-Fan Energy Efficient Blade Stall Stall Flutter Tests				18. Distribution Statement [REDACTED] Unitl December 31, 1987	
19. Security Classif. (of this report) Unclassified		20. Security Classif. (of this page) Unclassified		21. No. of Pages 114	
22. Price*					

FOREWORD

All of the testing reported herein was performed at the United Technologies Research Center facilities in East Hartford, Connecticut, under the direction of personnel from Hamilton Standard, a Division of United Technologies Corporation. The assistance of UTRC personnel in the performance of this testing is gratefully acknowledged. This work was accomplished under contract NAS3-22755 for the NASA-Lewis Research Center in Cleveland, Ohio. Mr. Oral Mehmed of the NASA-Lewis Research Center was the Project Technical Monitor for this contract.

The data reduction was performed by Mr. Donald J. Marshall, and the analysis and reporting was conducted by Mr. Arthur F. Smith. Mr. Bennett M. Brooks was the Hamilton Standard Project Manager.

PRECEDING PAGE BLANK NOT FILMED

TABLE OF CONTENTS

	<u>Page</u>
ABSTRACT	i
FOREWORD	iii
TABLE OF CONTENTS	v
SUMMARY	vii
SYMBOLS	ix
1.0 INTRODUCTION	1
2.0 DESCRIPTION OF EXPERIMENTAL PROGRAM	3
2.1 Model Description	3
2.2 Test Models	3
2.3 Wind Tunnel Facility	4
2.4 Propeller Dynamometer	5
2.5 Model Instrumentation	5
2.6 Test Procedures	6
2.7 Operating Conditions	7
2.8 Data Reduction	7
3.0 ANALYTICAL TECHNIQUES	9
3.1 Method Description	9
3.2 Calculated Instabilities	10
4.0 TEST DATA EVALUATION AND COMPARISON WITH CALCULATIONS	11
4.1 Response Frequencies	11
4.2 Total Stress Results	11
4.3 Spectral Analyses	14
4.4 Modal Response for the SR-3	16
4.5 Comparison with NASA-Lewis Tests	17
5.0 CONCLUSIONS	19
6.0 RECOMMENDATIONS	21
7.0 REFERENCES	23
TABLES	25
FIGURES	30
APPENDIX A - TOTAL VIBRATORY STRESS PLOTS	67
APPENDIX B - SR-3 STRESS PEAK FREQUENCY TABULATION...	93
APPENDIX C - SR-3 CAMPBELL DIAGRAMS	105

SUMMARY

Static stall flutter tests were conducted in an unattached open 5.5 meter (18 foot) test section of the UTRC wind tunnel on three Prop-Fan models. These models are designated the SR-2, SR-3 and SR-5 with the blades characterized by increasing sweep, from the unswept (straight) SR-2 blade to the highly swept SR-5 blade. The tests were conducted at zero flight speed, over a large range of blade angles and rotational speeds (RPM), including all areas of deep stall. Blade vibratory stress measurements were recorded for all operating conditions. Extensive analysis of these data was performed.

Perhaps the most significant test result seen is that increased blade sweep is beneficial in suppressing the high stress which is indicative of stall flutter. The unswept SR-2 model is the most susceptible to stall, responding with the highest stress levels. The moderately swept SR-3 and the highly swept SR-5 models remained stable at increasingly higher blade angles and RPM's than the SR-2, and also responded with lower stresses. As expected, all three models encountered high stressing at the highest blade angles and rotational speeds. It is believed that these were forced excitation responses due to vortex shedding, or buffeting.

The test data show that the strain gages were properly located to allow the various blade vibratory modes to be distinguished. Data analysis indicates that stall flutter responses occur in the third mode (torsion) for the SR-2 model and in the second mode for the SR-3 and SR-5.

Vibratory blade stresses measured during a similar independent test conducted in the NASA/Lewis 10x10 wind tunnel show very good agreement with the UTRC test data.

Stall flutter calculations were made using a recently developed flutter analysis method that can determine the stability of thin, highly swept blades, such as those used on Prop-Fans. The onset of stall flutter is analytically determined to be at operating conditions for which blade damping goes to zero. Negative damping indicates an unstable condition.

Flutter predictions for the three Prop-Fan models were made and compared to test data. Flutter boundaries were determined from the test data, based on the occurrence of steeply rising stresses with increasing blade angle or rotor RPM, since damping was not measured. The calculations show negative damping occurring at generally the same operating conditions for which high stresses were encountered during test. Very good agreement was seen for the SR-2 and SR-3 models, with less agreement for the SR-5 model which did not give strong flutter indications during test. However, the tested trend showing stability to increase with blade sweep was well predicted. The theory predicts that stall flutter will occur in the third mode for all three models. This agrees with the SR-2 test data, but not with SR-3 and SR-5 measurements.

SYMBOLS

AF	Blade Activity Factor	$= \frac{100,000}{16} \int_{0.2}^{1.0} \frac{b}{D} x^3 dx$
b	Blade Section Chord Width, m	
Cl	Blade Section Design Lift Coefficient	
CP	Power Coefficient = SHP/ $\rho n^2 D^5$	
D	Rotor Diameter, m	
N	Rotor Speed, RPM	
n	Rotor Speed, revolutions/sec	
Q	Rotor Torque, N-m	
SHP	Shaft Horsepower	
X	Non-Dimensional Blade Radius	
$\beta_{REF.}$	Reference Blade Angle, deg	
$\beta_{.75}$	Blade Angle at 3/4 Radius, deg	
ρ	Air Density, kg/m ³	

SI units of measurement used throughout unless specified otherwise.

1.0 INTRODUCTION

The occurrence of fuel shortages, increased fuel cost and the threat of future worsening conditions for air transportation has caused NASA to sponsor studies of new, more efficient, aircraft and propulsion systems. One of the promising concepts established by these studies is the advanced high speed turboprop, or Prop-Fan. This propulsion system differs from existing turboprops. The Prop-Fan has greater solidity than a turboprop, achieved by more blades of larger chord. The turboprop has straight blades with relatively thick airfoil sections; the Prop-Fan has swept back blades with thin airfoil sections to enhance performance and reduce noise. The turboprop cruises at no more than 0.65 Mach number; the Prop-Fan is designed to cruise at 0.7 to 0.8 Mach number. The diameter of the Prop-Fan is about 40 to 50% smaller than that of the turboprop. For maximum performance the Prop-Fan makes use of advanced core engines of the kind being used in modern turbofan engines. Performance is also enhanced by use of a spinner and nacelle aerodynamically contoured to reduce compressibility losses by retarding the high velocity flow through the root sections of the Prop-Fan blades.

Utilizing predicted and measured aerodynamic performance data, weight estimates, and noise projections, several Government sponsored studies by both engine and airframe manufacturers have concluded that a fuel savings of approximately 20 to 40% depending on operating Mach number should be achieved by a Prop-Fan aircraft, as compared with a high bypass ratio turbofan aircraft. With these encouraging results, a research technology effort has been instituted to establish the design criteria for this new propulsion system.

A major objective in the development of Prop-Fan configurations is to insure the structural integrity of the rotor. Since the Prop-Fan is such a significant departure from conventional propellers, with its highly swept, thin blades, the structural demands are substantial. The high speed operation of highly swept blades imparts large forces to the limited material inherent to the thin airfoil sections needed for efficient performance. It is imperative that the rotor be able to absorb the aerodynamic loads at all operating conditions, as well as the centrifugal loads associated with its unique shape and construction. The steady-state dynamic response of the blades must be low and flutter instabilities must be avoided, for safe operation.

As part of the continuing studies of Prop-Fan structural stability being conducted by Hamilton Standard, under contract to NASA-Lewis Research Center, static stall flutter tests were conducted on the SR-2 8-bladed, SR-3 8-bladed, and SR-5 10-bladed model Prop-Fan configurations. These tests were conducted during September and October, 1981 at the United Technologies Research Center.

This report summarizes the results of this static stability investigation. Included are trends of the measured blade stress test data with operating conditions for the three models. Blade vibratory stress data were analyzed for the peak stress amplitudes of the total signal as well as for the frequencies and amplitudes of the spectral components. In addition, stall flutter stability boundaries were predicted using a theoretically based calculation procedure for comparison to test results. The comparisons were used to evaluate the accuracy of the prediction methods and to recommend improvements to increase their effectiveness as Prop-Fan design tools.

2.0 DESCRIPTION OF EXPERIMENTAL PROGRAM

2.1 Model Description

Three Prop-Fan models were installed on an isolated nacelle in the United Technologies Research Center wind tunnel and were tested to determine the dynamic stability in stall (see Ref. 1). The models were designated SR-2, SR-3 and SR-5 and are shown installed in Figures 1 through 3, respectively. The blades are made with a solid metal construction, and the planforms are characterized by increasing sweep, from the straight bladed SR-2 model Prop-Fan to the highly swept SR-5 model Prop-Fan. Figure 4 is a schematic showing these planforms along with strain gage locations which will be discussed later.

The SR-2 is an eight-bladed model constructed of steel. The SR-3 is an eight-bladed model and the SR-5 is a ten-bladed model, both of which were constructed of titanium. Table I shows some of the design parameters for these configurations. All of these configurations are derived from full scale designs that are intended to operate at a rotational tip speed of 800 ft./sec. and at 0.8 Mach number flight speed. Figure 5 shows the variations of many of the geometric parameters of each design.

2.2 Test Models

Each of the three test models comprised an approximate 1/8 scale, variable pitch (ground adjustable), 62 cm (24.5 in.) diameter Prop-Fan configuration. Each model consisted of a unique hub, blades, and spinner as well as a common nacelle afterbody. The blades, hub, and spinner were designed and fabricated by Hamilton Standard. The nacelle afterbody was fabricated by UTRC per Hamilton Standard design. Each model was designed for counterclockwise rotation (viewing upstream).

The blade roots were equipped with a gear-sector that engaged a common ring gear in the hub, which assured blade pitch angle synchronization and simplified blade angle changes. The gear-section mechanism permits an infinite adjustment in blade angle over approximately a 90 degree range. However, a locking pin, which is inserted in the ring gear and indexing plate holes, results in incremental settings of 1 degree. The maximum blade pitch angle settings for all three models was limited to 80 degrees. The minimum setting varied for each of the three models and was limited by mechanical interference at the blade roots to -14.3 degrees for the SR-2, -8 degrees for the SR-3, and +11 degrees for the SR-5 model. Blade pitch angle was measured by placing the particular blade in a horizontal position and employing an inclinometer fixture on the face side of the blade at 0.78 radius, known as the reference station. Blade pitch angle is defined as the acute angle between the blade chord and the plane of rotation. Prior to installation, each model rotor was statically balanced on knife edges, and material was removed from the heavy side of the hub by drilling holes to provide a static balance.

2.3 Wind Tunnel Facility

The United Technologies Research Center (UTRC) Large Subsonic Wind Tunnel (LWST) shown in Figure 6 is a single-return, closed-throat facility with interchangeable 5.5 and 2.4 meter (18 and 8-ft.) octagonal test sections. Maximum tunnel velocity is approximately 90 m/s (200 MPH) in the 5.5 m (18-ft.) test section and near sonic Mach numbers can be obtained in the 2.4 m (8-ft.) test section.

For the subject static test program, the tunnel circuit was arranged (Figure 7) to reduce tunnel wall effects and to minimize recirculating flow through the plane of the propeller. This was accomplished by locating the 5.5 m (18-ft.) diffuser in its normally stowed position, thus permitting unobstructed airflow to enter the downstream end of the test section. Flow recirculation through the tunnel circuit was minimized by blocking the open circuit which normally mates to the diffuser and by exhausting the propeller airflow through the air exchanger valves which were set in the 1 m (3-ft.) open position.

The LSWT has available both static and dynamic data acquisition and recording systems. This test program used the static system called Online Computer Controlled Acquisition Recording (ONCOAR). Its minicomputer initialized and controlled that data acquisition equipment, acquired data, displayed and recorded the acquired data, and transmitted the data via a Multi-Serial Transmission (MST) line to another high speed digital minicomputer system for on-line processing. The reduced data were then displayed in tabular form on a computer terminal or in graphical form on a cathode ray tube. ONCOAR is capable of acquiring analog data on up to 25 different channels, using up to eight scanivalve or temperature scanner solenoids. In addition, the system was set up to accept input from up to 14 digital channels. This list includes six channels for the main balance, one each for model pitch and yaw attitudes, barometric pressure, test section pressure differential, tunnel stagnation temperature, two channels for Events Per Unit Time (EPUT) signals and one for a precision pressure transducer/regulator. ONCOAR is capable of recording and storing up to 1200 pieces of analog or digital data in any combination within the above limits.

In this test, ONCOAR recorded a total of 219 pieces of data per point on nine analog channels and four digital channels. Approximately 30 seconds were required to acquire the data, and an additional 10-15 seconds were needed (depending on computer workload) to transmit, reduce, and display the on-line data for a total of approximately 40-45 seconds per data point. The raw data, which had been recorded on floppy disc by ONCOAR, were transferred to a nine-track magnetic tape in large computer compatible format for further processing off-line. This off-line processing can be used for correcting data as well as for refining processing procedures.

A dynamic data recording system supplied by Hamilton Standard was used to monitor and acquire time variant blade stress data. This system provides eight channels of signal conditioning and amplification, FM recording and playback capability, oscilloscope monitor, and switching gear to acquire up to 16 channels of strain gage type data.

2.4 Propeller Dynamometer

The Prop-Fan model was driven by the UTRC Prop-Fan test rig dynamometer (PTR). It uses two variable-speed motors housed within a streamline cast-steel pod with an integral support strut (Figure 8). The motors are mounted in hydrostatic bearings to restrain all motion except axial and rotational motion about the longitudinal axis of the dynamometer. These motions are restrained by load cells which measure thrust and torque of the model Prop-Fan. Each motor has a nominal rating of 280 kW (375 hp) at 12,000 RPM; together they provide a maximum torque of up to 450 N-m (330 lb-ft.) over the entire speed range. Model speed is controlled by variable frequency power supplied by two motor generator sets and measured with an events per unit time meter and a 60-tooth gear signal generator. Prop-Fan rotational direction for this test was counterclockwise looking upstream. The dynamometer is faired such that there is a minimal axial static pressure gradient through the plane of the Prop-Fan and so that the Prop-Fan rotor and spinner surfaces are the only portions of the metric system exposed to the airstream. Pressure instrumentation is provided within the dynamometer to correct measured thrust for any differential pressure between the front face of the hub and an equal area in the rear fairing.

The Prop-Fan dynamometer was mounted on the floor at the downstream end of the 5.5 m (18-ft.) test section (facing south). This positioned the models within 25 cm (10-in.) of the open tunnel circuit (Figure 9). The Prop-Fan drew air from the courtyard in an area unconfined by tunnel walls and discharged it into the tunnel circuit. With the tunnel circuit blocked at the extreme south end of the courtyard and the air exchanger valves open approximately 1 m (3-ft.), the flow created by the Prop-Fan passed out the air exchanger valves and could not recirculate through the plane of the propeller. The relationship of the dynamometer, test section, courtyard, and blocked off tunnel circuit is shown in Figures 10 and 11.

Dynamometer instrumentation consisted of: thrust and torque load cells, a 1/rev reference signal, a 60/rev signal for RPM, vertical and lateral plane vibration transducers, bearing and motor thermocouples, and internal cavity pressure taps. The instrumentation electrical and pneumatic lines were routed down through the hollow PTR pylon to the tunnel floor and from there to appropriate monitoring and recording devices in the control room.

2.5 Model Instrumentation

Each of the three test model Prop-Fans was instrumented with strain gages on the camber surface to measure bending and torsional stresses on four blades. The strain gages were located at the maximum principle stress locations of the natural modes, as determined by analysis. The locations of these strain gages for each blade model are documented in Figure 4. The blade strain gage configuration for each of the three rotors is described in Table II. Blades were numbered sequentially around the rotor in a clockwise direction when viewed from the rear. Blade strain gages are identified by BGx-y, where BG designates blade gage, x is the blade number and y is the gage number. The

electrical lead wires were routed from the strain gages along the trailing edges of the blades and through the hub to a slip ring assembly mounted on the upstream surface of the hub. An electronic, two-position switch on the rotating portion of the slip ring assembly permitted the selection of either of two groups of five strain gages to be monitored. The electrical leads from the stationary portion of the slip ring assembly were routed out the front end of the spinner (Figures 2 and 3) through a pneumatic air cooling line and from there to the appropriate HSD monitoring equipment in the tunnel control room. Air cooling was provided to each of the eight rotating elements of the slip ring through a 1.3 cm (0.5-in.) diameter tube connected to a 138 kPa (20 psig) filtered air supply.

A static pressure probe was mounted in the plane of the airflow entrance to the 5.5 m (18-ft.) test section approximately 218 cm (86-in.) radially from the prop centerline (Figures 9, 10 and 11) to provide an indication of tunnel through flow as a result of propeller thrust. This probe was connected to a high accuracy, low pressure transducer, SETRA 140 Pa (0.02 psig) capability, which provided wind gust data to the dynamic data system, as well as steady-state data to the static ONCOAR data system. In addition, a tunnel spanning pressure rake was mounted 109 cm (43-in.) starboard of the prop centerline (Figures 9, 10 and 11) to provide steady-state wind speed data. The 13 elements on this rake were routed to a water manometer board in the tunnel control room. However, due to the low velocities, and hence low pressures, this system could not provide the desired resolution. For most of the tests, local tunnel velocity was measured solely by the static probe/SETRA system. Also, a conventional, vertical axis, cup anemometer was used for visual reference of the ambient wind condition (Figure 10).

2.6 Test Procedures

The primary objective of the test program was to define the stall-flutter boundaries, if any, of the SR-2, SR-3, and SR-5 Prop-Fan models under static flow conditions. This was accomplished by conducting rotational speed sweeps from 2000 RPM to maximum and back to 2000 RPM, at fixed blade pitch angles, while continuously monitoring blade stresses and recording these stresses on FM tape. Performance data, including rotor thrust, torque, total pressure rise, and nacelle surface pressure distribution, were acquired at regular, discrete rotor speed intervals.

Typically, a test run was conducted as follows: the blade pitch angle, at 0.78 radius, was set using the appropriate fixture and inclinometer; water cooling, oil lubrication, and hydrostatic pressure and scavenge systems were activated; a start zero was acquired on both ONCOAR and on the FM system; the rotor was brought on-line at a rotor speed of approximately 2000 RPM; all ten strain gages were monitored prior to rotor acceleration; rotor speed was increased from 2000 RPM to maximum in a slow, continuous sweep while blade stresses were monitored.

The rotor speed sweep was restricted by blade stress limits which differed for each of the three models. In addition, a speed sweep could be limited by the maximum available electric rotor torque. For this program, this appeared to be approximately 410 N-m (300 ft-lb.). The ultimate limit in rotor speed if stresses and power permitted was 9000 rpm, which corresponds to a rotor tip speed of approximately 293 m/s (960 fps). Steady-state and dynamic data were recorded at the maximum rotational speed and then in increments of 500 RPM between the maximum speed and 2000 RPM. This procedure was repeated at different blade pitch angles and model configurations for approximately 55 data runs. The conditions at which the three models were tested are summarized in Table III. Also summarized in Table III are the conditions for which calculations were performed and will be discussed later.

Since the test program was conducted under static (no flow) conditions, thrust and torque tare data were not acquired nor applied to the actual performance data.

2.7 Operating Conditions

The operating conditions used for the calculations cover a large range of blade angle settings and rotational speed settings. These conditions are presented in Table III for the test runs as well as those for the computations. Since the calculations involve the use of the lengthy MSC NASTRAN program for the mode shapes and frequencies, the number of runs was minimized in order to reduce the computer usage. The MSC NASTRAN program was therefore run at blade angles of -10° and 55° . The frequencies used in the stability analysis were interpolated for conditions with blade angles other than those calculated using MSC NASTRAN. The mode shapes of the nearest MSC NASTRAN case were used for the stability analysis.

The blade angle schedules in Table III for the static test conditions are different for each of the models. The RPM schedule is the same for each model except that the upper limit is restricted by either a power limit or a stress limit. All test points and calculations were at sea level conditions.

2.8 Data Reduction

Blade vibratory stress data were displayed and monitored, on-line, on a multichannel oscilloscope. Hamilton Standard personnel interpreted these time-variant data in a continuous, on-line manner throughout the test program. Test conditions were selected and operational limits were observed as a result of this (on-line) monitoring. In addition, stress data, for each steady state data point and all rotor accelerations, were recorded on FM tapes which were retained for comprehensive, detailed analysis.

The analog tapes were analyzed by obtaining total vibratory stress amplitudes using electronic peak stress converters and recording the resulting signals on strip charts. As a second step, samples 30 seconds in length from the magnetic tape were processed using a real time analyzer. These samples were time averaged to produce spectral analyses of the data. This information, in turn, was then stored on tape for a permanent record of each case. The data were then transmitted to a high speed digital mini-computer for processing. At this point, a computer program was used to pick out the peak amplitudes and the associated frequencies. These were then tabulated and printed according to case number and condition. Automatic routines were developed that produce Campbell diagrams and vibratory stress vs. RPM for each blade angle. These items are discussed further in the spectral analysis section (see 4.3) of this report.

3.0 ANALYTICAL TECHNIQUES

3.1 Method Description

The method used to estimate stall flutter boundaries involves several parts. The various computer programs used are listed by designation and purpose in Table IV. The primary analysis used to calculate these boundaries is the F203 analysis, and the other programs are used to generate data for or from this analysis.

The F203 stability analysis was developed by J. Turnberg (Reference 2) primarily for classical flutter. It is a linear eigen-value solution that uses unsteady aerodynamics accounting for compressibility effects and blade sweep. For classical flutter, the quasi-steady lift analysis uses the value of 2π for the lift curve slope. The computer program has a separate portion for stalled conditions that is used to calculate stall flutter. Here the unsteady aerodynamic analysis uses a parabolic pressure distribution for determining the unsteady forces. For the quasi-steady terms in stall, the program uses the lift curve slope at the local angle of attack for a particular operating condition. In addition, the analysis uses a method developed in Reference 3 for stalled flow. This method complements the eigen-solution and gives results that are very similar. It uses an energy balance that relates the energy developed by the aerodynamic forces to the strain energy in order to determine the damping of the system. It employs the same unsteady aerodynamic terms as are used in the stall flutter eigen-solution.

The stability analysis F203 is also a modal analysis that requires three-dimensional modes, developed in the blade chord coordinate systems, at each blade spanwise station. Generally, other linear aeroelastic analyses describing rotating aeroelastic surfaces will approximate the geometric blade angle relative to the plane of rotation using small angle assumptions. In static operation, this angle is very large, up to 70 degrees for a Prop-Fan. The F203 analysis uses the blade chord as a coordinate system such that the small angle is made on the section angle-of-attack, which is small for most applications. The input requires that the mode-shapes and modal masses be transformed to the above mentioned coordinate system. Generally, the mode shapes and frequencies are developed by the beam analyses, H025 and H027, or the finite element methods, NASTRAN or BESTRAN. A program called F214 makes the necessary transformations from finite element methods while approximating the blade motions by three-dimensional beam type displacements. Chordwise deformations are approximated by a rigid section. The methods used in the present analysis are discussed in more detail in Reference 2.

Figure 12 shows a block diagram of the procedure used in the stall flutter analysis. It can be seen in this diagram that the output from the finite element methods are input for the F214 coordinate transformation program. (It should be mentioned that there is an earlier modification to the F.E. data by a program called "MODES". This rotates the data for each element into the shaft plane and modifies the format. It is not shown on the block diagram.) The operation of the F214 program can be implemented by the CLIST Control Program as shown by the block diagram in Figure 12. An output file from F214 is created containing the transformed mode shapes, modal masses and frequencies.

- The aerodynamic properties used for the F203 stability analysis are initiated in a data bank accessed by the H444 performance analysis, where the data for several airfoil shapes are stored. Once the performance has been determined at the operating condition of interest, the lift and moment slopes are then determined as a function of angle of attack at each radial station for this operating condition. These slopes determine the unsteady and quasi-steady loads in the stability analysis.

As shown in Figure 12, the running of the F203 stability module is controlled by the F203CL CLIST. Here the transmission of the input and output files is managed, and the plot program is executed. The plot program PLT203 was created to run from a file that consists of data for many F203 runs. The results of this program are plots of the printed output, where damping and frequency are plotted as functions of blade angle.

It is suggested here that the stall flutter boundaries predicted by this analysis may be conservative. This is partially due to the fact that stall flutter is a limit amplitude phenomenon, and can exist at small amplitudes. If the limit amplitude is small enough, then it is possible that flutter will not be noticed experimentally, because it will be lost in stresses due to turbulence or other causes. The present analysis is a linear analysis and can, therefore, predict only the onset of flutter, which could be at low stress levels. Thus, the predicted boundary would appear conservative, in relation to the point of measured high stresses.

3.2 Calculated Instabilities

Calculations to estimate stability boundaries were made for the SR-2, SR-3 and SR-5 model blades using the F203 stability analysis. Values of total damping were calculated for 5000, 7000 and 9000 RPM, at many blade angles, as shown in Table III. Figures 13 and 14 show the damping to critical damping ratio for all three models as a function of blade angle at 7000 and 9000 RPM, respectively. The onset of stall flutter is assumed to be at the point where the damping goes through zero. At 7000 RPM, it is seen that increasing the sweep is beneficial in delaying the stall flutter to a higher blade angle. Note that the SR-5 does not flutter at 7000 RPM but is delayed until 9000 RPM. All of the stall flutter predictions are third mode instabilities. No instabilities were calculated for the first or second modes. Figure 15 shows the typical damping ratio relationships between the modes for the SR-3 model Prop-Fan blade. The flutter boundaries, as functions of blade angle and RPM, will be shown later in discussions of the test results.

4.0 TEST DATA EVALUATION AND COMPARISON WITH CALCULATIONS

4.1 Response Frequencies

The calculated blade response frequencies for the SR-2, SR-3 and SR-5 model blades are shown in Figure 16, where blade frequency is plotted as a function of rotational speed. Also shown in this figure are data points taken from spectral analyses of the analog blade stress data, some of which will be discussed later. As previously mentioned, the SR-2 blade frequencies were calculated using the beam methods H025 and H027, while the SR-3 and SR-5 blade frequencies were calculated using the MSC NASTRAN analysis.

It is seen that good agreement exists in all modes between the test results and the computations for the SR-2. Note that the slopes of the second and third mode show good agreement. For the swept models, the SR-3 and SR-5, good correlation is made for the first two modes with poorer correlation occurring for the third, fourth and fifth modes. However, good agreement is seen for the slopes of the higher modes for these two models. Both swept blade models show a measured response between the second and third calculated mode. The nature of this response is not understood at this time.

4.2 Total Stress Results

As previously indicated, total peak vibratory stress was recorded on strip charts for the SR-2, SR-3 and SR-5 model Prop-Fan blades. The stress data from those charts were tabulated and selected data were plotted on curves of total vibratory stress (infrequently repeating peak stress*) as a function of RPM for various blade angles. These plots are shown in Appendix A for the three Prop-Fan models. Additionally, cross plots were made to produce stress contour plots for the model Prop-Fan blades. These are contours of constant total vibratory stress, plotted on curves of reference blade angle vs. RPM, and are shown in Figure 17 through 19. Note that the takeoff design operating point for each blade is shown for reference.

Isostress Contour Plots - Figure 17 shows the total stress contours for the tip bending gage and the shear gage outputs of the SR-2 model (blade number 5). Both gages show the highest stress at a reference blade angle of 40 degrees and 7000 RPM. From Figure 16, it is seen that this is very close to the third mode 5P critical speed. The buildup seems gradual with increasing RPM and less gradual with increasing blade angle. This effect is probably due to the fact that a change in reference blade angle has a greater effect on the blade angle of attack than a change in RPM. These results are typical for conventional propellers that encounter high stresses in the static condition. Since the third mode is the torsion mode, it is not surprising that stall conditions combined with critical speed effects would cause a stress buildup. It is also noted that the gradual buildup makes it difficult to find a precise definition of a stall flutter boundary, especially one where the damping might be considered as having a value of zero.

*The infrequently repeating peak is defined as the maximum stress peak that repeats itself two or three times during the stress data sample period.

The calculated flutter boundaries for the SR-2 are also shown in Figure 17. The calculated boundaries represent the torsion (third) mode while the measured total stress represents all the modes. A spectral method by which the modal stresses can be separated will be discussed in the next section.

Similar isostress contour plots are presented in Figure 18 for the SR-3 model Prop-Fan. This figure represents the output from the inboard bending, the shear and the tip bending gages, respectively. In order to smooth out some of the irregularities in the data, the values of stress were averaged between blades 1, 2, 5 and 6 for the shear and tip bending gages, and between blades 1 and 5 for the inboard bending gage. These curves show three entirely different patterns. For example, the shear gage shows a very gradual increase in stress with varying RPM and blade angle. However, the inboard bending gage shows a sharp increase in stress near 40 degrees blade angle and 6000 RPM. The tip bending gage indicates a sharp rise in stress near 30 degrees blade angle, but shows a gradual increase with RPM.

Subsequent viewing of oscillograph records clearly shows different predominant frequencies of similar amplitude occurring on different gages of the same blade for some records. This indicates that stalled flow can excite several different modes simultaneously. It can also be concluded that the strain gages were effectively placed to measure the response of each mode. Interestingly, the flutter indications predicted for the shear gage seem to occur experimentally for the tip bending gage. Spectral studies made for the SR-3, and discussed later in this report, shed more light on this apparent discrepancy.

Figure 19 shows stress contour plots for the SR-5 model blade. They represent the output from the inboard bending gage and the shear gage, respectively. The shear gage shows a very high stress peak at 6500 RPM. This can be attributed to the fact that it is very close to a 6 per revolution critical speed for the 4th experimental mode, as shown in the Campbell diagram in Figure 16. This mode coincides with the 3rd predicted mode. High 4th mode response is also indicated on spectral plots, to be shown later in the report.

The calculated stall flutter boundary predictions are also shown in Figure 19. These were developed for the 3rd mode and represent the boundary of zero damping. It is seen that this predicted boundary occurs at very high RPM and does not coincide with any sudden stress rise. Some of the lack of correlation between test and prediction might be due to the fact that the test results include aerodynamic excitation other than stall flutter, such as buffeting. Also, it may be difficult, in some cases, to distinguish between stall flutter response and a critical speed crossover.

Stall Flutter vs. Buffet - It may be useful to discuss the differences between stall flutter and buffeting. Buffeting is defined as a forced excitation due to an instability of the air, such as vortex shedding, shock oscillation, or turbulence. Stall flutter is an instability due to the interaction between the air and the blade. In stall flutter conditions, the motion of the blade and the aerodynamic loading on the blade are strongly interdependent. In buffet conditions, the motion of the blade has little effect on the loading.

Generally, as blade angle is increased the Prop-Fan progresses from normal load conditions to stall and then to deep stall. Stall flutter can occur as the Prop-Fan becomes stalled and buffet occurs in deep stall. At a specific operating condition, the local angles of attack along to blade span increase as the blade angle is increased, with stall first occurring inboard and then progressing outboard.

In order to define when the Prop-Fan is stalled, the blade reference station (0.78 radius) is generally a good point to consider as being a stall control station. The conditions at which the current Prop-Fan blades stall was not investigated for this analysis. However, from preliminary estimates it is thought that stall occurs at a reference blade angle between 30 and 35 degrees, for Prop-Fans at static (zero forward speed) conditions. Although the boundary between stall flutter and buffet regions is not clear, it is thought that buffet occurs at blades angles which are substantially higher than blade angles for which stall flutter occurs. For this discussion, the buffet region is defined to be at blade angles of approximately 45 degrees and larger.

Blade Stall vs. Rotor Torque - Prop-Fan rotor torque can be an indication of the loading condition on the blades. Figure 20 shows the measured shaft torque, as a function of reference blade angle for various RPM, for the SR-2, SR-3, and SR-5 model Prop-Fan configurations. Each plot shows a variation in RPM from 5500 to 8500 RPM.

Generally the torque increases with blade angle and RPM for all configurations. It is seen from these curves that there is a change in the torque at or near the blade angles where stall might be expected. The SR-2 shows the greatest effect, where the torque increases rapidly near a blade angle of 28 degrees, peaking at 30 degrees and returning to the torque curve at 33 degrees.

The SR-3 data show a decrease in torque near a blade angle of 31.5 degrees. It is not known if there is a torque rise just before this point because of insufficient data. The change in torque seems less severe than that observed for the SR-2.

The SR-5 data show a small depression at a blade angle of 34 degrees for the higher RPMs. This is a lesser effect than that seen for the SR-3. The low RPM SR-5 data show little of this effect.

The effect of stall on the torque curves is most severe for the SR-2 and least severe on the SR-5 with the SR-3 falling in between. This indicates that the influence of stall on the torque is affected by blade sweep, since the major difference between the configurations is sweep, the SR-2 being non-swept and the SR-3 and SR-5 having increasing sweep, respectively.

It is also noted that the torque change occurs at an earlier blade angle on the SR-2 and progressively later on the SR-3 and SR-5, respectively. The test data discussed above (Figures 17 to 19) show that a high stress rise occurs at blade angles near where the torque inflections occurred. Also, the highest stresses occurred on the SR-2, with progressively lower stresses on the SR-3 and SR-5. This indicates that stall and/or stall flutter occurs at similar conditions as the inflections on the torque curves. It is therefore concluded that the torque curves can indicate the presence of stall or stall flutter conditions.

It is recommended that in future static tests on Prop-Fan models, fine variations be made in RPM and blade angle in the area just below, in and above the stall condition, and that torque measurements be made at each steady state condition. This would be helpful in defining the condition of blade stall onset and its relation to blade stress.

Blade Stress vs. Damping - It should be noted that some of the difficulty, in comparing calculated stall flutter boundaries to the experimental results, is due to the nature of the parameters which are used to define the boundary for each. The calculated stall flutter boundaries are linearly determined to be at the point where the critical damping ratio goes zero. The experimental flutter point is determined to be where there is a sudden rise in vibratory stress with increasing RPM, usually to a high stress value. This ignores the fact that in a non-linear system, the damping can go to zero at flutter onset but can also be zero at some limit amplitude. It is conceivable that the limit amplitude could be small, while the damping is zero. It may be misleading to investigate stall flutter conditions by comparing the two different parameters of damping and stress, as was done here. A better result may be expected if a non-linear aeroelastic analysis is used to produce stress predictions that could be compared to the experimental stresses. At the time of this work, however, a reliable analysis of this nature was not available.

4.3 Spectral Analyses

Measurements of total stress cannot be used to fully characterize blade dynamic behavior. For example, total stress values do not allow the stress contributions of each mode or P-order response to be distinguished. Spectral information is helpful in evaluating modal stresses. This is examined in the form of spectral plots of vibratory stress as a function of frequency.

SR-2 Results - Figure 21 is a spectral plot of measured stress for the blade tip bending gage output on the SR-2 model operating at 7000 RPM and a reference blade angle of 36.2 degrees. Figure 22 is a spectral stress plot of the shear gage at 8500 RPM and a reference blade angle of 31.5 degrees. These two figures represent conditions in the high stress areas for each gage, as seen in Figure 17. They are not the conditions of highest stress, but are located in the area of steep stress rise.

The indications from Figures 21 and 22 are that, for the SR-2, the flutter occurs in the third mode at or near 600 Hz. This mode is considered the primary torsional frequency (See Figure 16). The third mode response level seen in Figure 21 is large due to its proximity to the 5P critical speed. Figure 22 shows substantial twice per revolution response. This is unexplained, except that it is a relatively low stress, and this condition may be close enough to the 2P critical speed to give some magnification to the 2P stress. Figure 23 shows a spectral plot for the mid-blade bending stress at 5000 RPM and reference blade angle of 50.3 degrees. Here the response is substantially in the first mode. This may be a buffet condition exciting the first mode with some 2P magnification due to the nearness of the 2P critical speed (See Figure 16).

SR-3 Results - Spectral plots from SR-3 testing are shown in Figures 24, 25 and 26. Tip bending stress is shown in Figure 24 for a condition of 9050 RPM and 31.7 degrees reference blade angle. This condition is in a steep stress rise area (See Figure 18) that is indicative of stall flutter. Figure 24 shows the tip bending to have a high 3P response accompanied by a moderate second mode contribution. The 3P response seems exaggerated by low damping associated with the 2nd mode response. The 4P, 5P and 6P responses could also be critical speed related (See Figure 16).

A more clear example of stall flutter response is shown in Figure 25. The tip bending gage spectrum in this figure is for a condition of 32.7 degrees blade angle and 7020 RPM. This is not near any critical speed and is also in the steep stress rise area. Figure 25 shows substantial second mode response with no apparent excitation. This is a strong indication of stall flutter response. There is also response present in the third, fourth and fifth experimental modes. Recall from Figure 16 that what is termed the fourth experimental mode is shown near the third predicted mode. This mode shows the least response in Figure 25, which is contrary to the stall flutter predictions discussed earlier.

Figure 26 represents a 5010 RPM and 50.3 degree blade angle condition. This is considered to be in a high stress buffet region due to the large blade angle, as discussed earlier. This is probably not a stall flutter condition. Figure 26 shows primarily 1st mode response. The contour plots in Figure 18 also show mostly inboard and tip bending at this condition. Spectral plots of the shear gage signals (not shown) indicate comparatively little stress.

SR-5 Results - Two SR-5 spectral stress samples are shown in Figures 27 and 28. The first represents the output of a shear gage at 8500 RPM and a reference blade angle of 35.7 degrees, and the second is the output of an inboard bending gage at 6500 RPM and a reference blade angle of 49.8 degrees. All the stress peaks shown for these two curves indicate relatively low stresses, but the shear gage seems to be responding to white noise type excitations. This indicates the possibility of buffeting, and there seems to be no evidence of a self excited response. This is also seen in Figure 19, in that there is no sudden stress rise in either the shear or bending gage. The inboard bending spectral curve (Figure 28) shows a low level second mode response, and little of anything else.

The indications from these data are that the highly swept SR-5 Prop-Fan model has little or no stall flutter problem, the SR-3 has a moderate stall flutter response, while the SR-2 has a strong stall flutter response. Thus, sweep seems to have a suppressing effect on stall flutter.

4.4 Modal Response for the SR-3

The stress peaks that were obtained from the spectral analysis and used in the Campbell diagram of Figure 16 can be categorized as to frequency and mode. Table V indicates the frequency range assumed for each mode, based on the experimental responses. Plots of stress vs. RPM for various blade angles can be made for each mode and each gage. Diagrams of constant vibratory stress contours can be plotted from crossplots of these curves. For this report, only the isostress contour plots for the SR-3 model will be shown.

Figure 29 shows the modal isostress contour plots for the SR-3 model Prop-Fan stall flutter tests at the UTRC. Here, the measured modal stress is plotted as a function of rotational speed and reference blade angle. Each mode is shown for the particular gage that generally has the highest response. Only the first five modes are shown in Figure 29; one contour plot for each. For the first plot (1st mode), it is seen that the high stresses occur at a reference blade angle of about 50 degrees and at RPM's greater than 6000. This is well above what is considered stall, possibly indicating that these stresses are due to buffeting, which involves mostly the 1st bending mode. Note that the identifying gage is the inboard bending gage, which is most responsive to the first mode. Also shown on this curve are the operational limits of the test. These limits were established by drive power limits, RPM limits and blade allowable total stress limits.

The second mode is characterized by high stress, probably under conditions for which the blade first encounters strong stall over most of its span. This indicates stall flutter responding in the second bending mode. These data corroborate the spectral results, discussed earlier. Note that the high stresses are found primarily in the tip gage. Also, the stress does not seem to be related to a critical speed, whereas the high stress observed in the first mode could indicate the 2P crossover; see Figure 16. The higher modes (3, 4 and 5) show little response. It should be noted that the calculated results indicate that stall flutter should occur in the third mode. This is inconsistent with the test results which show high stress occurring in the second mode.

4.5 Comparison with NASA-Lewis Tests

Low speed stall flutter tests were conducted at NASA-LeRC in the 10 x 10 wind tunnel during October 1981, and are reported in Reference 4. Some of the tests were run at static conditions with a small component of velocity due to induction in the tunnel. Assuming this effect is negligible, the total vibratory stress results observed at the UTRC were compared with those obtained at NASA-LeRC. These comparisons are shown in Figures 30 through 32, where total vibratory stress is plotted as a function of rotational speed for various blade angles.

Figure 30 shows the total blade vibratory stresses for the SR-2 model Prop-Fan. Shown are the outputs from the mid-blade bending, the shear and the tip bending gages for reference blade angles of approximately 32 degrees and 40 degrees. Generally, the test results at the UTRC give stresses that are similar to those obtained at NASA, except near or at critical speeds, where the UTRC results show higher stresses. This may be due to the fact that, at the UTRC the rotor was subject to the effects of turbulence due to weather conditions, since the test was open to the atmosphere.

Figure 31 shows the results from the inboard bending, the shear and the tip bending gages of the SR-3 model Prop-Fan blade. The comparisons are made for reference blade angles of approximately 32 degrees and 60 degrees for shear and tip-bending, and approximately 32 degrees and 50 degrees for the inboard bending. Note that the vibratory stresses are lower for the SR-3 model than for the SR-2 (Figure 30) due to the benefits of sweep. The correlation between the results from the NASA-Lewis tests and the results from the UTRC tests, for the SR-3, is also very good. For the SR-3 bending gages, the vibratory stresses obtained from UTRC are somewhat higher than the NASA measurements, which is the opposite from the SR-2 results. However, the UTRC results for the SR-3 indicate higher response near the critical speeds than the NASA results, as also occurred for the SR-2 model.

Figure 32 shows the results from the inboard bending, the shear, and the chordwise bending gages on the SR-5 model Prop-Fan. Shown are the results for the approximate reference blade angles of 32 degrees and 50 degrees. Again, the UTRC vibratory stress results are somewhat higher than the NASA data but the correlation is still very good. As for the other blade models, the UTRC SR-5 tests show higher response in the critical speed regions probably due to higher turbulence.

5.0 CONCLUSIONS

As a result of the test and analysis program summarized in this report, the following conclusions were reached regarding the static stability of the SR-2 straight blade, the SR-3 moderately swept blade and the SR-5 highly swept blade Prop-Fan models:

1. Increased sweep tends to suppress the high blade stresses caused by stall flutter and buffet.
2. Correlation between tested and predicted Campbell diagram modal frequencies was excellent for the first and second modes for all blade models.
3. Correlation between tested modal frequencies and beam method calculations for the SR-2 model, at the higher frequencies, was good. Finite element method frequency modal calculations for the SR-3 and SR-5 models showed less agreement with test data at the higher frequencies.
4. Comparisons were made between measured stall flutter boundaries, based on steeply rising stresses with RPM and blade angle, and calculated boundaries based on zero blade damping. Good agreement between test and prediction was indicated for the SR-2 and SR-3 models, while less agreement was seen for the SR-5 model, which did not give strong flutter indications during test.
5. Tested stall flutter response for the SR-2 straight blade occurred in the torsional third mode, as was predicted. Test data for the SR-3 and SR-5 swept blades show stall flutter response primarily in the second bending mode while the calculated results predict that stall flutter should occur in the torsional third mode.
6. Modal isostress contour data indicate that stall flutter and buffet occur in different operating regions, with buffet occurring for very high blades angles.
7. Total vibratory stresses measured at static conditions at the UTRC were compared to those obtained in the 10 x 10 wind tunnel at NASA-LeRC, for the SR-2, SR-3 and SR-5 models. Both the absolute stress amplitudes and the trends with varying RPM agree very well for these two independent tests.

6.0 RECOMMENDATIONS

1. Since it was shown that there was little difference between testing in the wind tunnel at NASA-Lewis or testing in the atmosphere at UTRC, it is suggested that future static tests can be conducted in a wind tunnel. This will eliminate duplication of rig setup.
2. It is recommended that in future static tests on Prop-Fan models, fine variations be made in RPM and blade angle in the area just below, in and above the stall condition, and that torque measurements be made at each steady state condition. This would be helpful in defining the condition of blade stall onset and its relation to blade stress.
3. The tests reported herein show variations of measured blade stress with rotational speed (RPM) and with blade angle. It was observed that at or near critical speeds, the testing was limited to those RPM's for which the stresses were below the limits. If the test condition envelope was increased to include rotational speeds beyond these critical speed areas, the scope of the data could be increased. Additional understanding of the phenomena of stall flutter and buffeting would develop if this could be achieved.
4. The correlation between the current stall flutter theoretical predictions and the experimental results can be improved. Deficiencies in the analysis may be due to its linearity. The analysis is linear in both the aerodynamics and structural dynamics by assuming small amplitude displacements. The actual blade response in stall flutter very often has large amplitude displacements. This behavior requires that non-linear aerodynamics as well as non-linear structural response be included in the analysis for proper representation. Also, Coriolis forces due to rotation are non-linear for large amplitude vibrations.

It is recommended that a non-linear analysis be developed that can model the behavior described above. It is suggested that this analysis be a modal time step analysis and that it include the following features:

- Three-dimensional modes obtained from finite element methods.
- Curved beam description of modes.
- Large displacement equations of motion, to include four or five bending and twisting degrees of freedom with the capability of including chordwise bending for future growth.
- Complete induced flow capability such that various methods of induction can be selected, from momentum methods to vortex and pressure potential methods.
- Non-linear aerodynamics for steady state operation, including high angles of attack.
- Non-steady aerodynamic effects to include non-steady coefficients, accounting for phasing, to be added to the steady state description with the ability to substitute empirical data or theory (synthesizing of data).
- Three dimensional treatment of airloads, including radial and inter-blade effects.

5. It is also recommended that wind tunnel tests be conducted on two-dimensional Prop-Fan airfoil sections, to provide data for use in improving the theoretical analyses. These tests should include investigations of the following:

- Steady state data.
- Unsteady data (synthesis).
- High angle of attack.
- High Mach number effects (compressibility).
- Effects of sweep.

7.0 REFERENCES

1. Goepner, B.W., "Static Flutter Tests of HSD Prop-Fan Models", United Technologies Research Center Report R81-335414, February, 1982 (controlled circulation).
2. Turnberg, J., "Classical Flutter Stability of Swept Propellers." Proceedings of the AIAA/ASME/ASCE/AHS 24th Structures, Structural Dynamics and Materials Conference, May, 1983, Lake Tahoe, Nevada.
3. Steinman, D.B., "Aerodynamic Theory of Bridge Oscillations", American Society of Civil Engineers, Transactions, Paper No. 2420, October, 1949.
4. Smith, A.F., "Analysis and Test Evaluation of the Dynamic Response and Stability Of Three Advanced Turboprop Models at Low Forward Speed", NASA CR 175026, December 1985.

TABLE 1. PROP-FAN MODEL SUMMARY

	SR-2	SR-3	SR-5
NO. BLADES	8	8	10
MATERIAL	STEEL	TITANIUM	TITANIUM
DIAMETER	24.5 IN	24.5 IN	24.5 IN
DESIGN C_L	0.084	0.214	0.271
AF (TOTAL)	1632	1880	2100
AF (PER BLADE)	204	235	210

**TABLE II: STRAIN GAGE DESIGNATION MODEL PROP-FAN
UTRC STATIC STALL FLUTTER TESTS**

PROP-FAN MODEL	DESCRIPTION	RADIAL STATION, IN.	BLADE NO		GAGE DESIGNATION									
			1	2	3	4	5	6	7	8	9	10		
SR-2	Mid-Blade Bending	7.0	BG1-2	BG2-2	.	.	BG5-2	BG6-2		
SR-2	Shear-V Gage	7.5	BG1-3	BG2-3	.	.	BG5-3	BG6-3		
SR-2	Tip Bending	10.0	BG1-4	.	.	.	BG5-4		

SR-3	Inbd. Bending	4.4	BG1-1	.	.	.	BG5-1		
SR-3	Shear-V Gage	9.6	BG1-4	BG2-4	.	.	BG5-4	BG6-4		
SR-3	Tip Bending	10.7	BG1-6	BG2-6	.	.	BG5-6	BG6-6		

SR-5	Inbd. Bending	5.3	BG1-1	BG2-1	BG3-1	.	.	BG6-1	BG7-1	BG8-1	.	.		
SR-5	Shear-V Gage	8.9	BG1-5	BG6-5		
SR-5	Tip Bending	10.4	BG1-3	BG6-3		

TABLE III. OPERATING SCHEDULES

OPERATING SCHEDULE FOR COMPUTER RUNS*

MACH NO.: 0.0

BLADE ANGLE $= \beta.75^{**}$: -20 DEG. TO 70 DEG. IN 5 DEG. INCREMENTS FOR F203
-10 DEG. AND 55 DEG. FOR MSC NASTRAN

ROTATIONAL SPEED: 5000, 6000, 7000, 8000, & 9000 RPM FOR F203
5000, 7000, & 9000 RPM FOR MSC NASTRAN

SEA LEVEL CONDITIONS

* FOR ALL MODELS

** AT 75% RADIUS

OPERATING SCHEDULE FOR THE MODEL PROP-FAN STATIC TESTS AT UTRC

ROTATIONAL SPEED (ALL MODELS): 2000 TO 9000 RPM IN 500 RPM INCREMENTS

(END POINTS ARE MODIFIED DEPENDING ON POWER OR STRESS LIMITS AND
WINDMILL CONDITIONS)

SEA LEVEL CONDITIONS

BLADE ANGLE (DEG) $= \beta \text{ REF}^{***}$

SR-2	SR-3	SR-5
-8.3	-10.0	3.7
15.8	12.0	10.0
19.6	15.9	12.0
23.8	19.9	16.4
27.4	23.6	19.5
29.7	27.6	23.8
31.5	31.7	28.0
32.0	32.7	31.9
35.8	34.0	35.7
36.2	35.7	39.9
39.8	38.0	49.8
50.3	40.0	59.6
60.3	44.9	69.6
69.9	50.3	79.7
79.6	60.0	
	69.9	
	80.0	

*** FOR THE SR-2 AND SR-3: $\beta \text{ REF} = \beta.75 - 0.8 \text{ DEG.}$

FOR THE SR-5: $\beta \text{ REF} = \beta.75 + 0.5 \text{ DEG.}$

TABLE IV
HAMILTON STANDARD COMPUTER PROGRAMS USED IN THE
STALL FLUTTER ANALYSIS CODE

<u>DESIGNATION</u>	<u>PURPOSE</u>
MSC NASTRAN	Finite element analysis used to predict vibratory mode shapes and frequencies for swept, thin structures.
BESTRAN	Hamilton Standard finite element analysis used to predict vibratory mode shapes and frequencies for swept, thin structures.
H025	Beam type analysis used to predict vibratory bending mode shapes and frequencies for straight propeller blades.
H027	Beam type analysis used to predict vibratory torsion mode shapes and frequencies for straight propeller blades.
H444	General Goldstein-type performance strip analysis for propellers. Provides power, thrust, section force data and angles of attack. Section lift and moment curve slopes are determined for use in the stall flutter analysis, F203.
MODES	Converts mode shapes from finite element methods or beam methods to a beam type description for use in the F203 flutter analysis.
F214	This program transposes all co-ordinate system motions into the blade section co-ordinate system in order to take advantage of small angle assumptions.
F203	Eigen-solution modal stability analysis. Calculates damping and frequency using unsteady aerodynamics.
PLT203	Plots the damping and frequency results obtained in F203.

**TABLE V. FREQUENCY RANGES FOR THE VARIOUS MODES
OF THE SR-3 MODEL BLADE RESPONSE DURING
THE STATIC STALL FLUTTER TESTS AT UTRC**

MODE	RESPONSE FREQUENCY RANGE, HZ
1ST	160 - 260
2ND	380 - 450
3RD	605 - 640
4TH	670 - 755
5TH	815 - 900

ORIGINAL PAGE IS
OF POOR QUALITY



FIGURE 1. SR-2 MODEL PROP - FAN STATIC TEST
INSTALLATION AT UTRC

ORIGINAL PAGE IS
OF POOR QUALITY

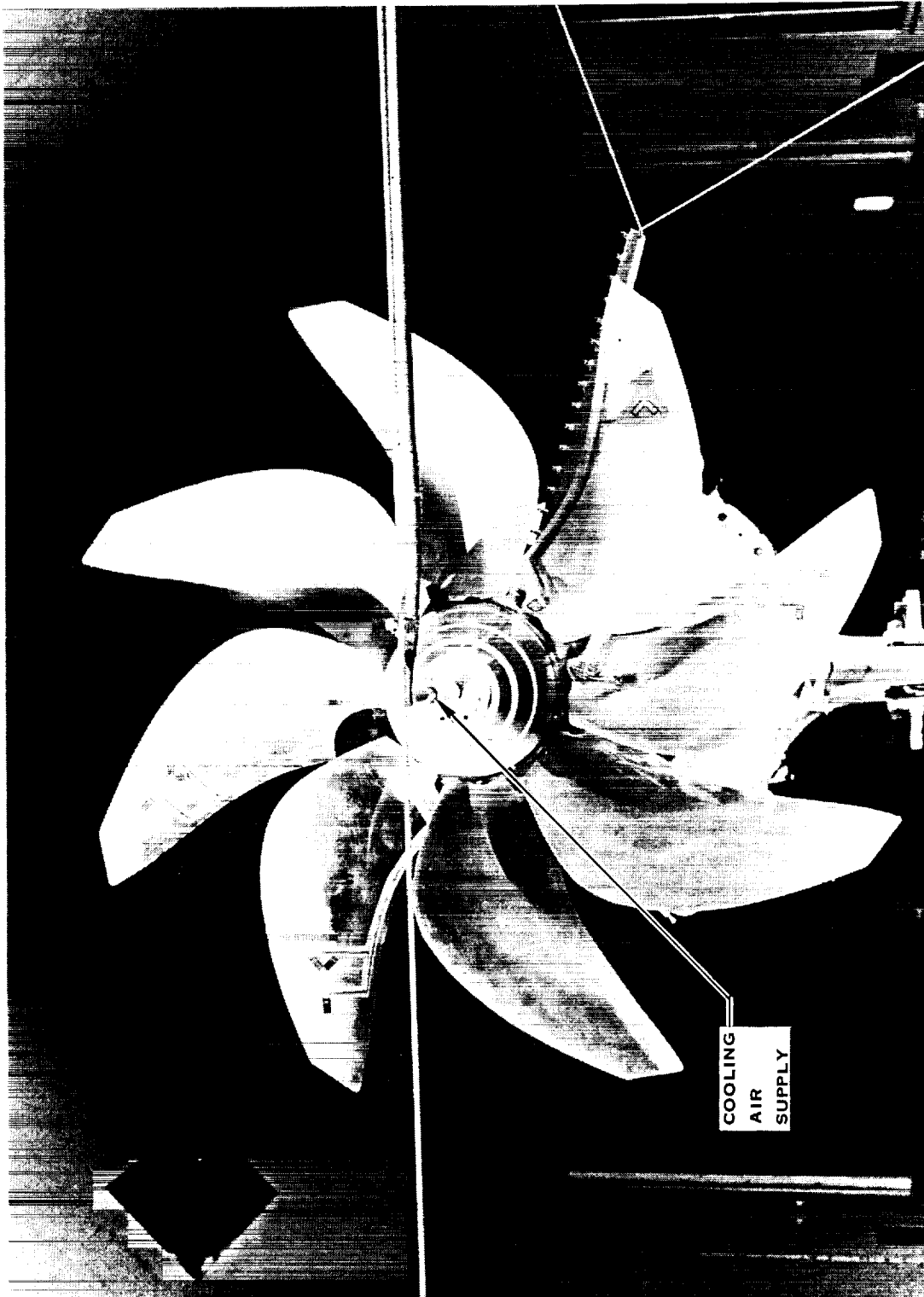


FIGURE 2. SR-3 MODEL PROP - FAN STATIC TEST
INSTALLATION AT UTRC

ORIGINAL PAGE IS
OF POOR QUALITY



FIGURE 3. SR-5 PROP - FAN MODEL STATIC TEST
INSTALLATION AT UTRC

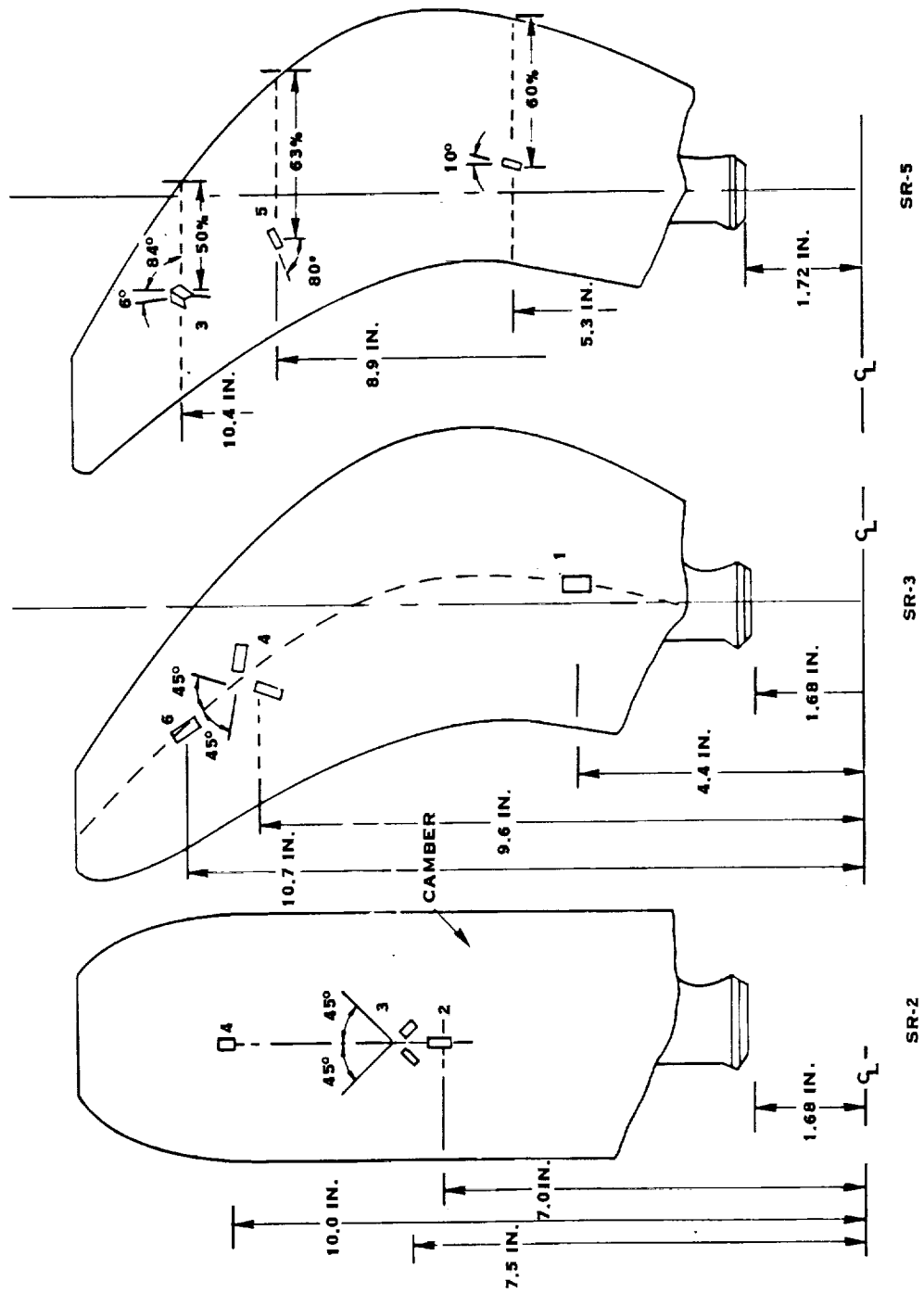
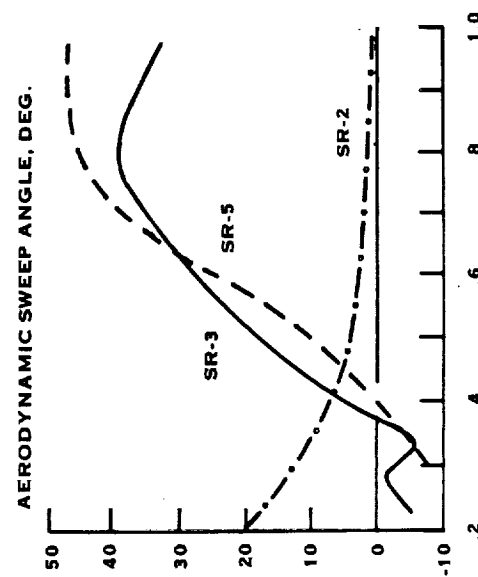
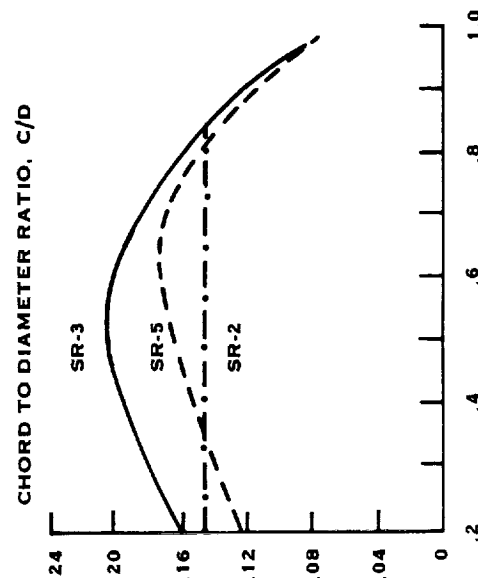
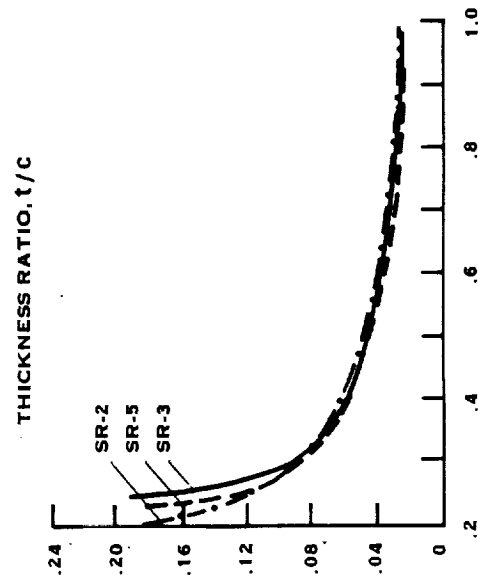
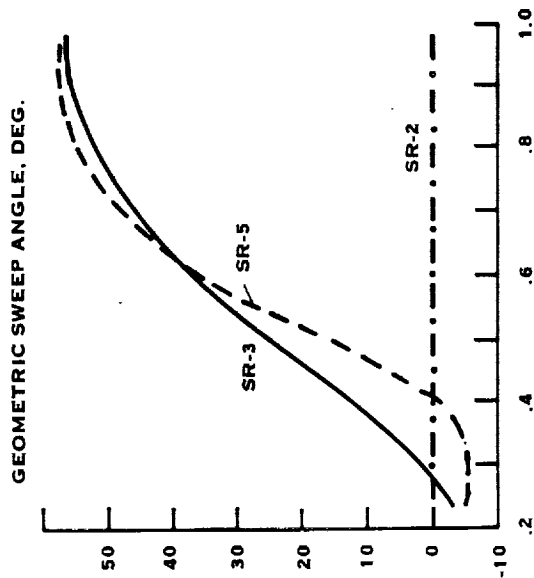
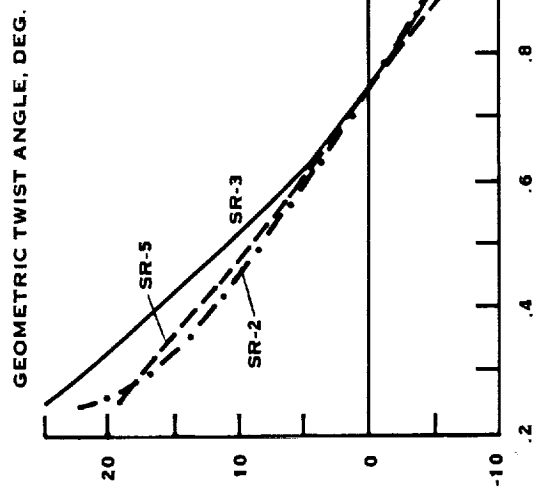


FIGURE 4. SR-2, SR-3, AND SR-5 PROP-FAN MODEL BLADES PLANFORM AND GAGE LOCATION - CAMBER SIDE



NORMALIZED RADIUS

FIGURE 5. PROP - FAN MODEL CHARACTERISTICS

ORIGINAL PAGE IS
OF POOR QUALITY

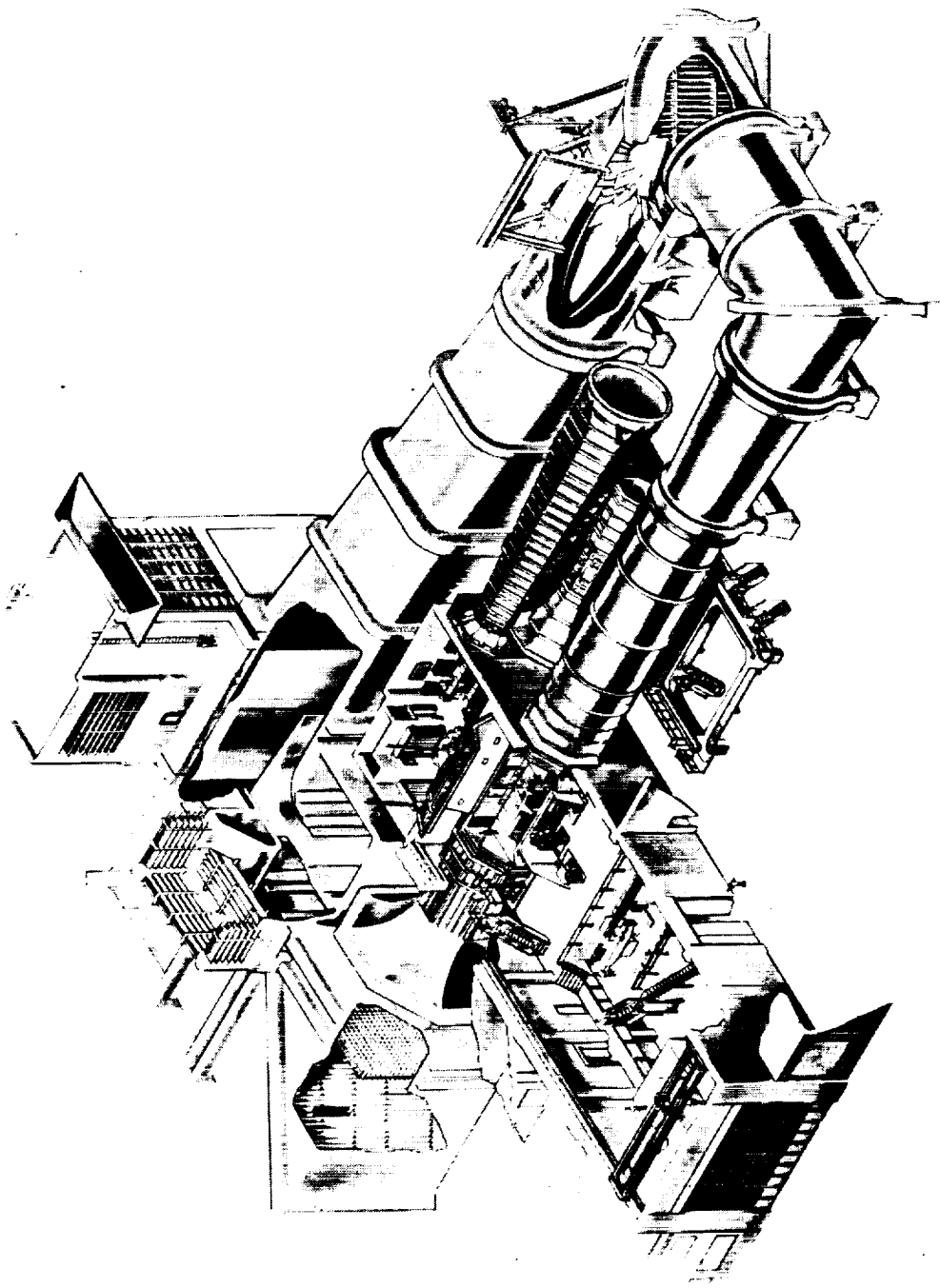


FIGURE 6. UTRC LARGE SUBSONIC WIND TUNNEL

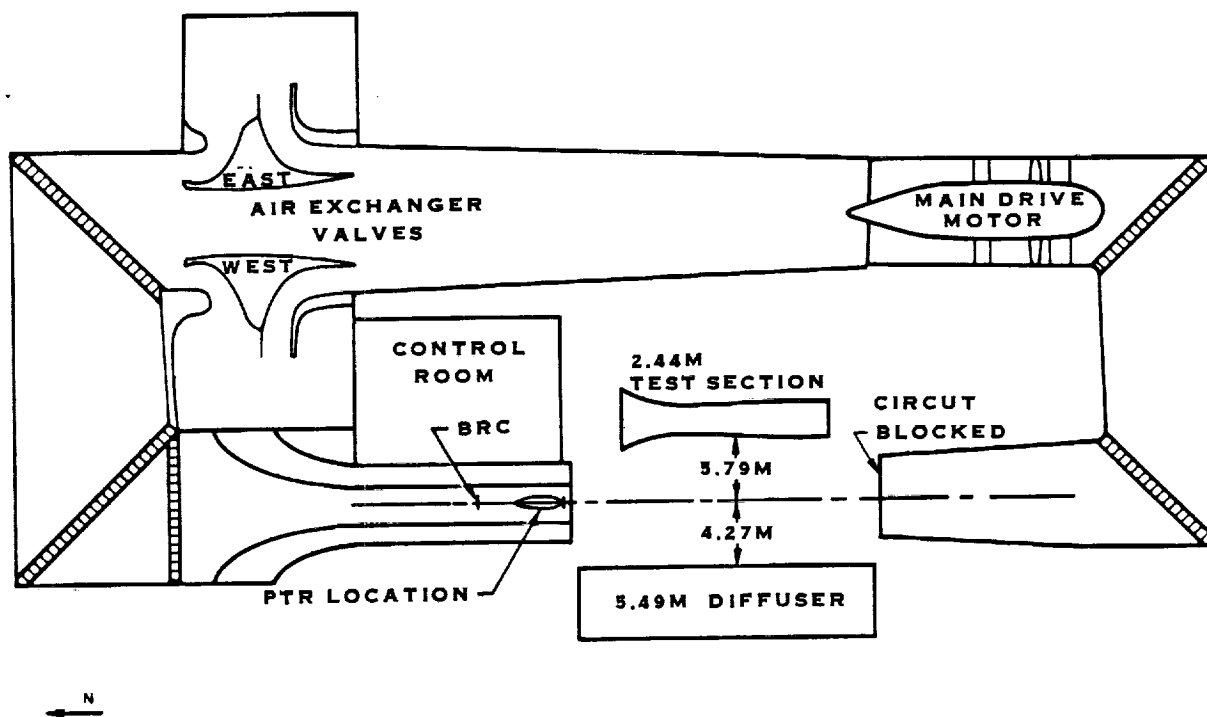


FIGURE 7 WIND TUNNEL CIRCUIT

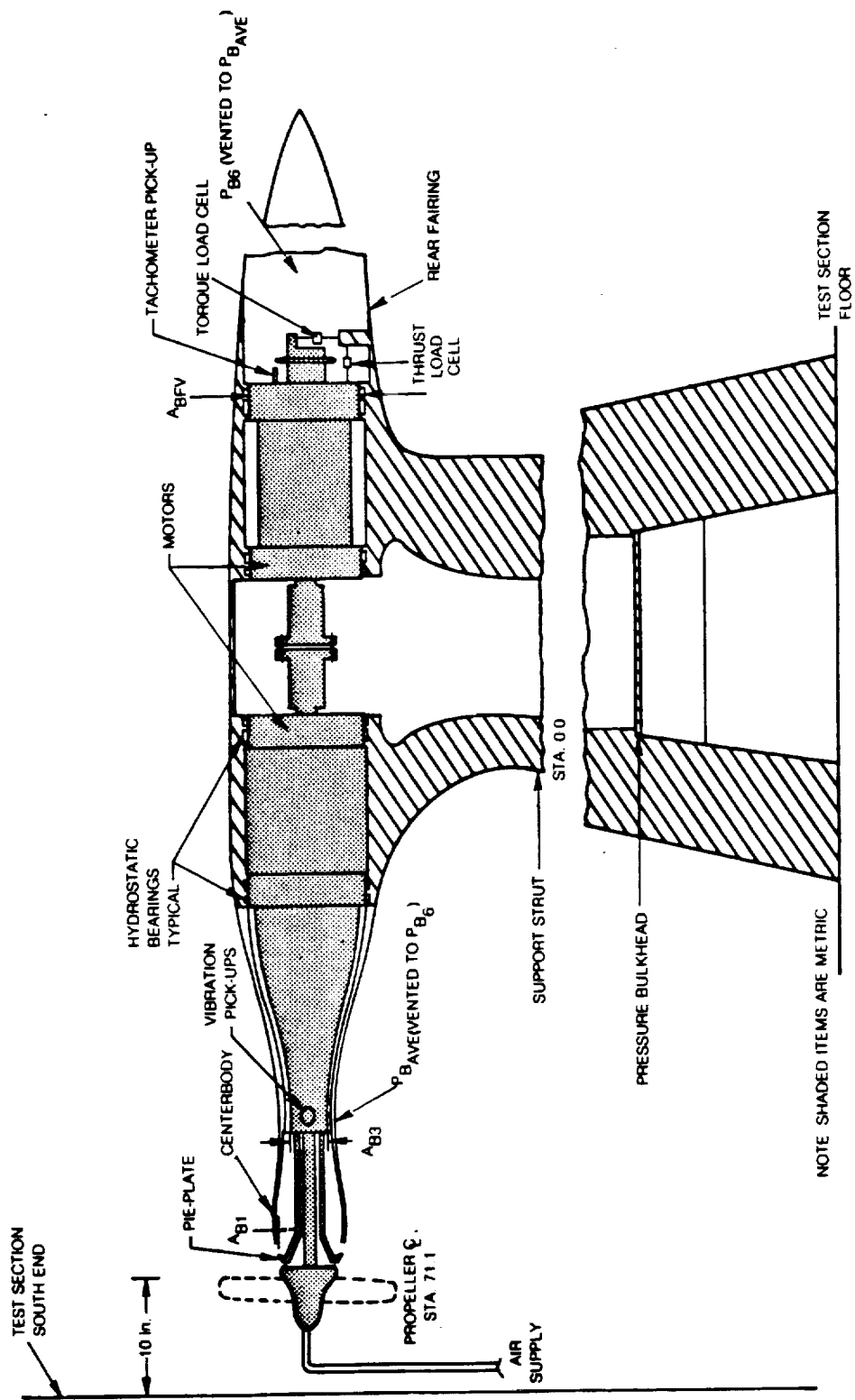


FIGURE 8 PROPELLER DYNAMOMETER DETAIL

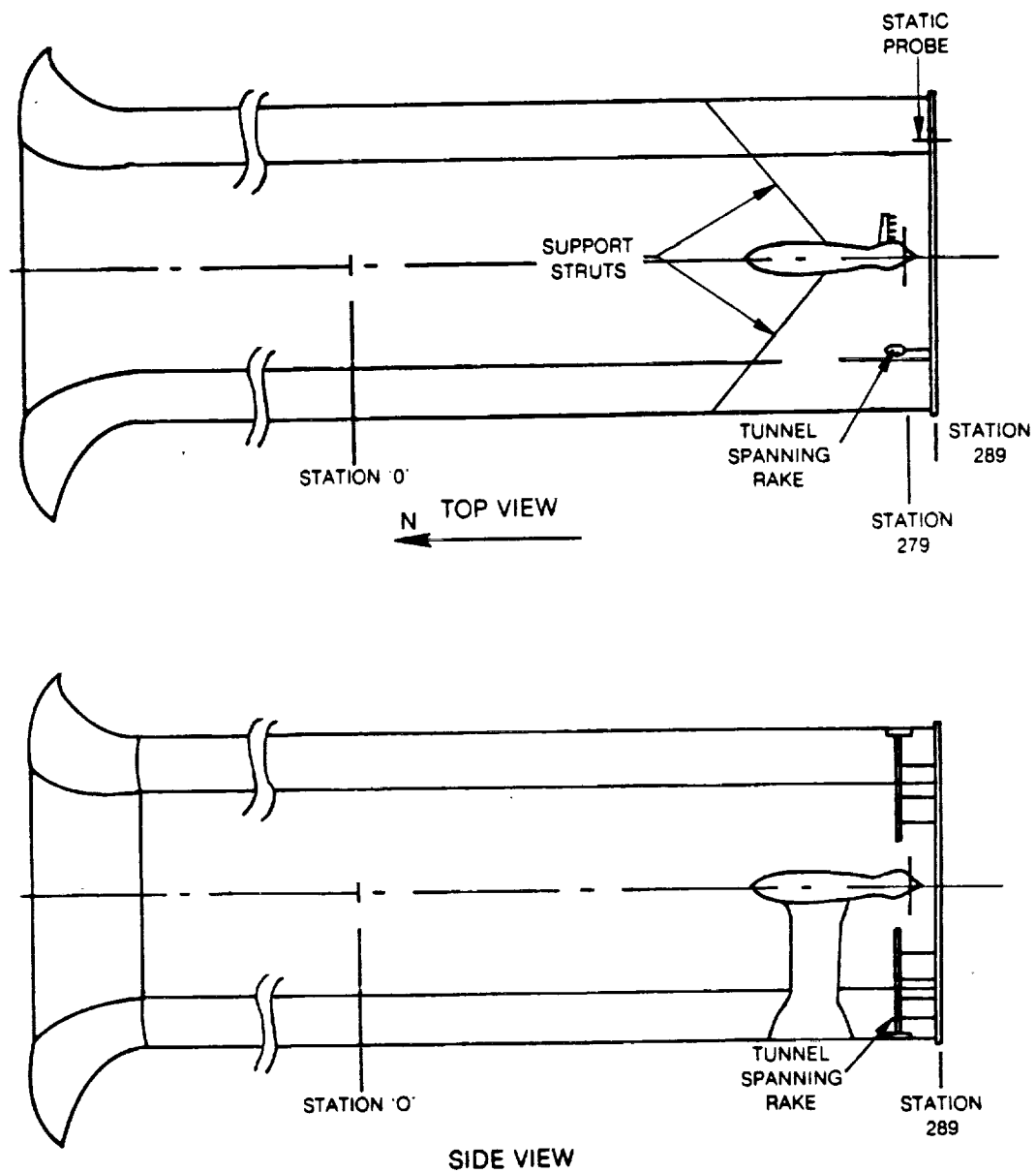


FIGURE 9 PROPELLER DYNAMOMETER INSTALLATION

ORIGINAL PAGE IS
OF POOR QUALITY

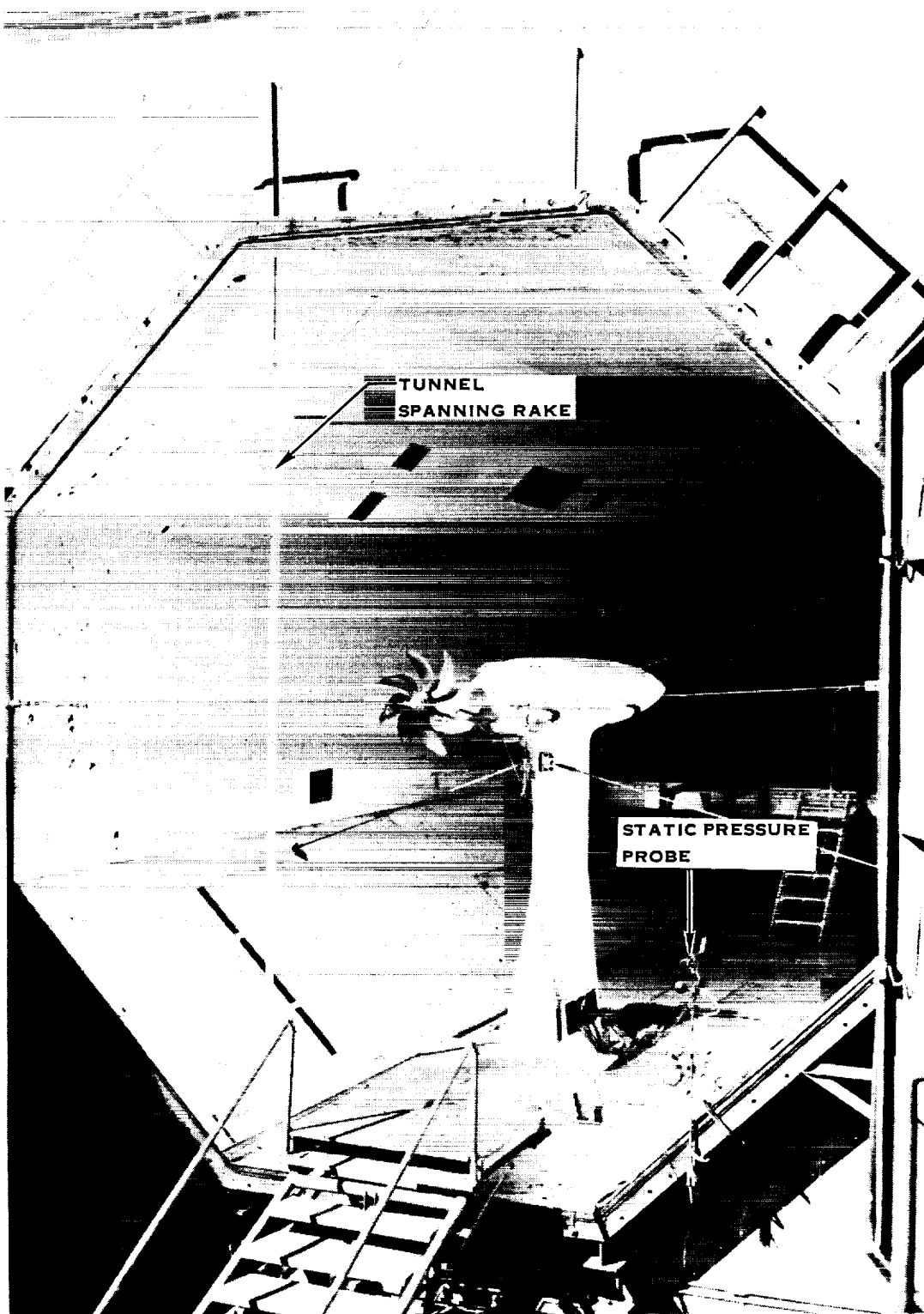


FIGURE 10. PROP - FAN MODEL INSTALLATION LOOKING DOWNSTREAM

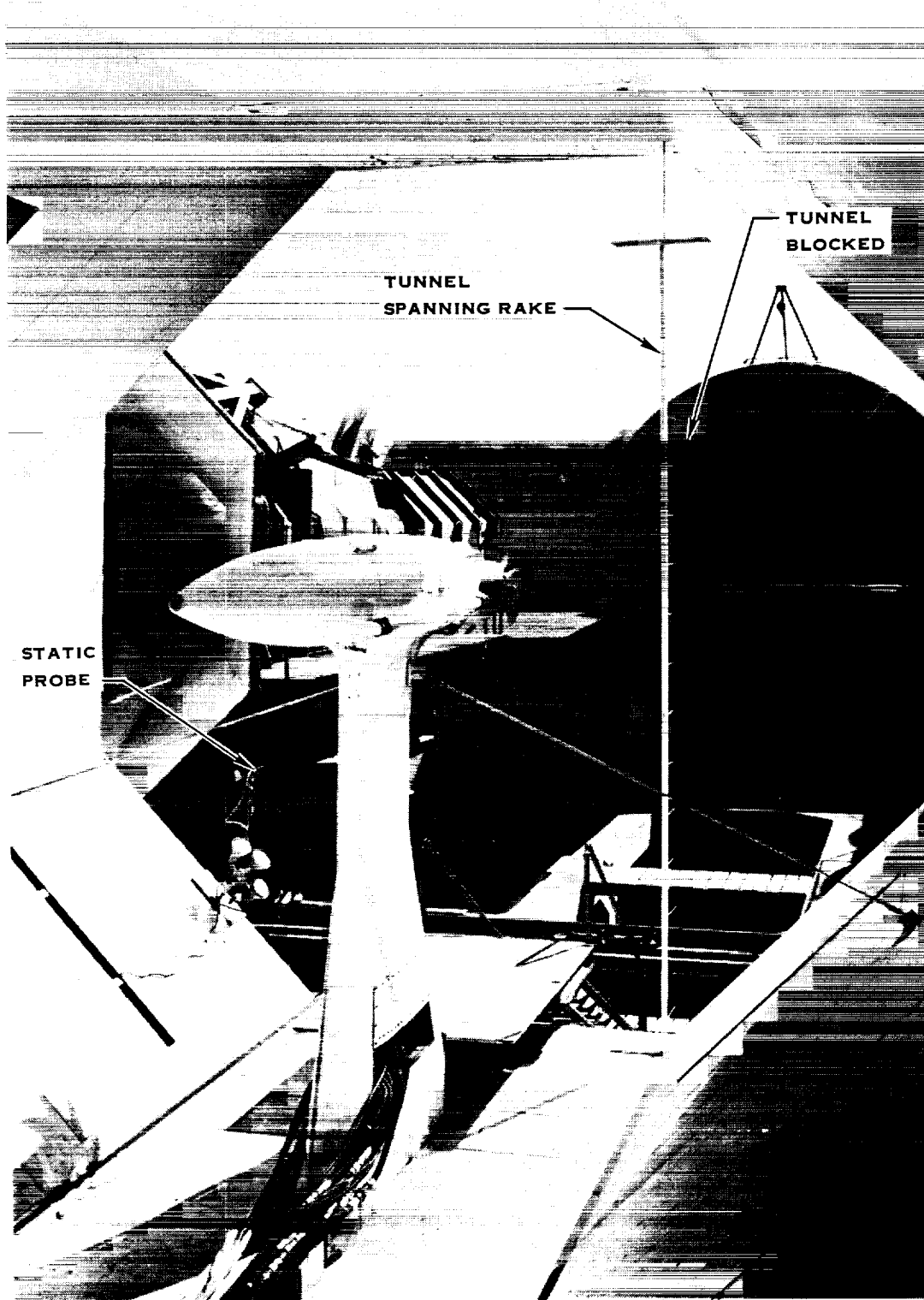


FIGURE 11. PROP - FAN MODEL INSTALLATION LOOKING UPSTREAM

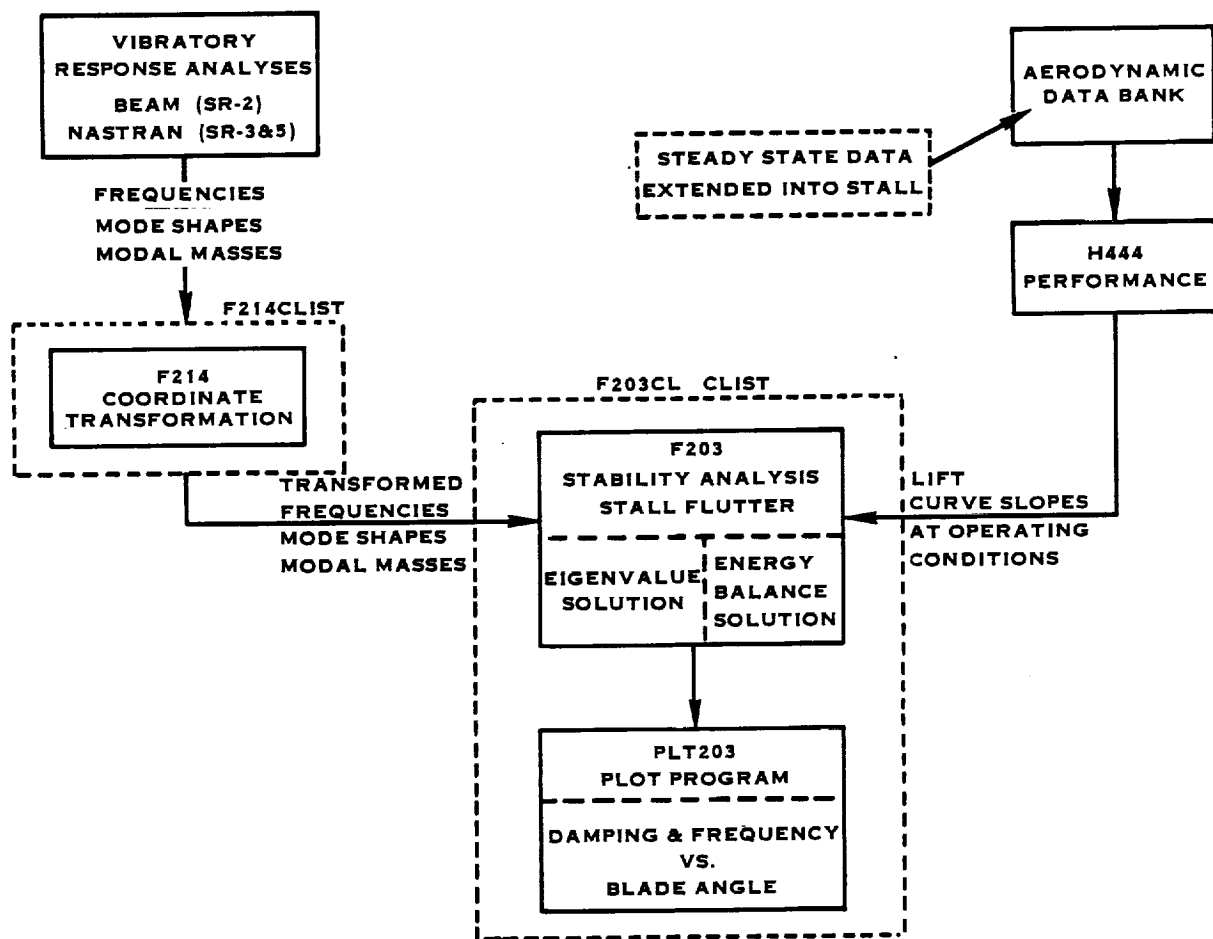
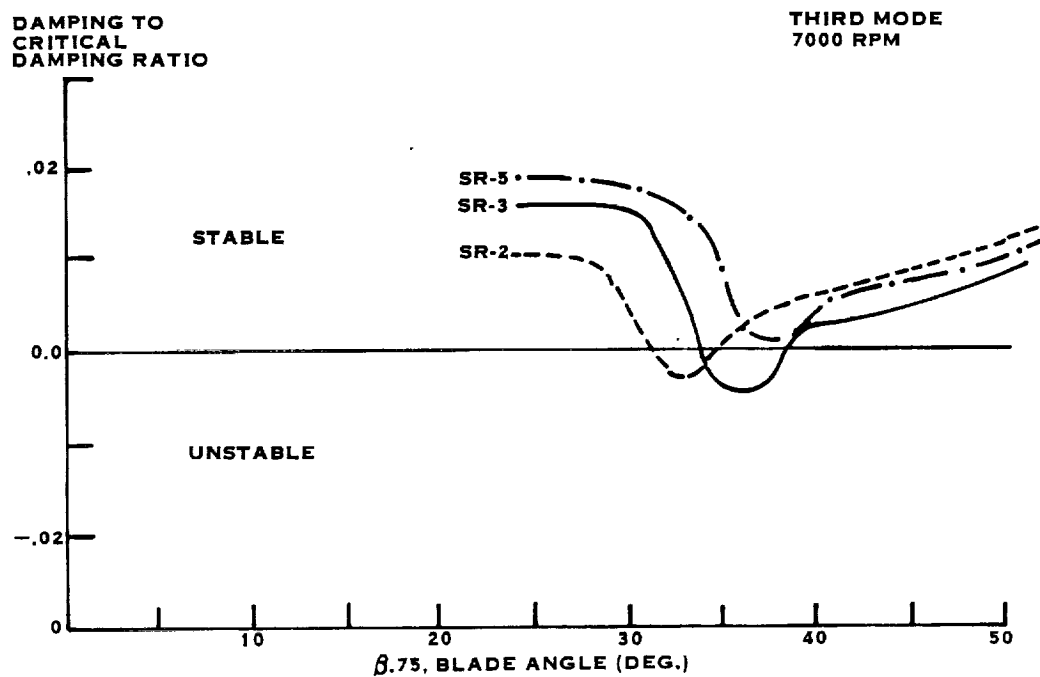


FIGURE 12. BLOCK DIAGRAM FOR STALL FLUTTER ANALYSIS



**FIGURE 13. MODEL PROP-FAN UTRC WIND TUNNEL
STATIC TESTS STABILITY PREDICTIONS**

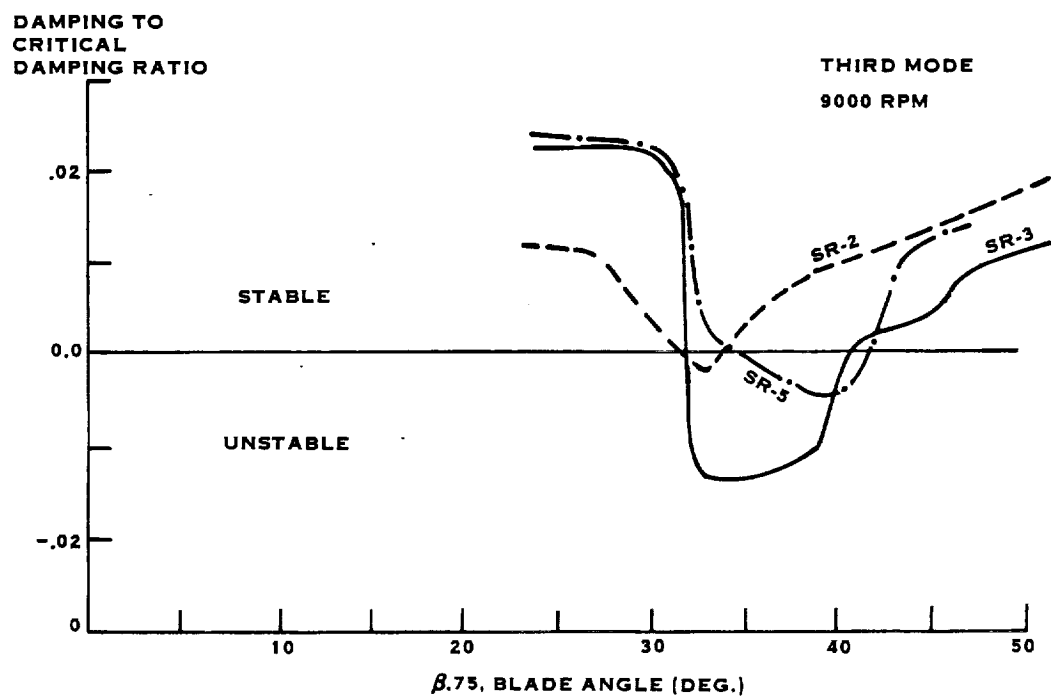


FIGURE 14. MODEL PROP-FAN UTRC WIND TUNNEL
STATIC TESTS STABILITY PREDICTIONS

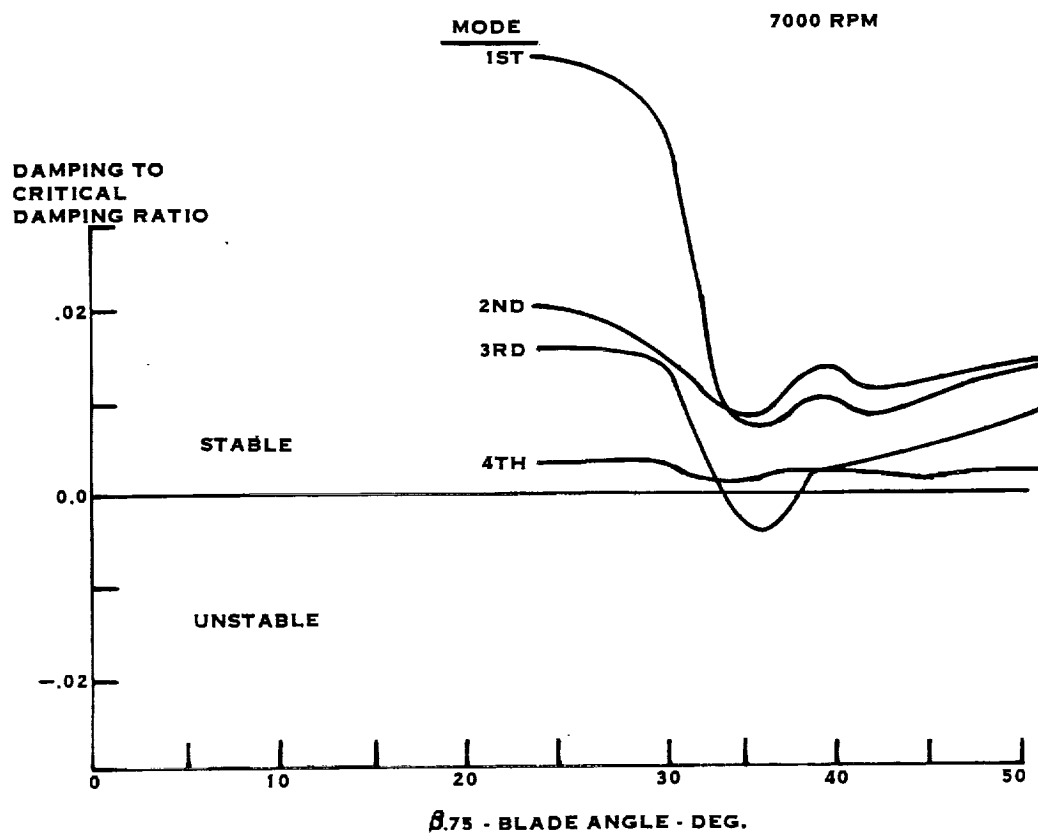


FIGURE 15. SR-3 MODEL PROP-FAN UTRC WIND TUNNEL
STATIC TESTS STABILITY PREDICTIONS

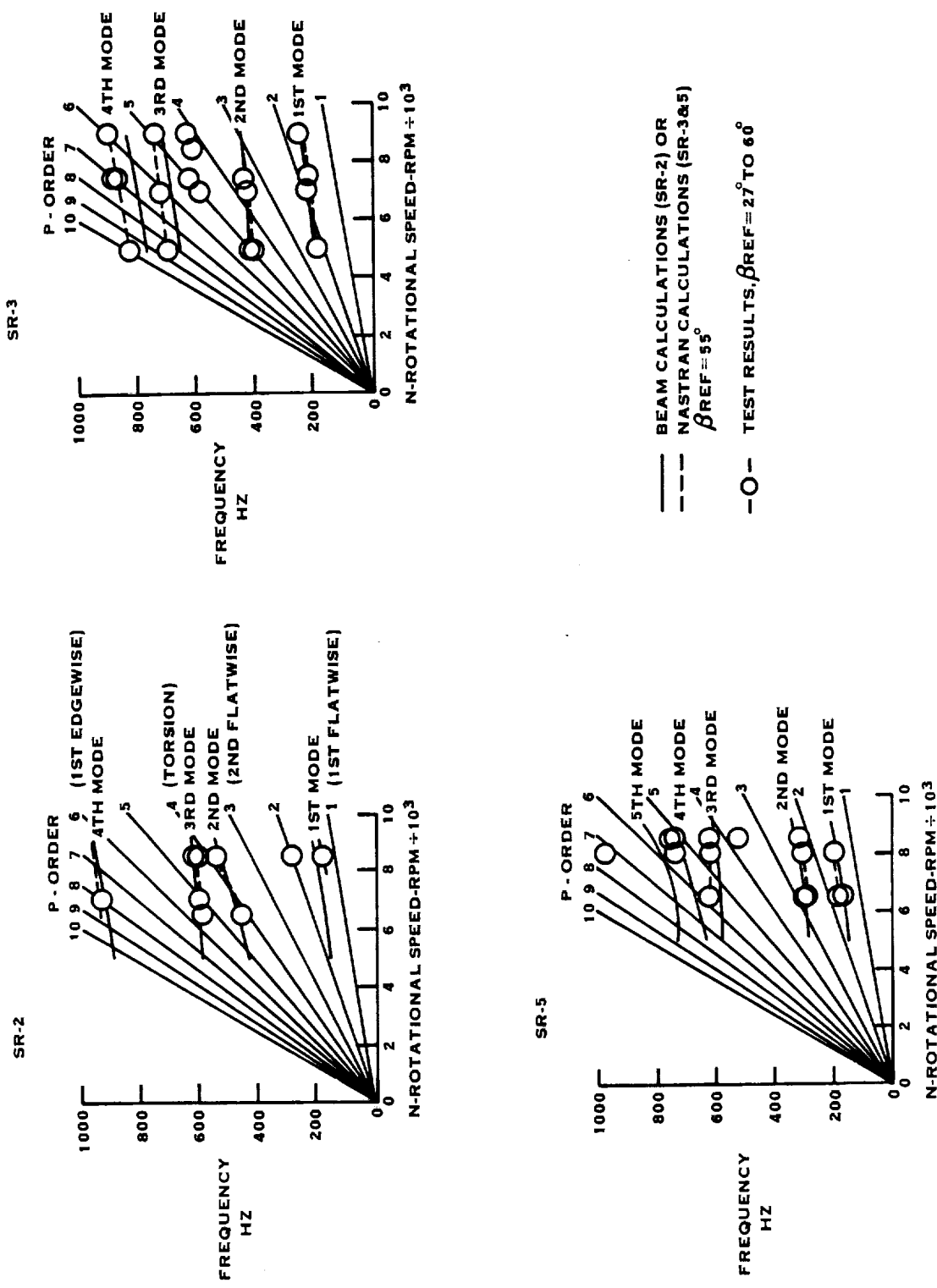
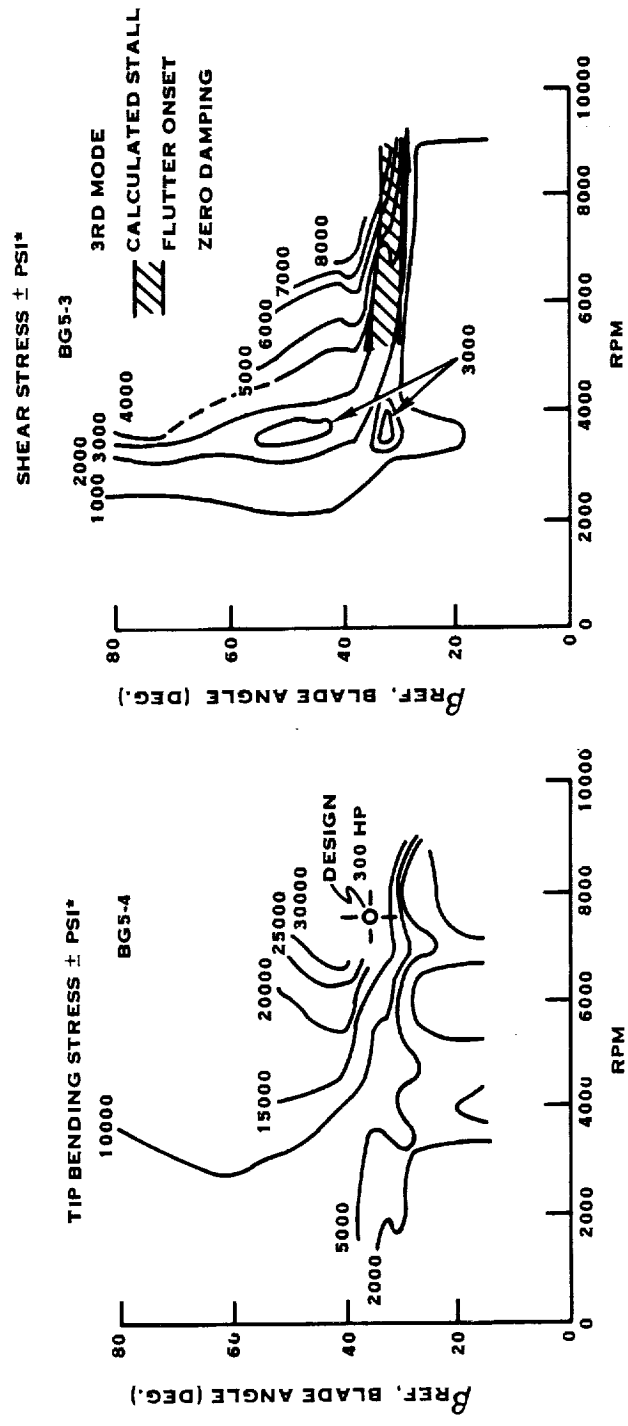
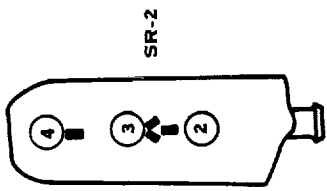


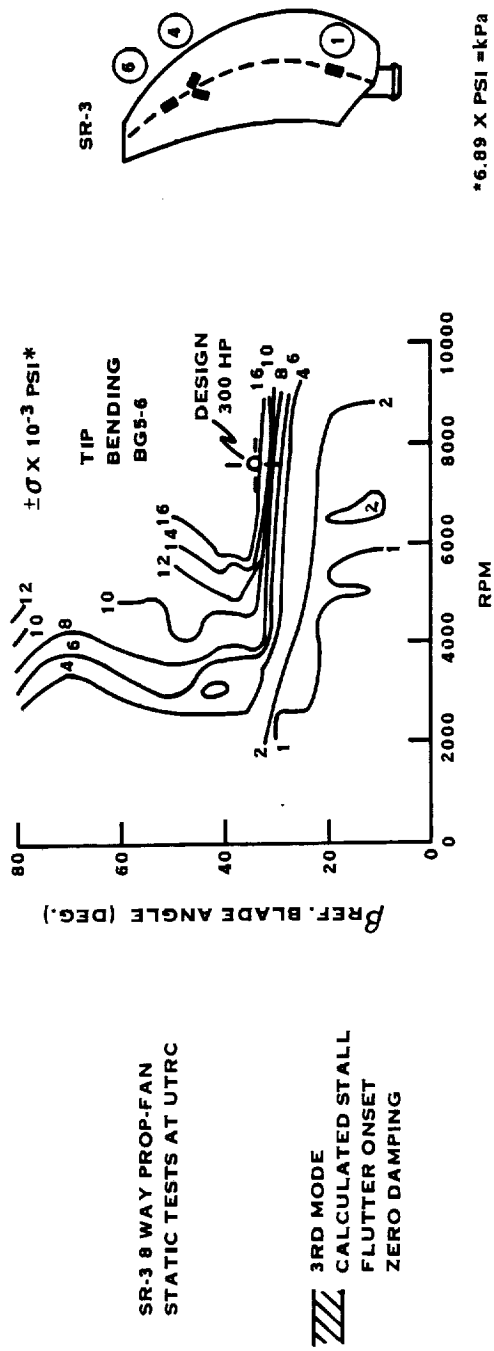
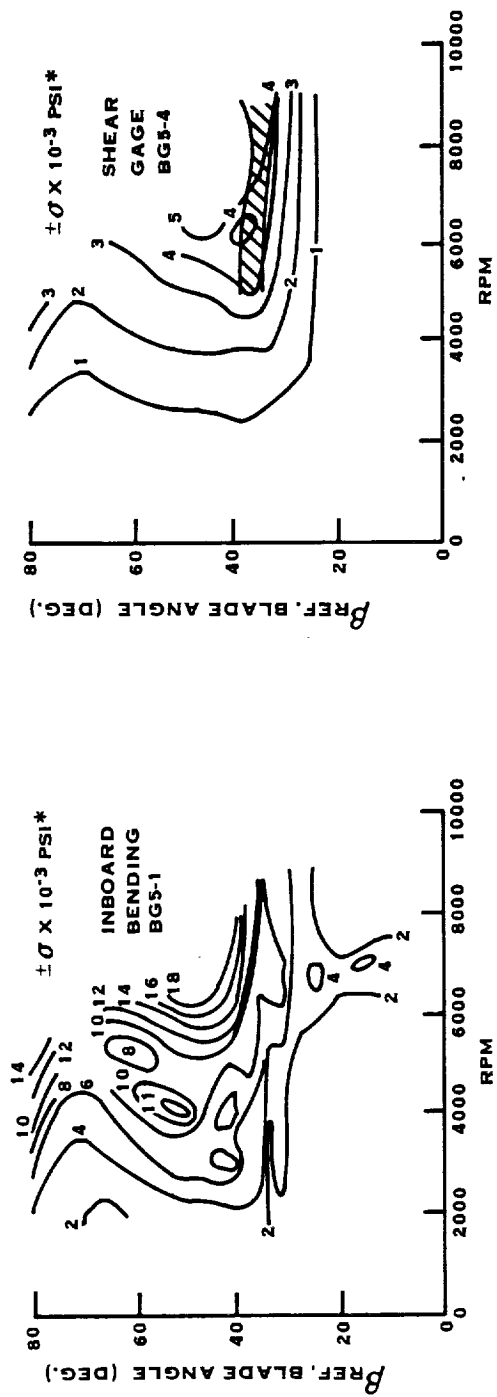
FIGURE 16. MODEL PROP-FAN STALL FLUTTER TESTS AT UTRC CAMPBELL DIAGRAMS

SR-2 8 WAY PROP-FAN
STATIC TESTS AT UTRC



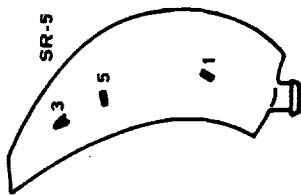
*6.89 X PSI = kPa

FIGURE 17. TOTAL VIBRATORY STRESS CONTOURS



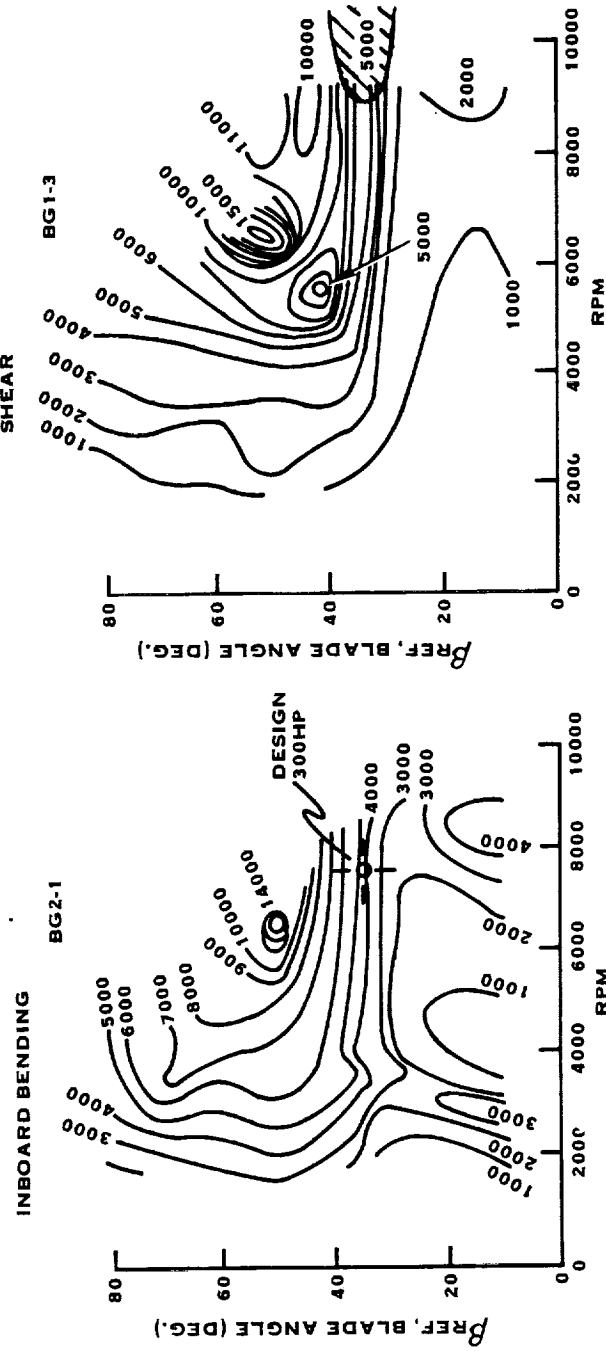
*6.89 X PSI = kPa

FIGURE 18. TOTAL VIBRATORY STRESS CONTOURS



SR-5 10 WAY PROP-FAN
STATIC TESTS AT UTRC
(\pm PSI)*

3RD MODE
CALCULATED STALL
FLUTTER ONSET
ZERO DAMPING



*6.89 X PSI = kPa

FIGURE 19. TOTAL VIBRATORY STRESS CONTOURS

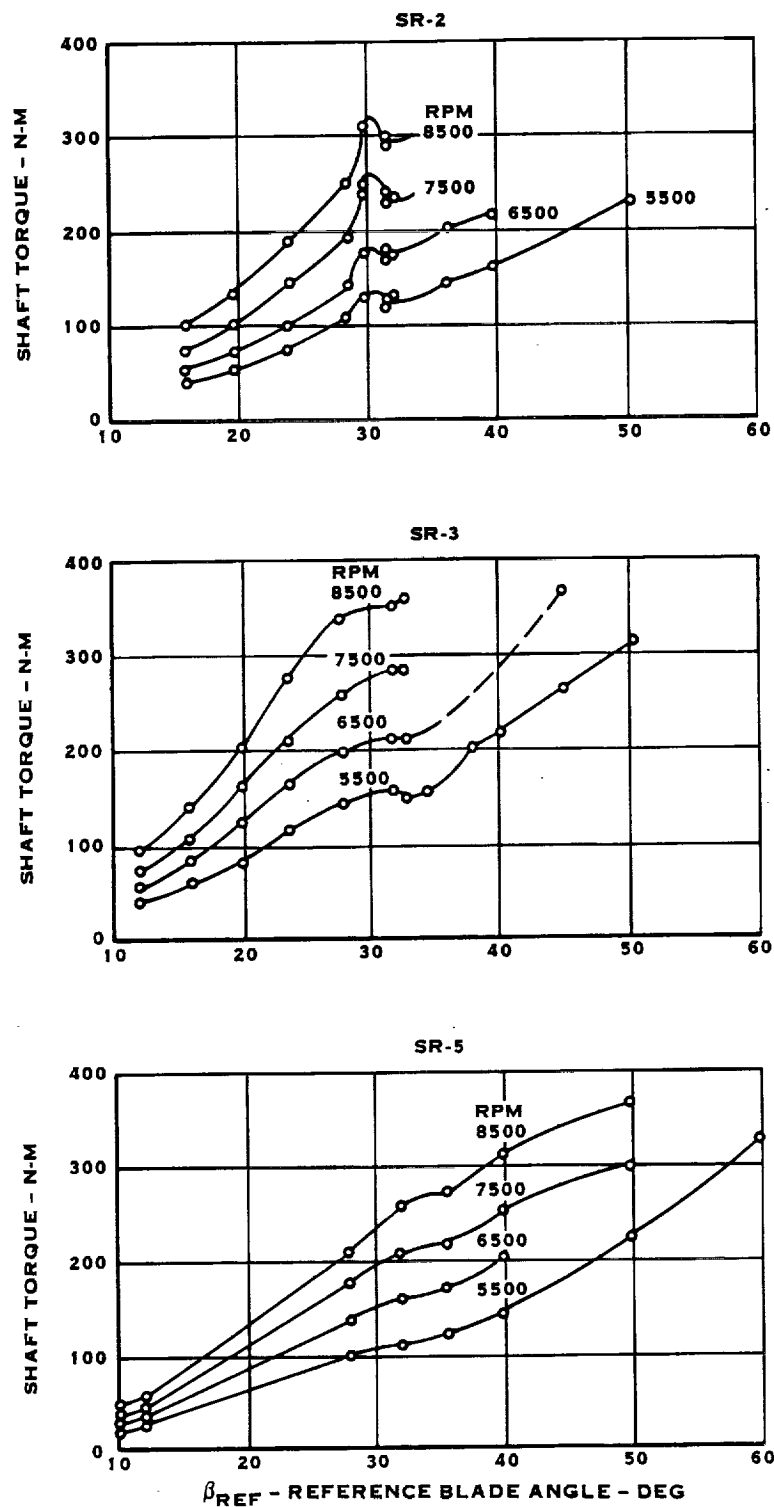


FIGURE 20. TORQUE VS. REFERENCE BLADE ANGLE FOR THE UTRC PROP-FAN STATIC TESTS, SR-2, SR-3 AND SR-5 MODELS

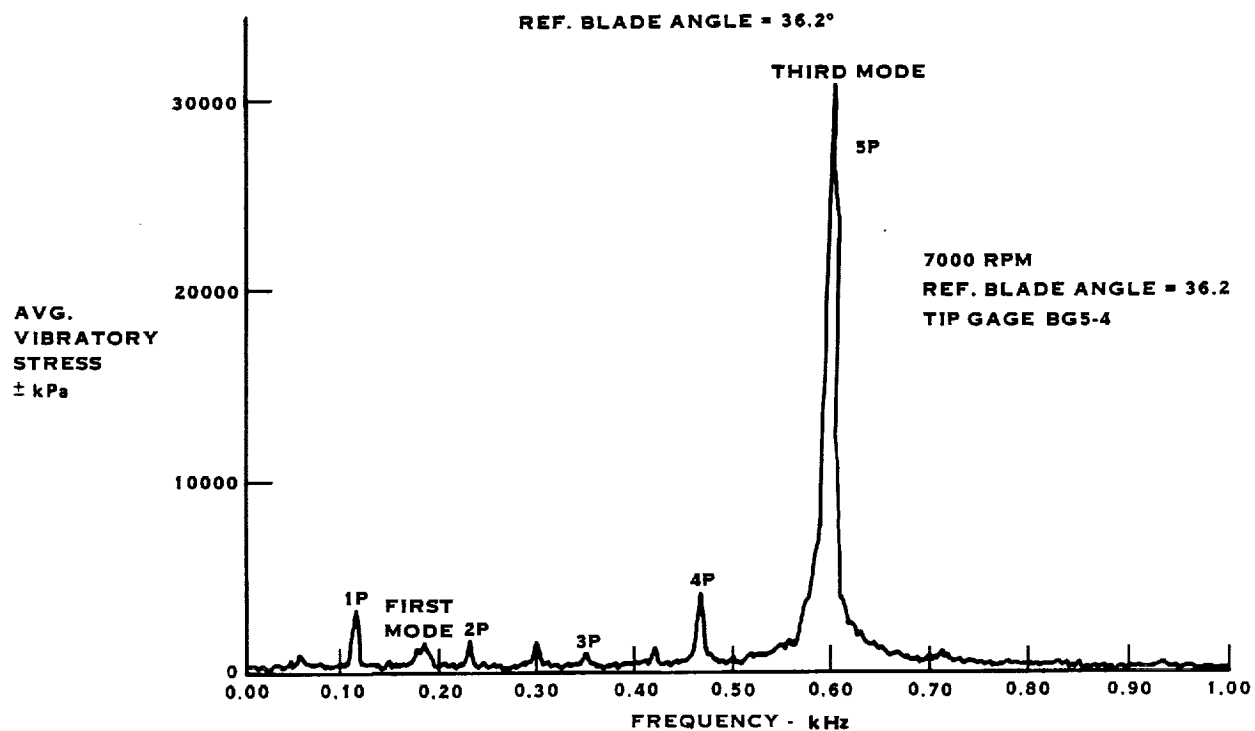


FIGURE 21. SR-2 PROP-FAN MODEL BLADE STALL FLUTTER TESTS AT UTRC

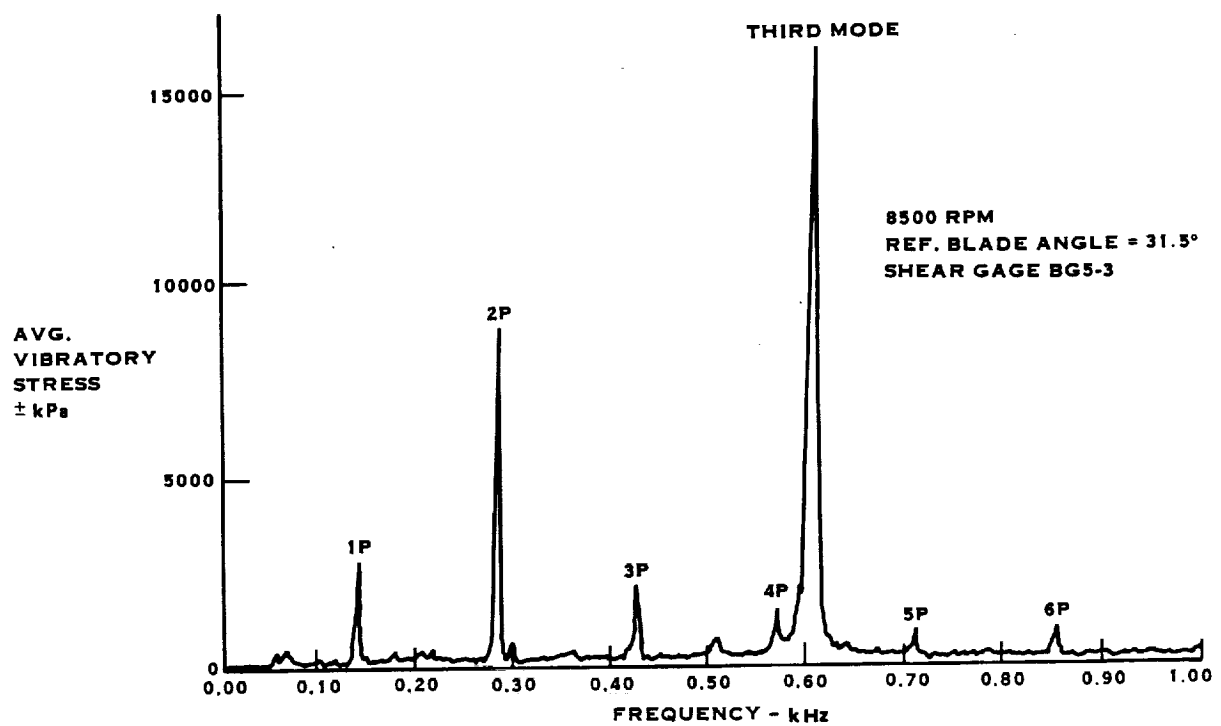


FIGURE 22. SR-2 PROP-FAN MODEL BLADE STALL FLUTTER TESTS AT UTRC

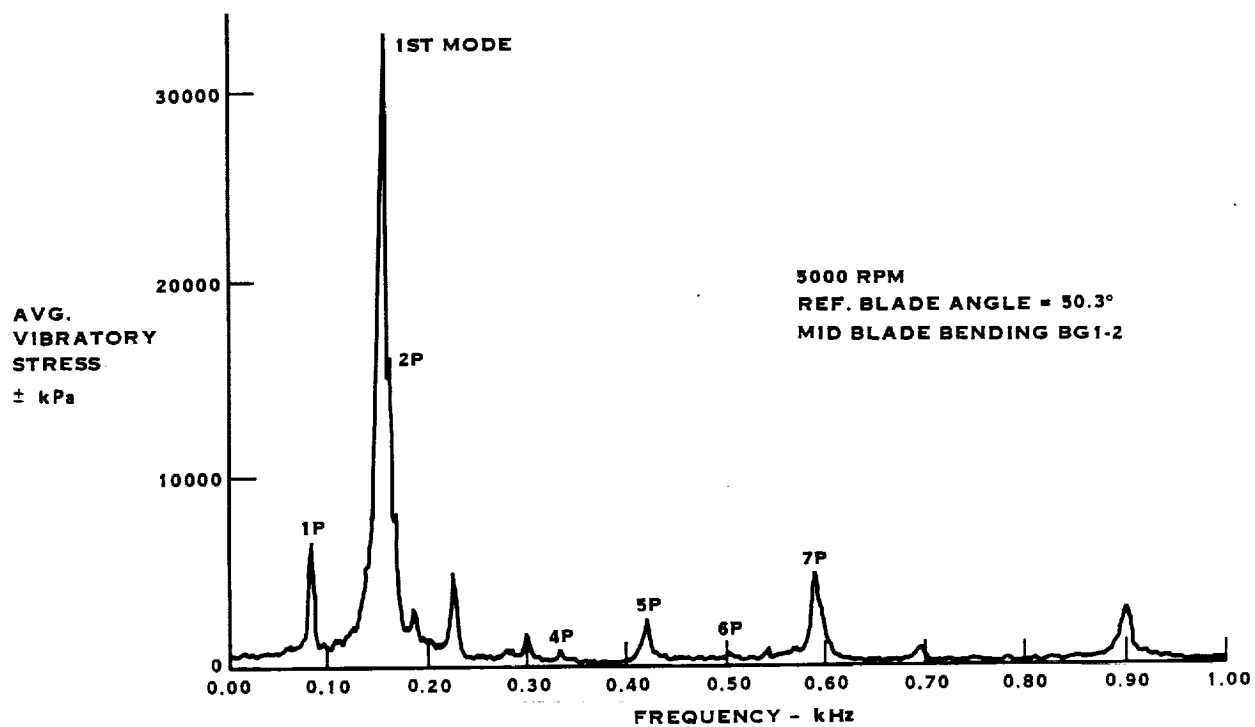


FIGURE 23. SR-2 PROP-FAN MODEL BLADE STALL FLUTTER TESTS AT UTRC

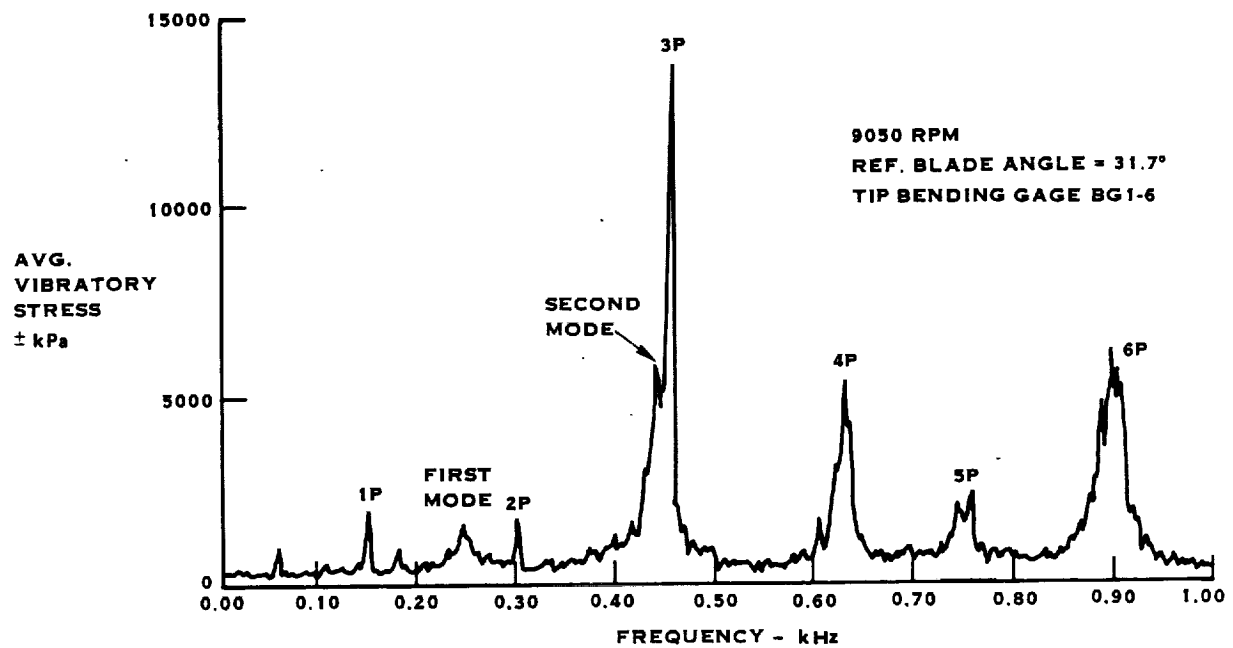


FIGURE 24. SR-3 PROP-FAN MODEL BLADE STALL FLUTTER TESTS AT UTRC

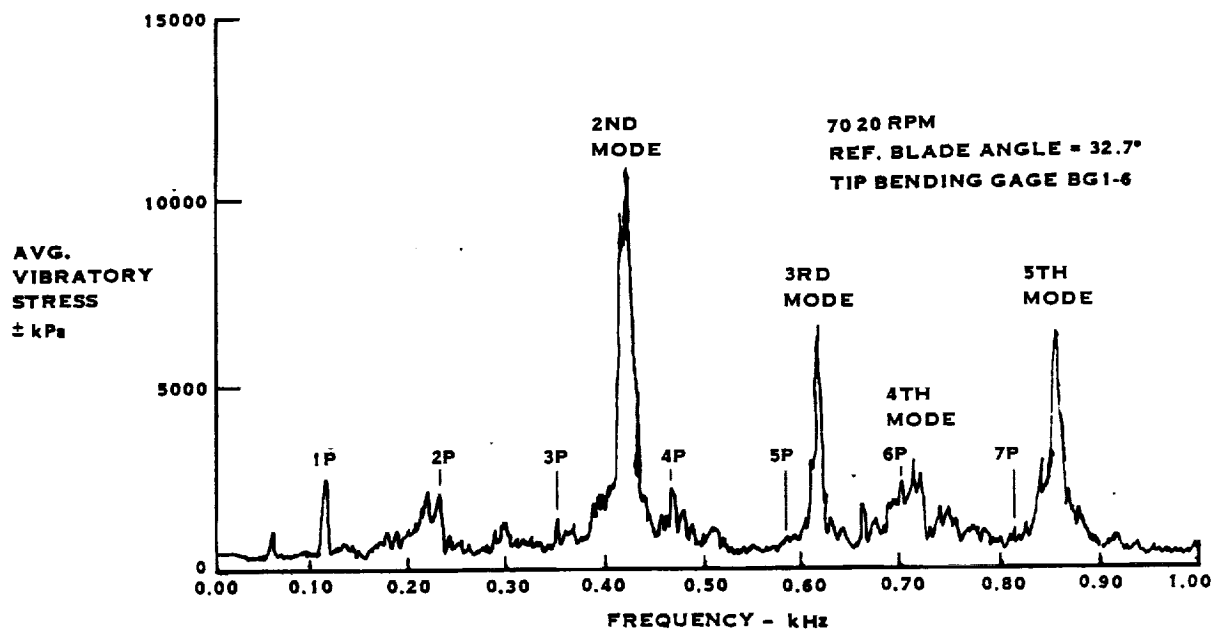


FIGURE 25. SR-3 PROP-FAN MODEL BLADE STALL FLUTTER TESTS AT UTRC

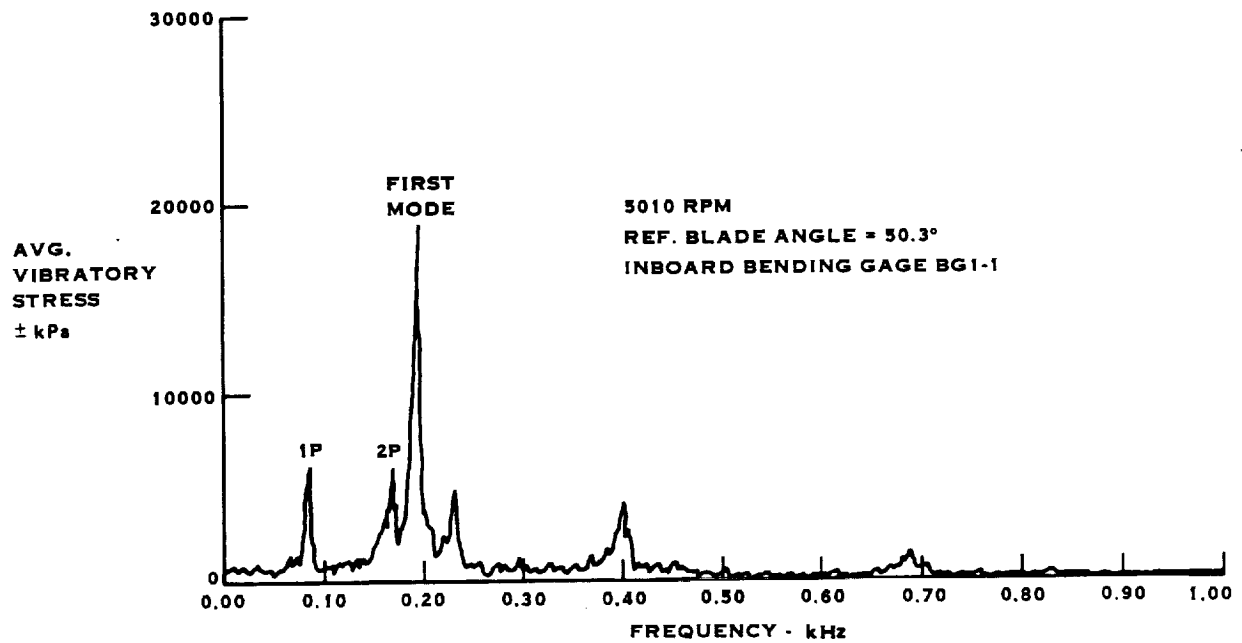


FIGURE 26. SR-3 PROP-FAN MODEL BLADE STALL FLUTTER TESTS AT UTRC

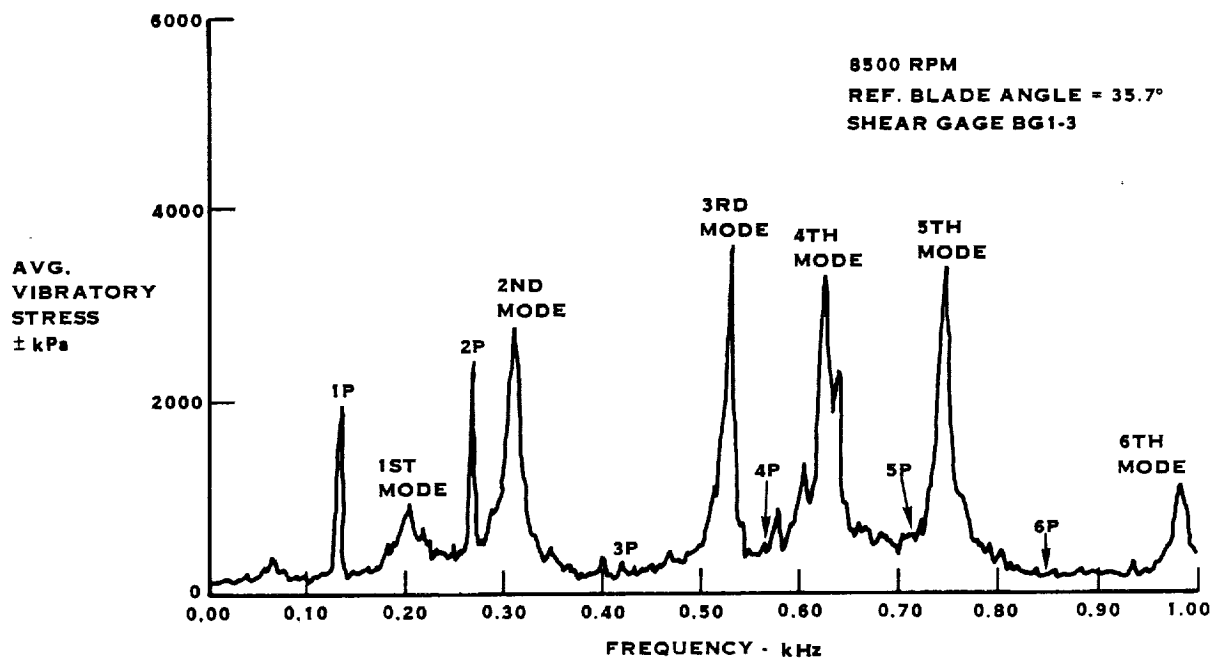


FIGURE 27. SR-5 PROP-FAN MODEL BLADE STALL FLUTTER TESTS AT UTRC

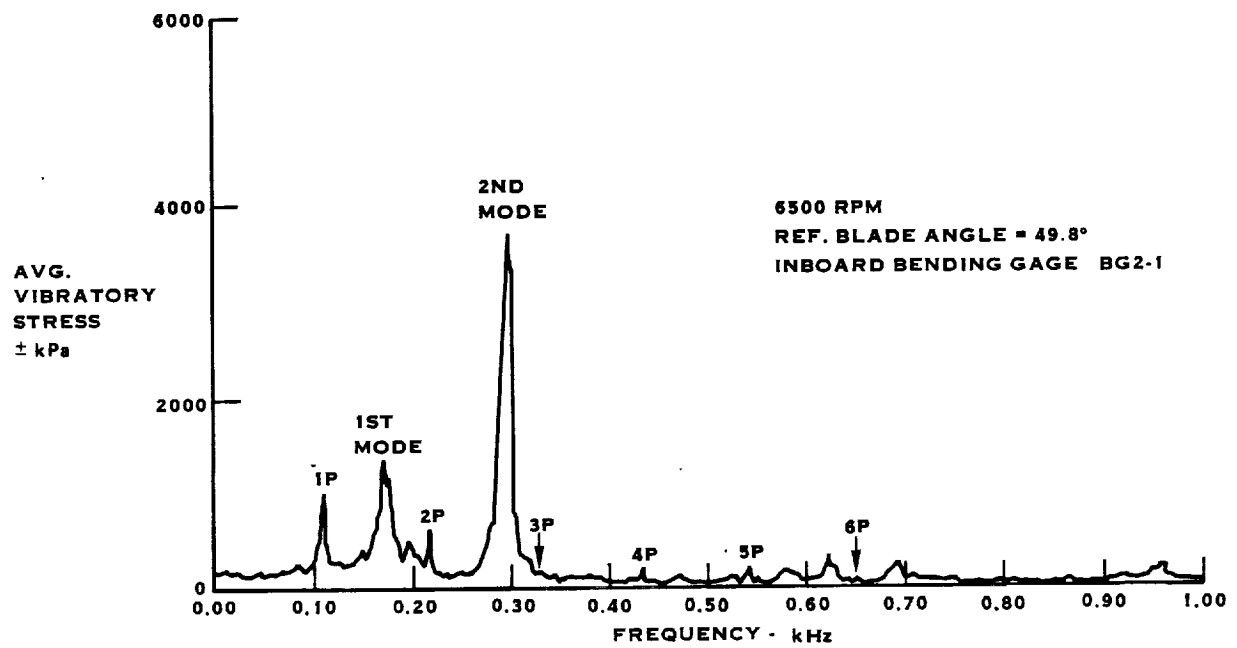
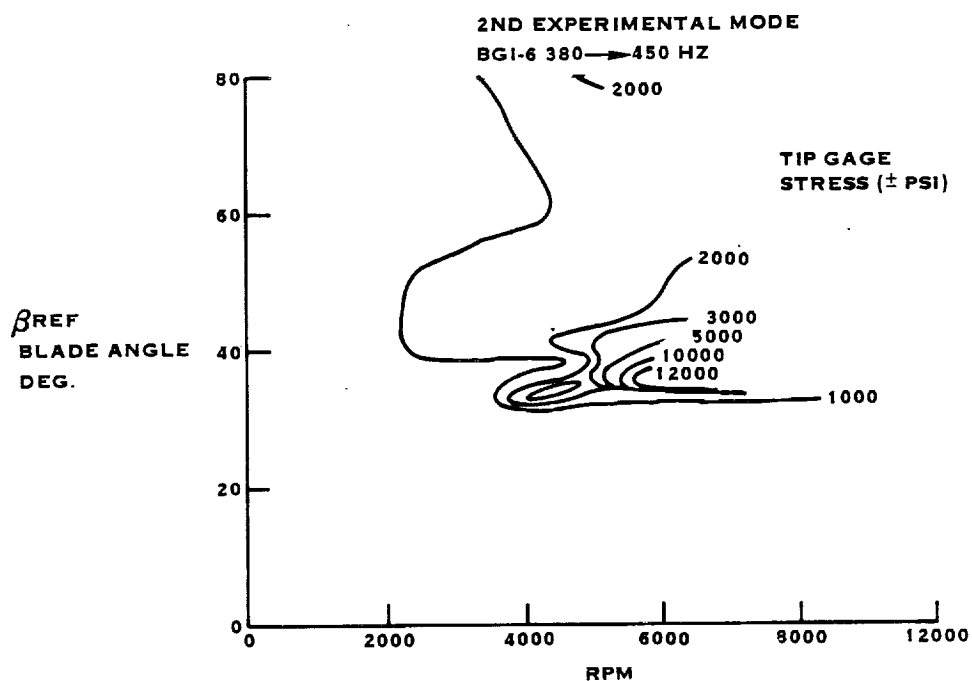
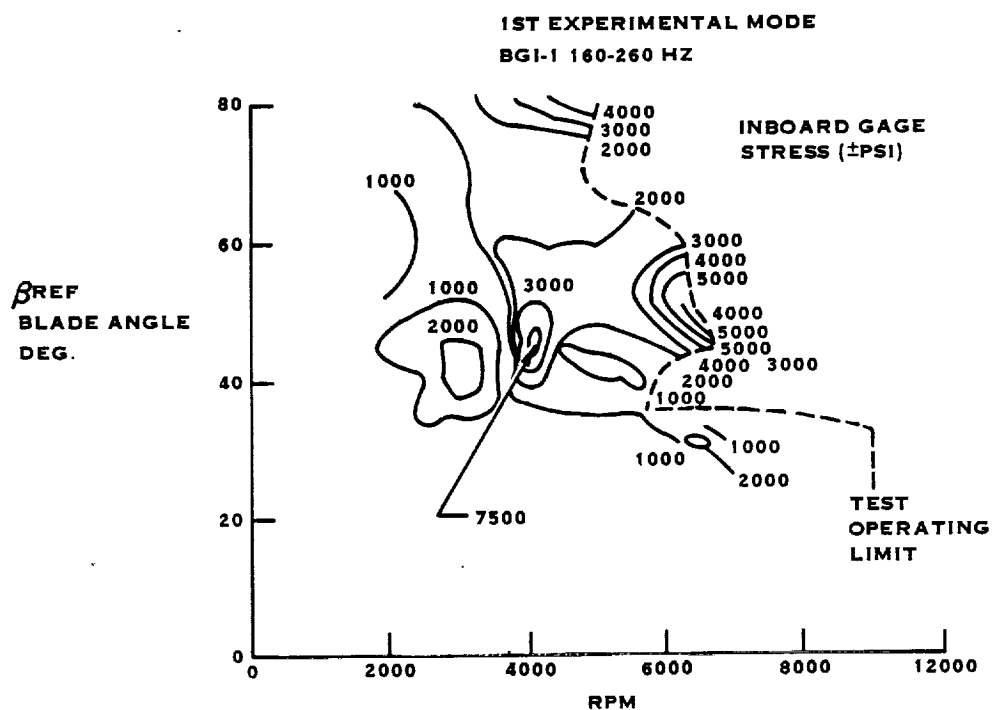


FIGURE 28. SR-5 PROP-FAN MODEL BLADE STALL FLUTTER TESTS AT UTRC



**FIG. 29 MODAL VIBRATORY STRESS (\pm PSI)*
CONTOURS FROM THE SR-3 MODEL
BLADE STALL FLUTTER TESTS AT UTRC
*(6.89 X PSI = kPa)**

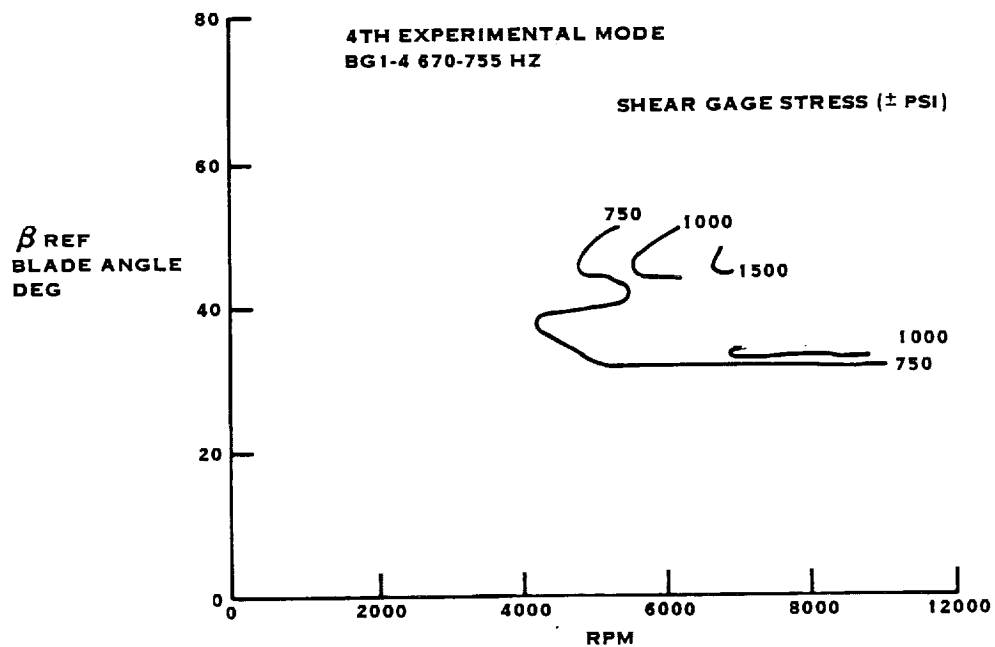
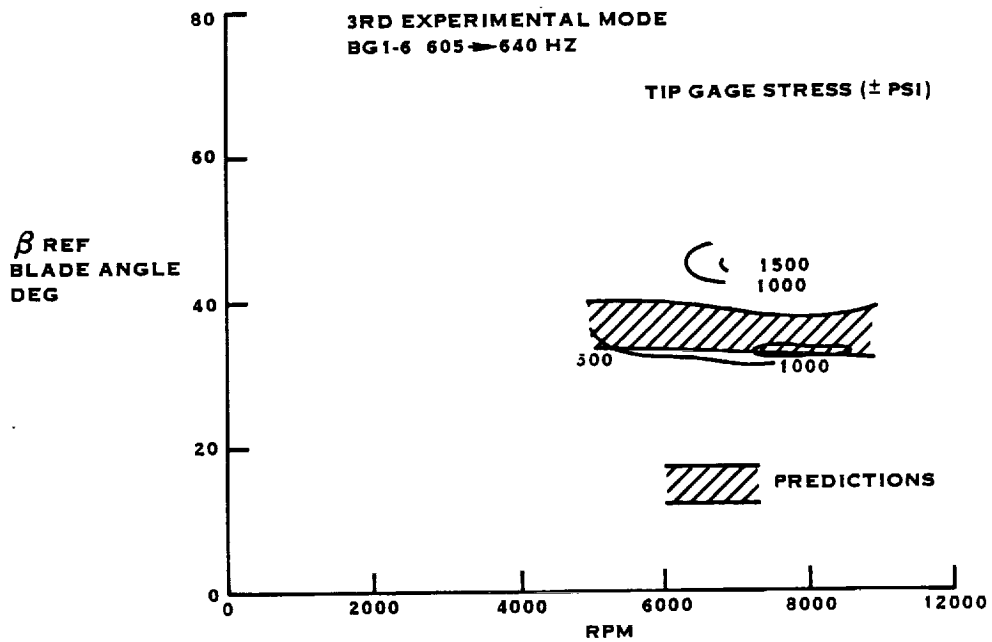


FIGURE 29. (CONT'D)

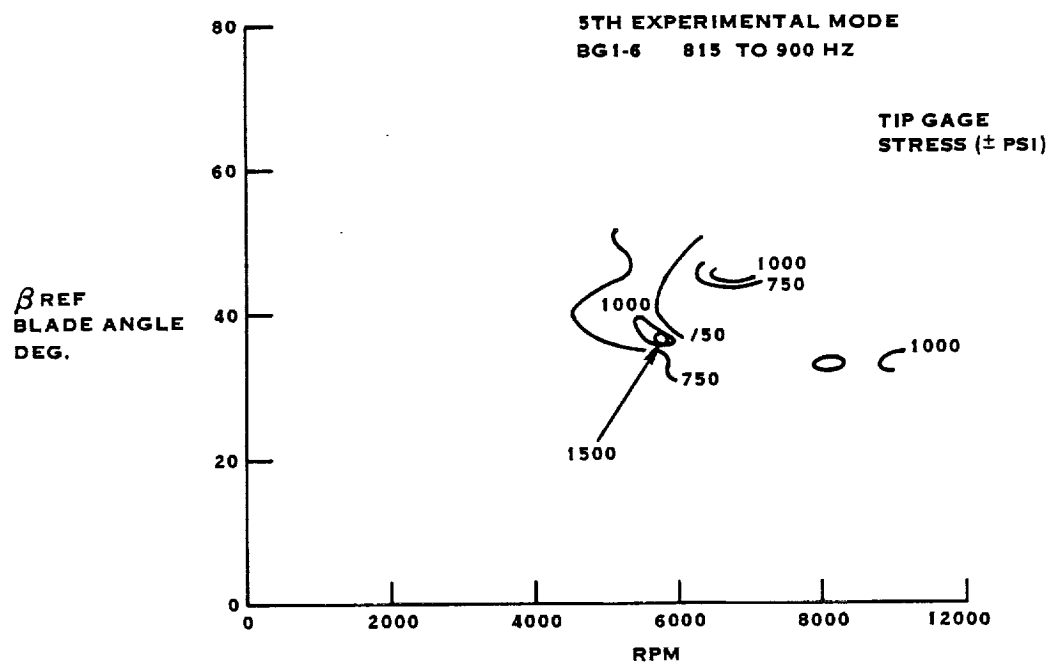


FIGURE 29. (CONT'D)

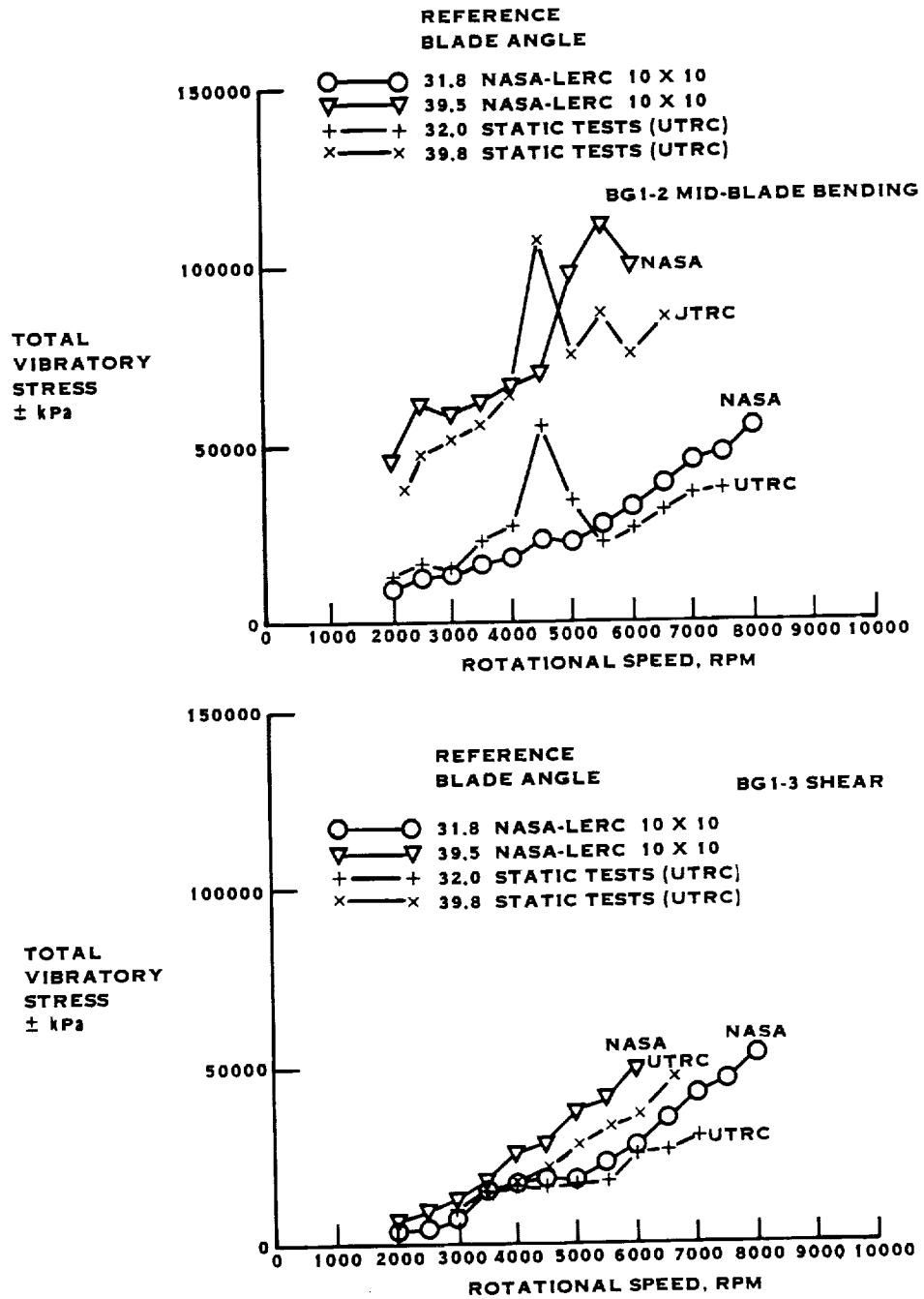


FIGURE 30. SR-2 MODEL PROP-FAN COMPARISON OF TESTS MACH NO. = 0.0 NO TILT

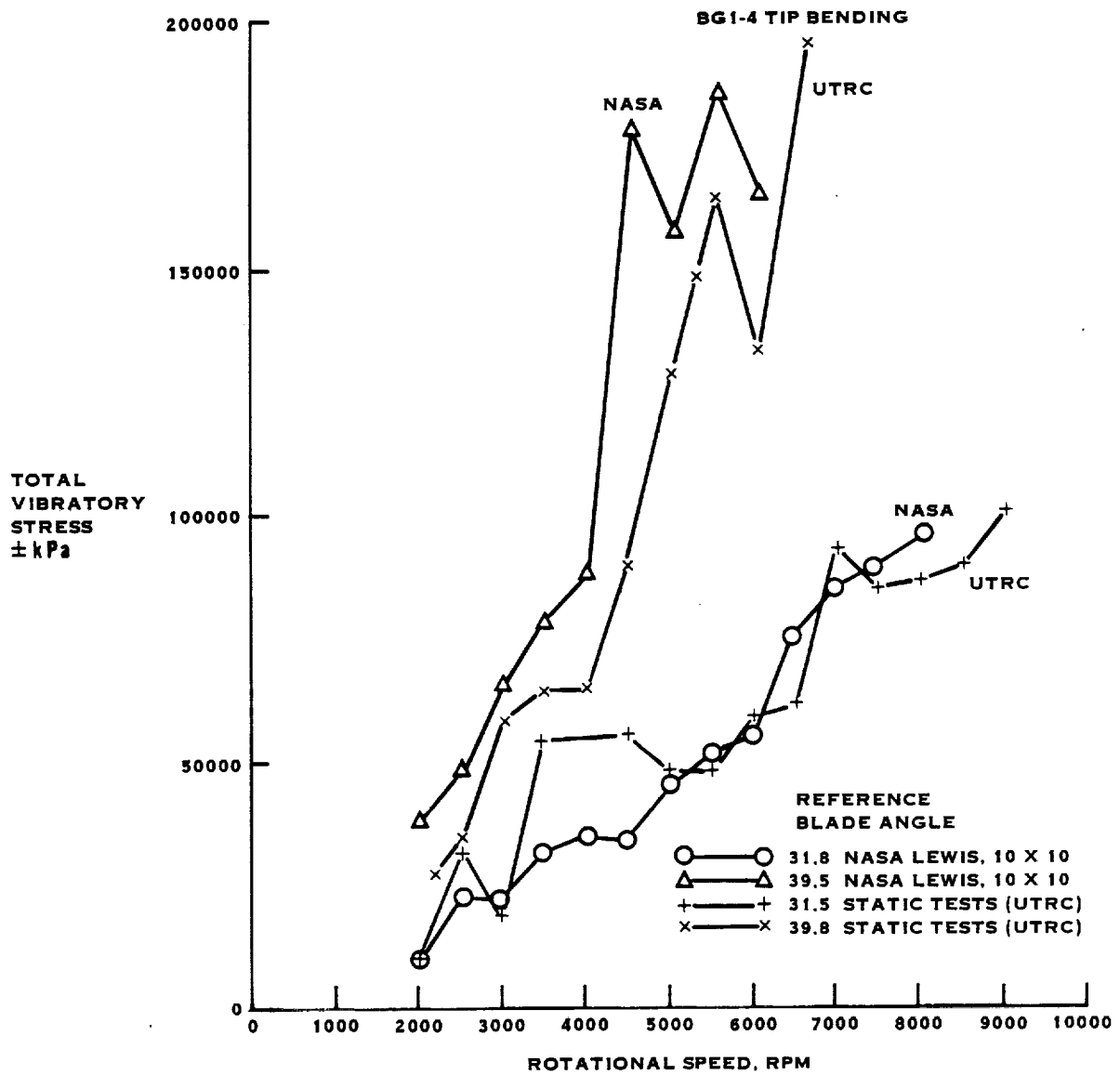


FIGURE 30. (CONT'D). SR-2 MODEL PROP-FAN COMPARISON OF TESTS
MACH NO. = 0.0 NO TILT

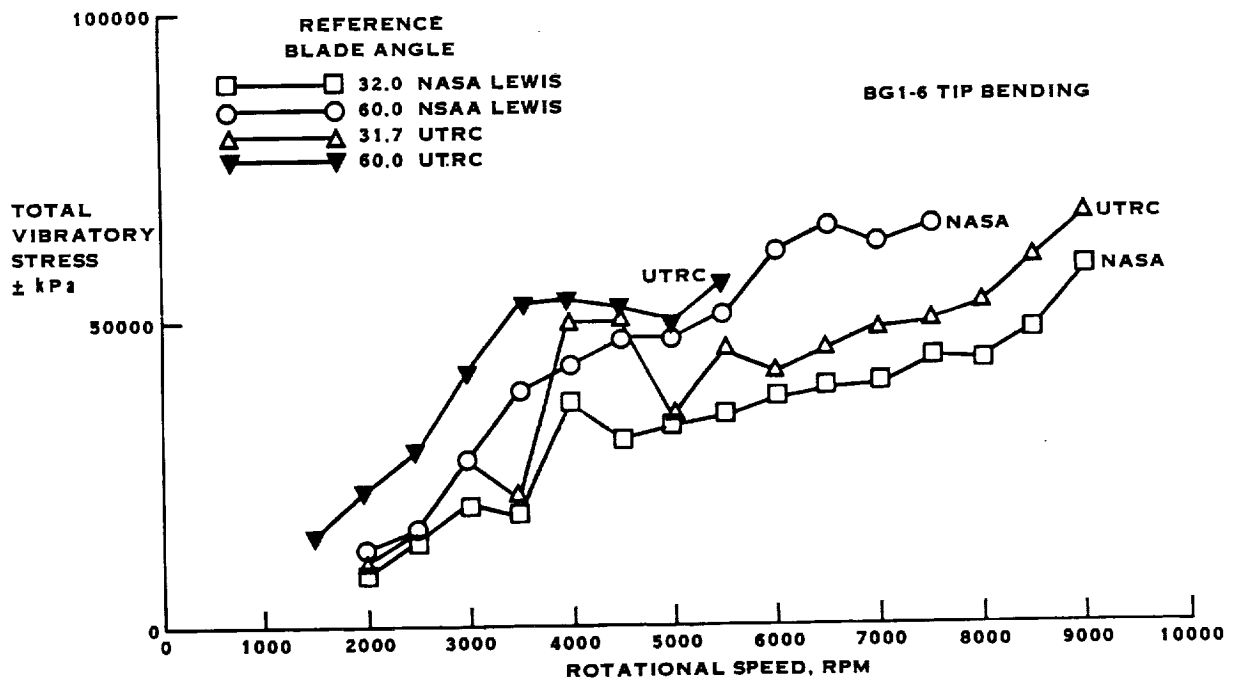
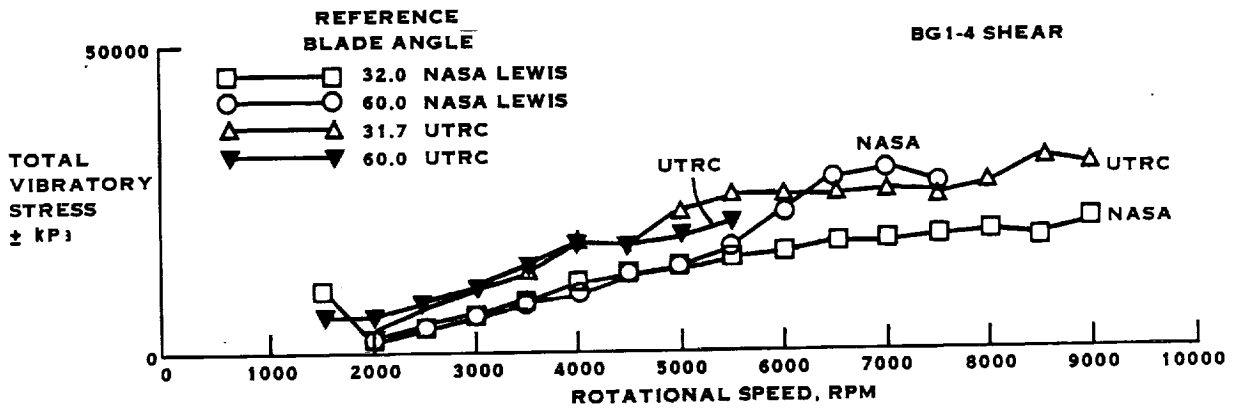


FIGURE 31. SR-3 MODEL PROP-FAN COMPARISON OF TESTS MACH NO. = 0.0 NO TILT

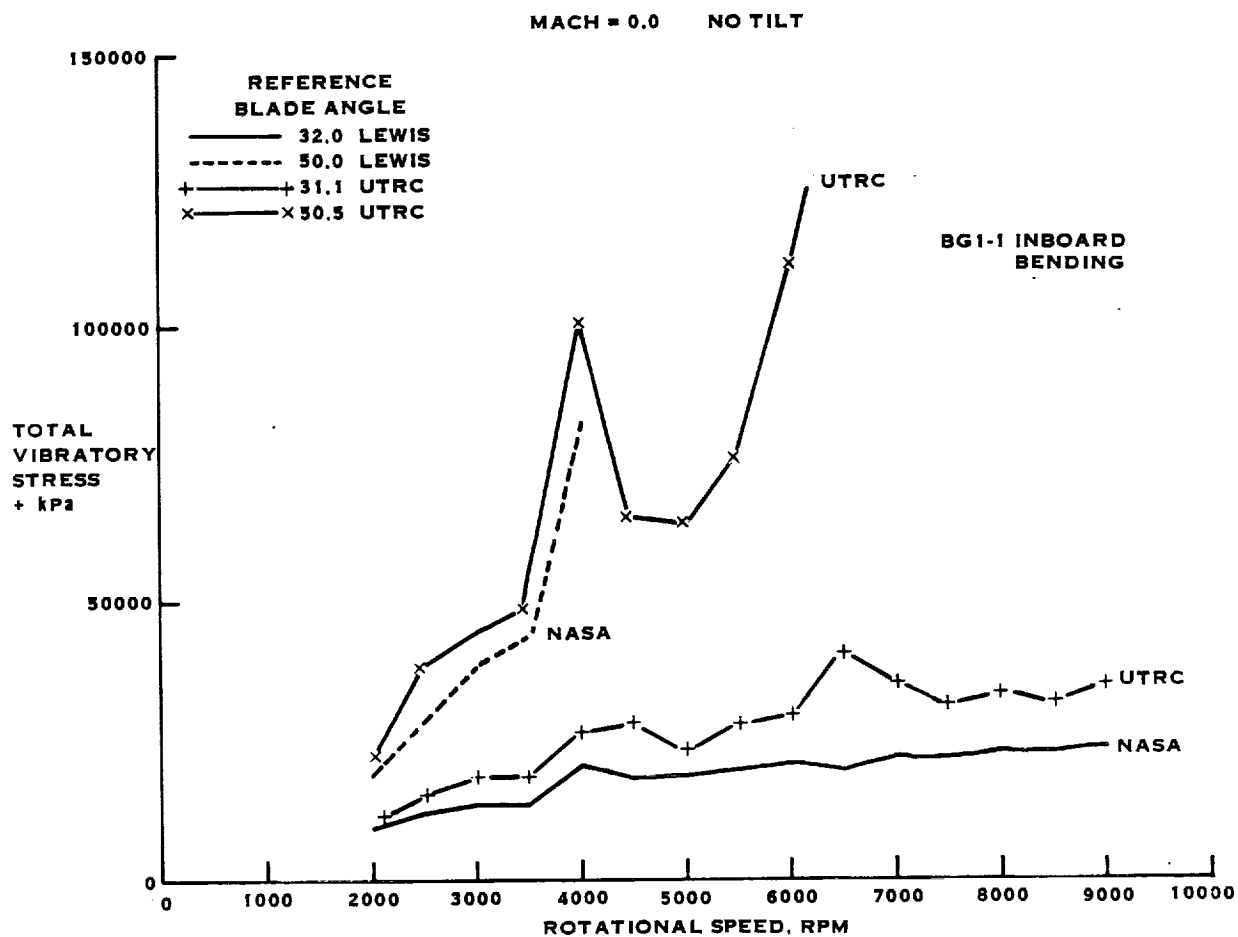


FIGURE 31. CONT'D. SR-3 MODEL PROP-FAN COMPARISON OF TESTS MACH NO. = 0.0
NO TILT

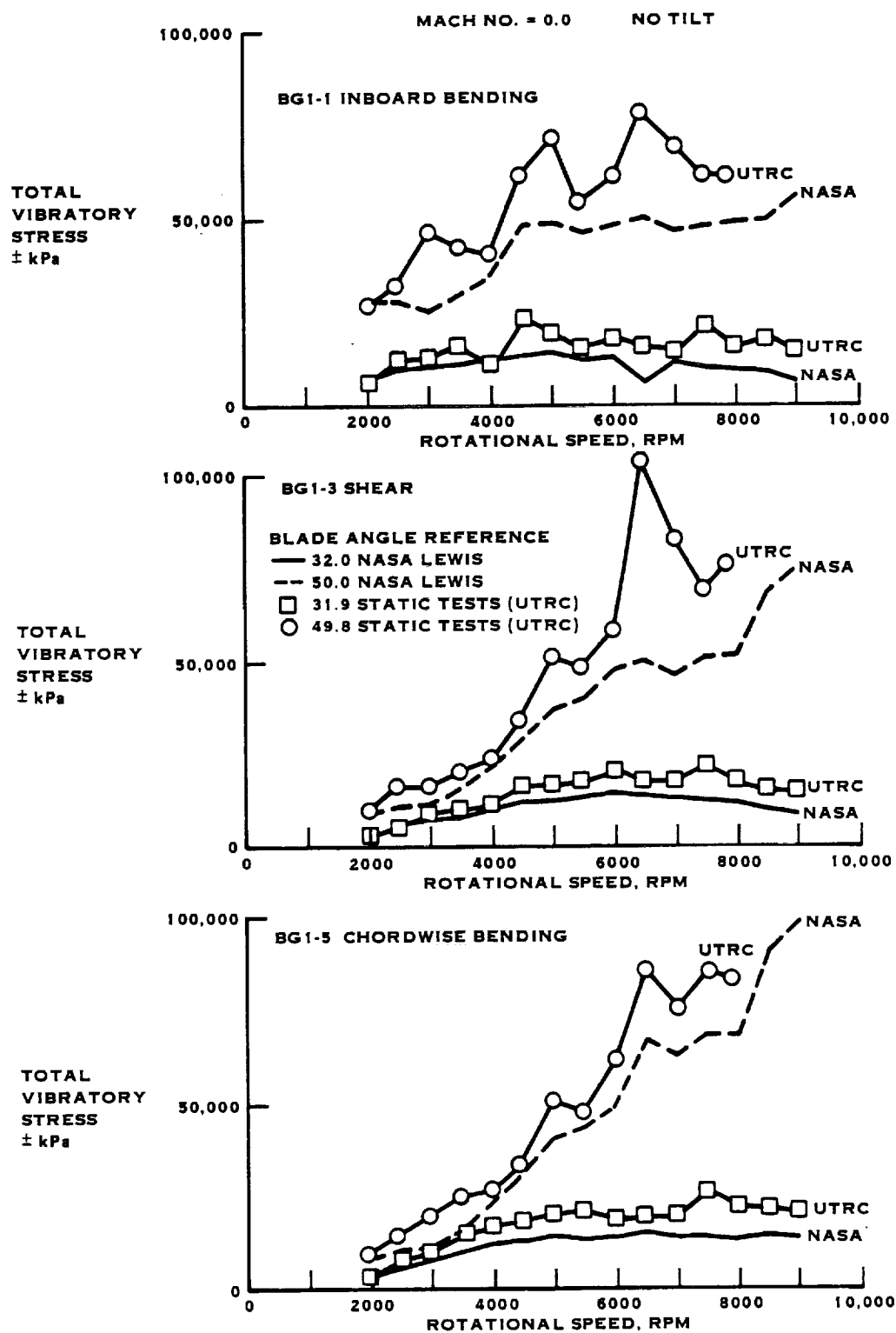


FIGURE 32. SR-5 MODEL PROP-FAN COMPARISON OF TESTS

APPENDIX A

TOTAL VIBRATORY STRESS* PLOTTED AS A FUNCTION
OF RPM FOR VARIOUS BLADE ANGLES AS OBSERVED IN
THE UTRC STATIC STALL FLUTTER TESTS ON THE SR-2,
SR-3 AND SR-5 MODEL BLADES

*Infrequently repeating peak stress as taken from brush charts.

APPENDIX A
TABLE OF CONTENTS

<u>FIG NO</u>	<u>PROP-FAN MODEL</u>	<u>BLADE ANGLE, DEG</u>	<u>STRESS TYPE</u>
A-1	SR-2	15.8, 19.6	SHEAR
A-2	SR-2	23.8, 27.4	SHEAR
A-3	SR-2	29.7, 32	SHEAR
A-4	SR-2	31.5, 36.2	SHEAR
A-5	SR-2	39.8, 50.3	SHEAR
A-6	SR-2	60.3, 69.9	SHEAR
A-7	SR-2	79.6	SHEAR
A-8	SR-2	15.8 through 32	TIP-BENDING
A-9	SR-2	36.2 through 79.6	TIP-BENDING
A-10	SR-3	10.0 through 32.7	TIP-BENDING
A-11	SR-3	34.0 through 44.9	TIP-BENDING
A-12	SR-3	50.3 through 80.0	TIP-BENDING
A-13	SR-3	10.0 through 32.7	TORSION
A-14	SR-3	34.0 through 80.0	TORSION
A-15	SR-5	10.0, 12.0	INBD. BENDING TIP BENDING SHEAR
A-16	SR-5	28.0, 39.1	INBD. BENDING TIP BENDING SHEAR
A-17	SR-5	35.7, 39.9	INBD. BENDING TIP BENDING SHEAR
A-18	SR-5	49.8, 59.6	INBD. BENDING TIP BENDING SHEAR

APPENDIX A
TABLE OF CONTENTS (Continued)

<u>FIG NO</u>	<u>PROP-FAN MODEL</u>	<u>BLADE ANGLE, DEG</u>	<u>STRESS TYPE</u>
A-19	SR-5	69.6, 79.7	INBD. BENDING TIP BENDING SHEAR
A-20	SR-5	10.0 through 59.6	INDB. BENDING
A-21	SR-5	59.6 through 79.7	INDB. BENDING

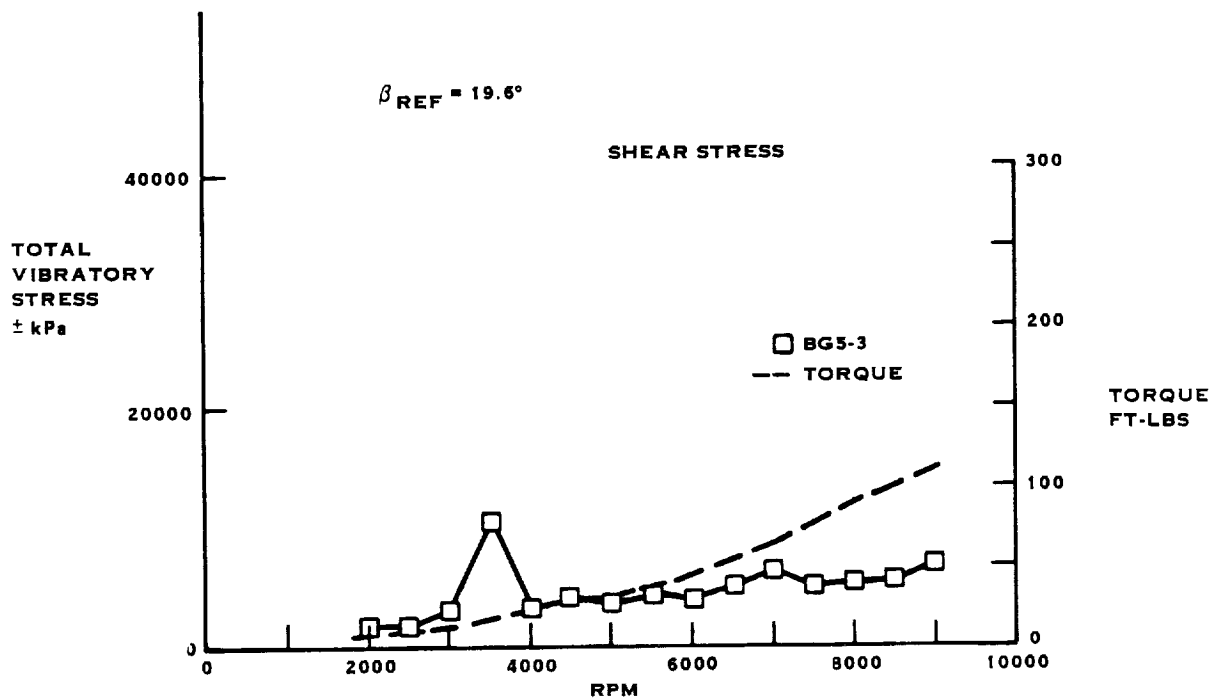
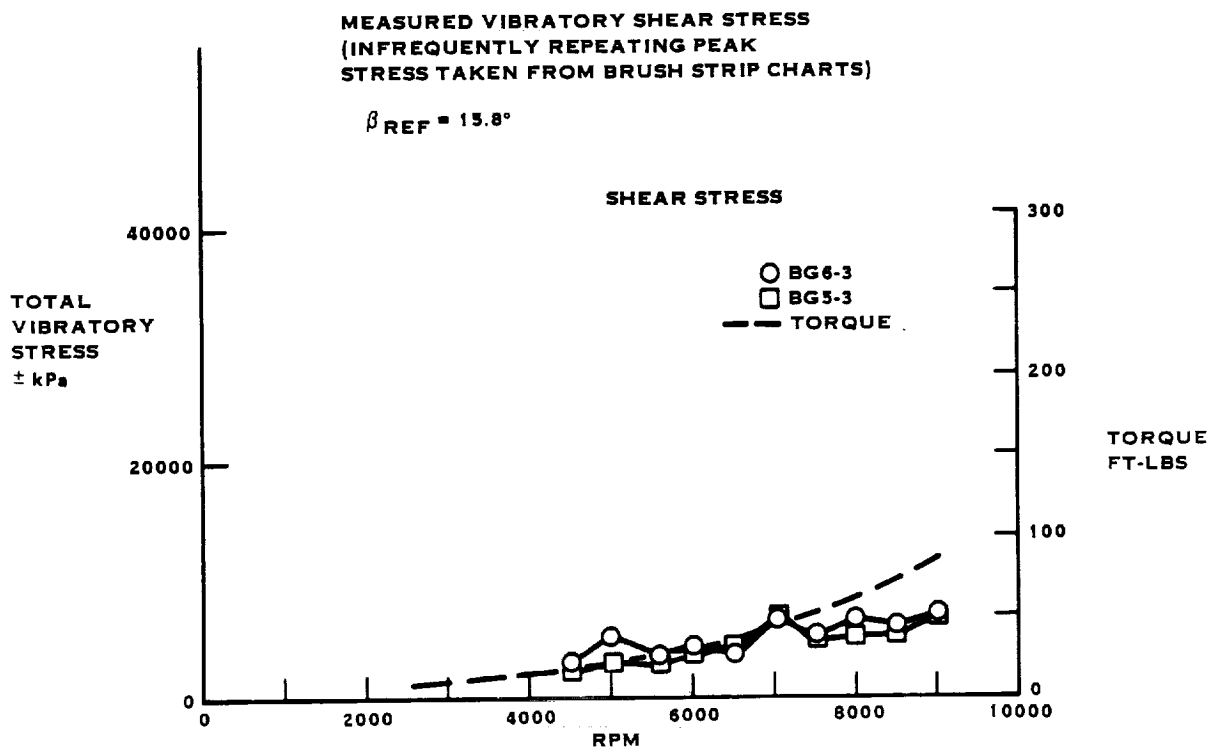


FIGURE A-1. SR-2 8 WAY STATIC PROP-FAN TESTS AT UTRC

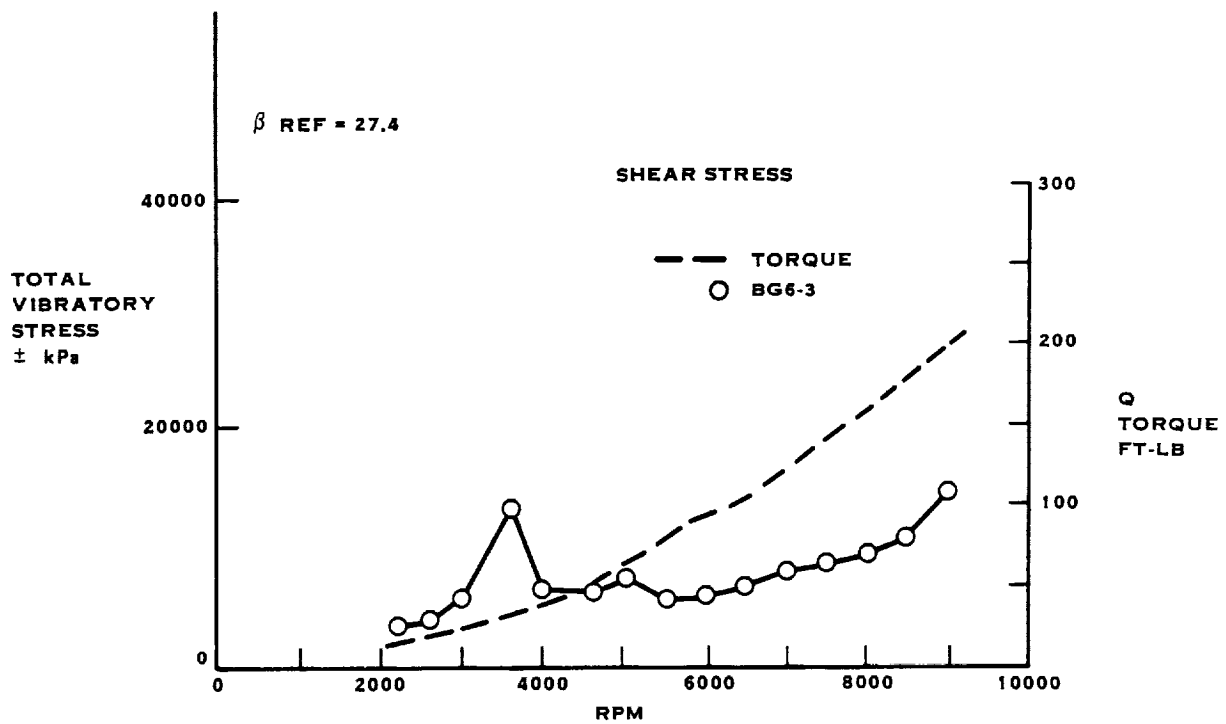
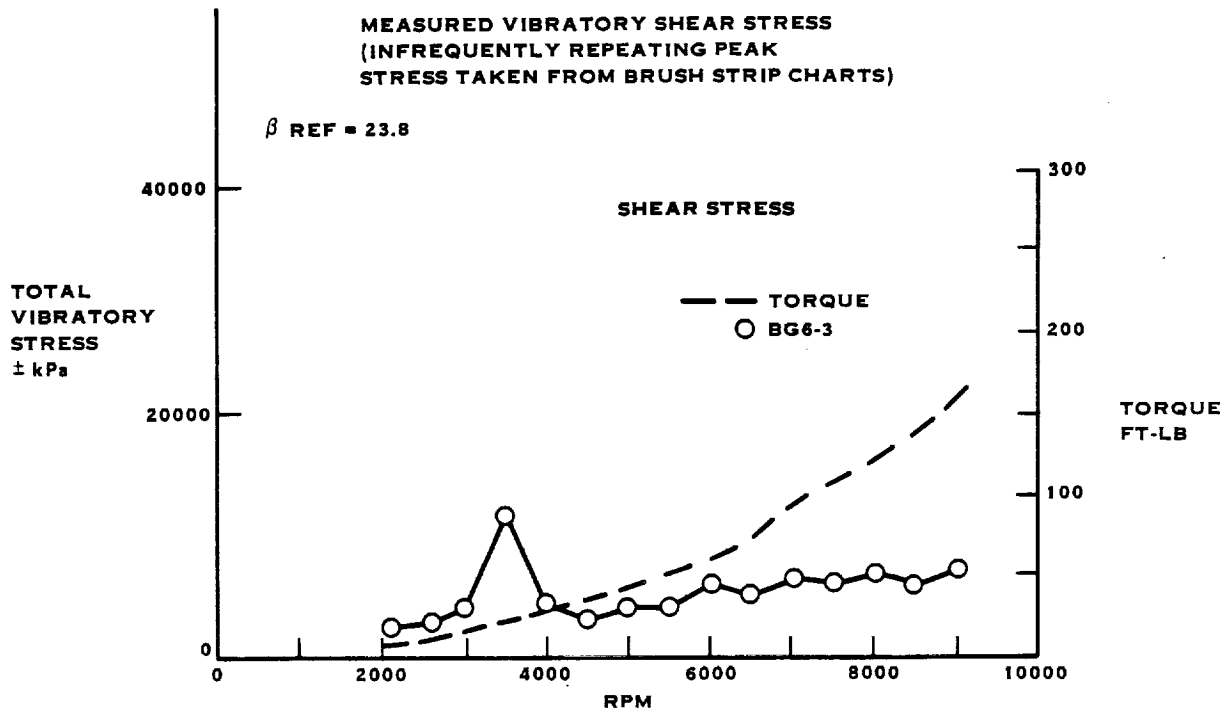


FIGURE A-2. SR-2 8 WAY STATIC PROP-FAN TESTS AT UTRC

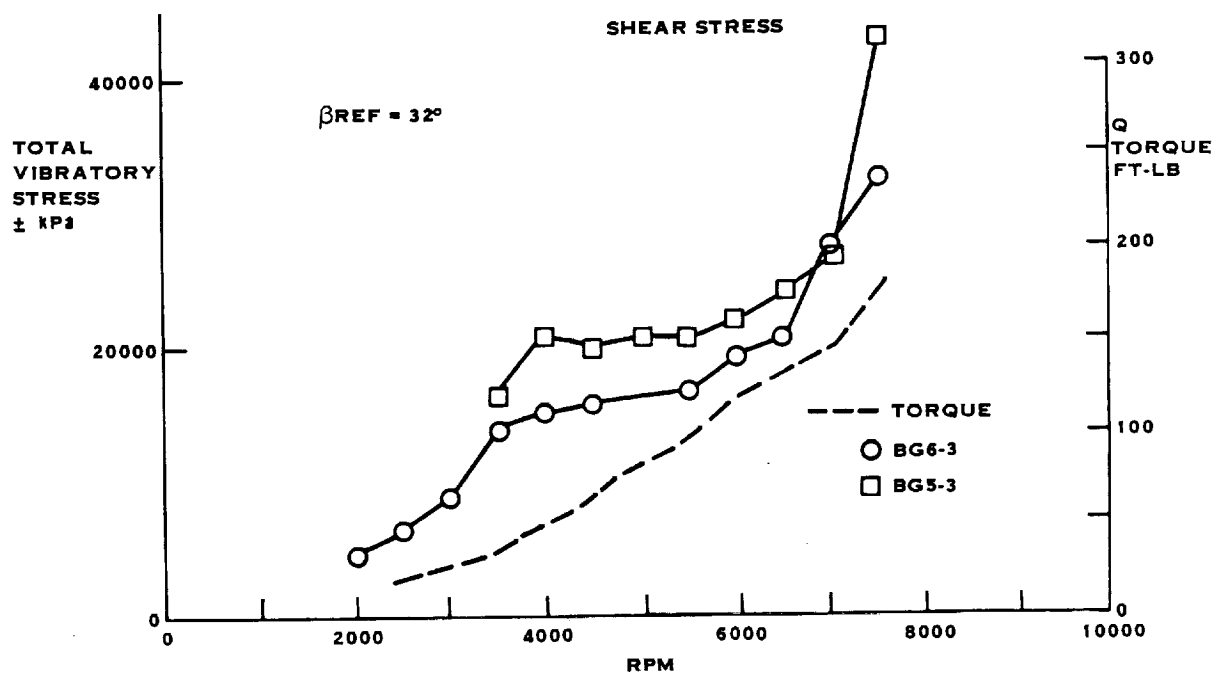
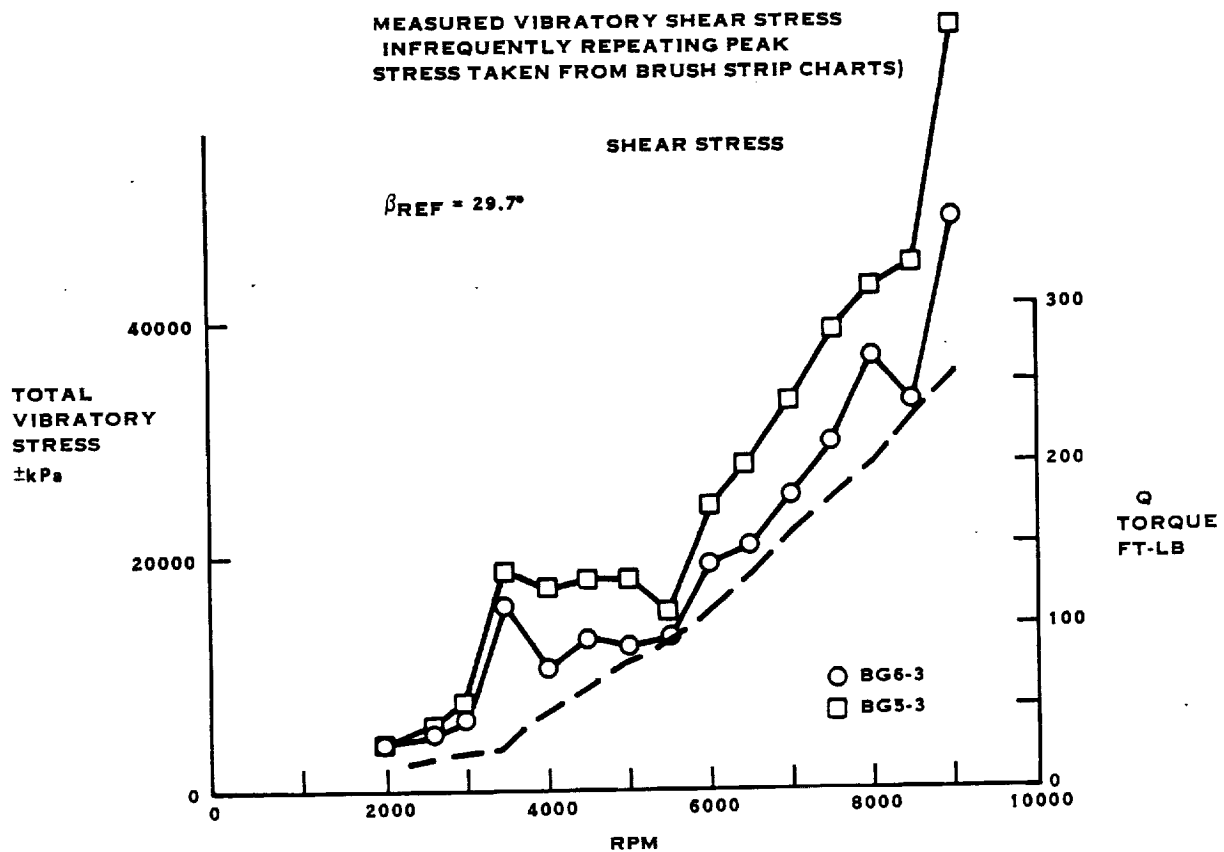


FIGURE A-3. SR-2 8 WAY STATIC PROP-FAN TESTS AT UTRC

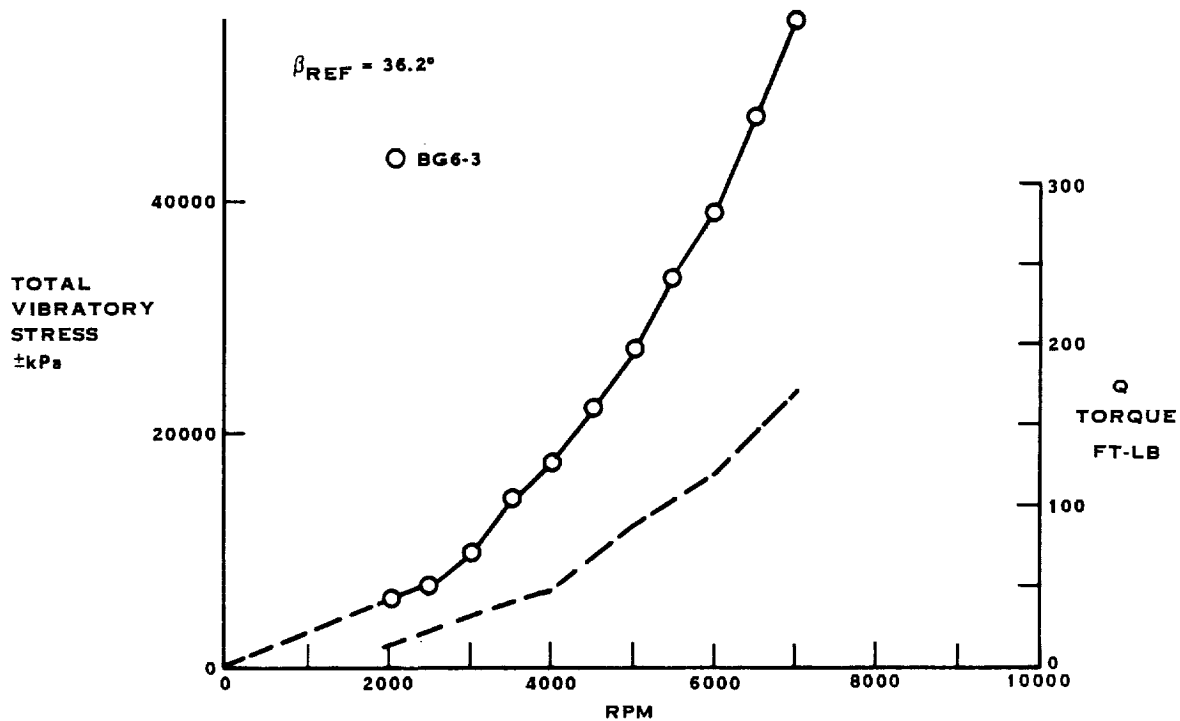
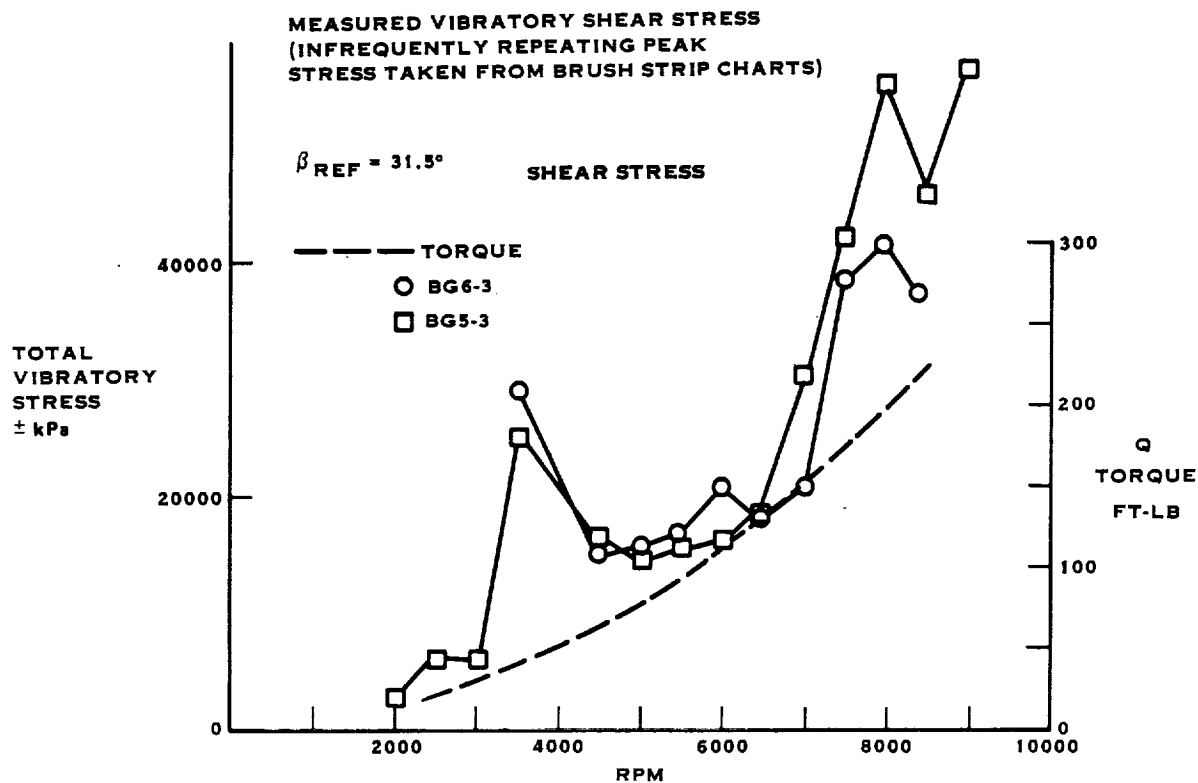


FIGURE A-4. SR-2 8 WAY STATIC PROP-FAN TESTS AT UTRC

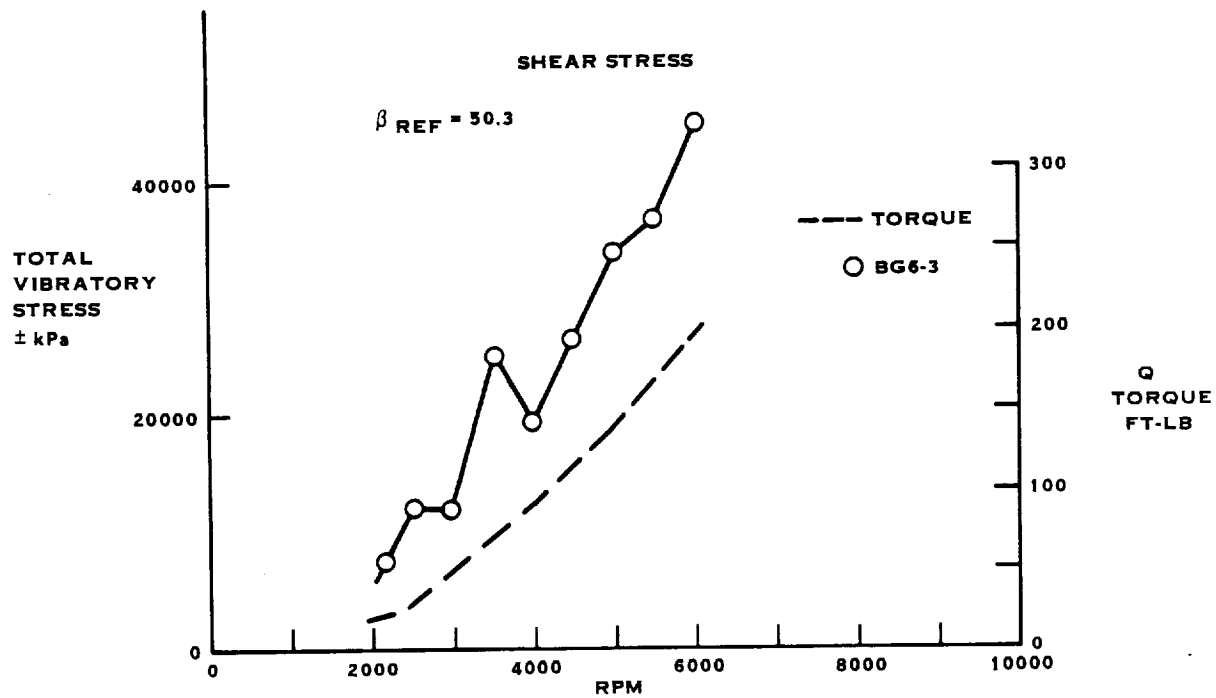
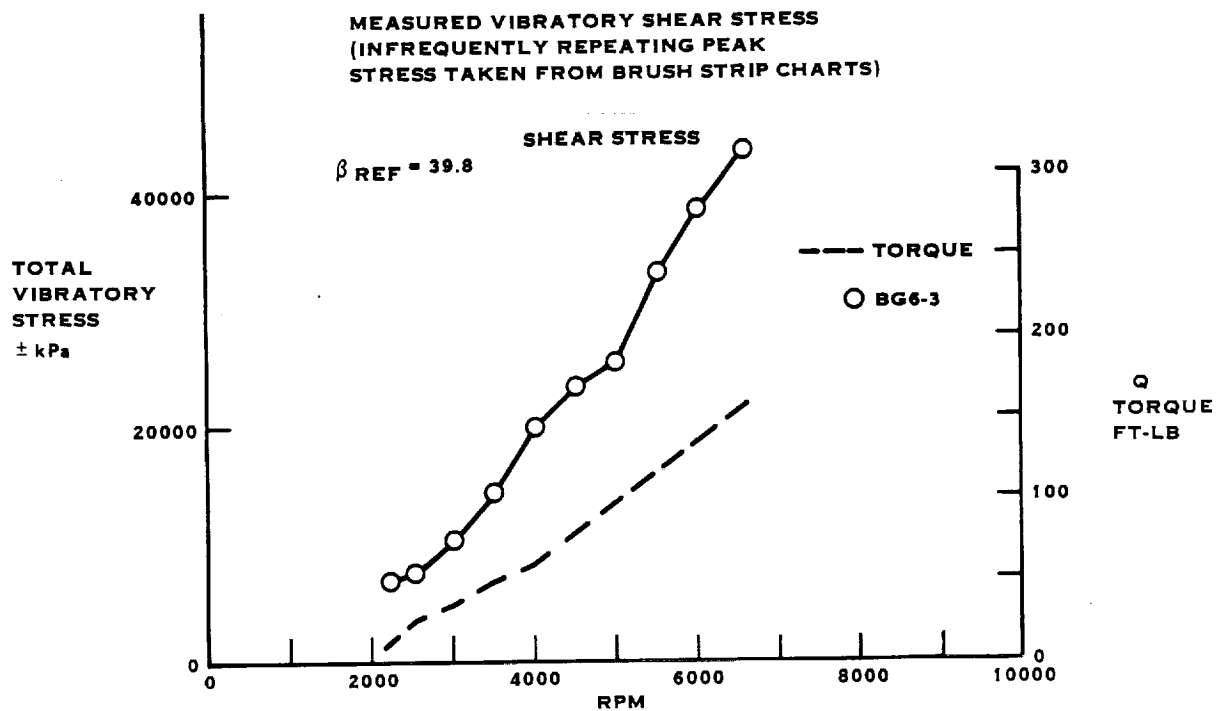


FIGURE A-5. SR-2 8 WAY STATIC PROP-FAN TESTS AT UTRC

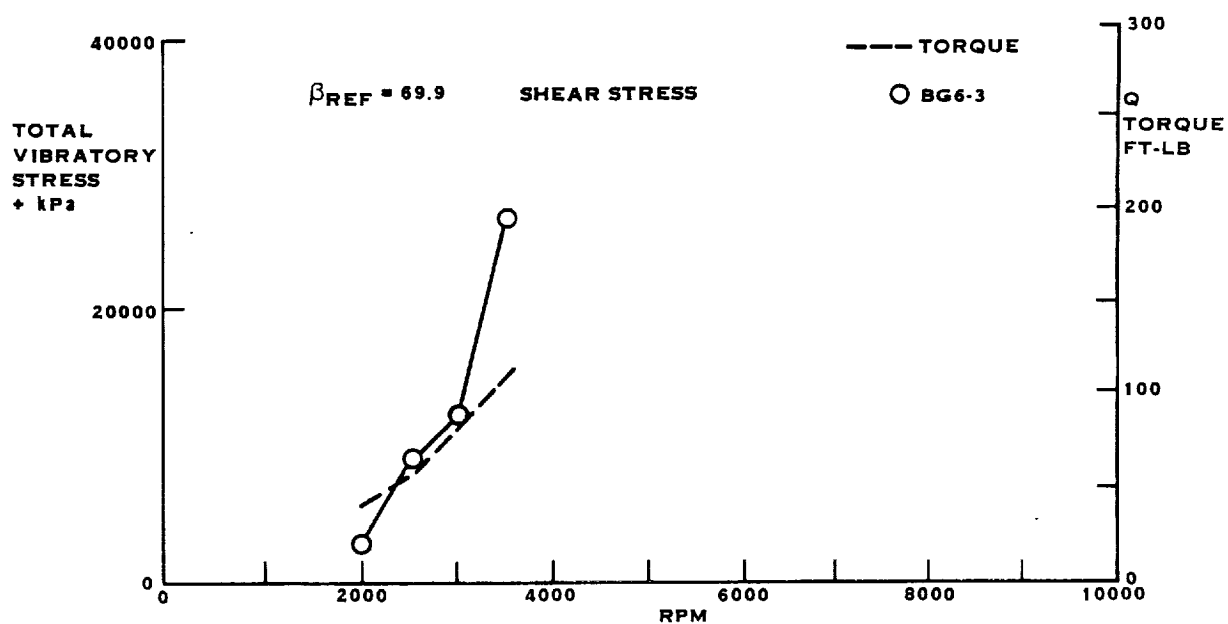
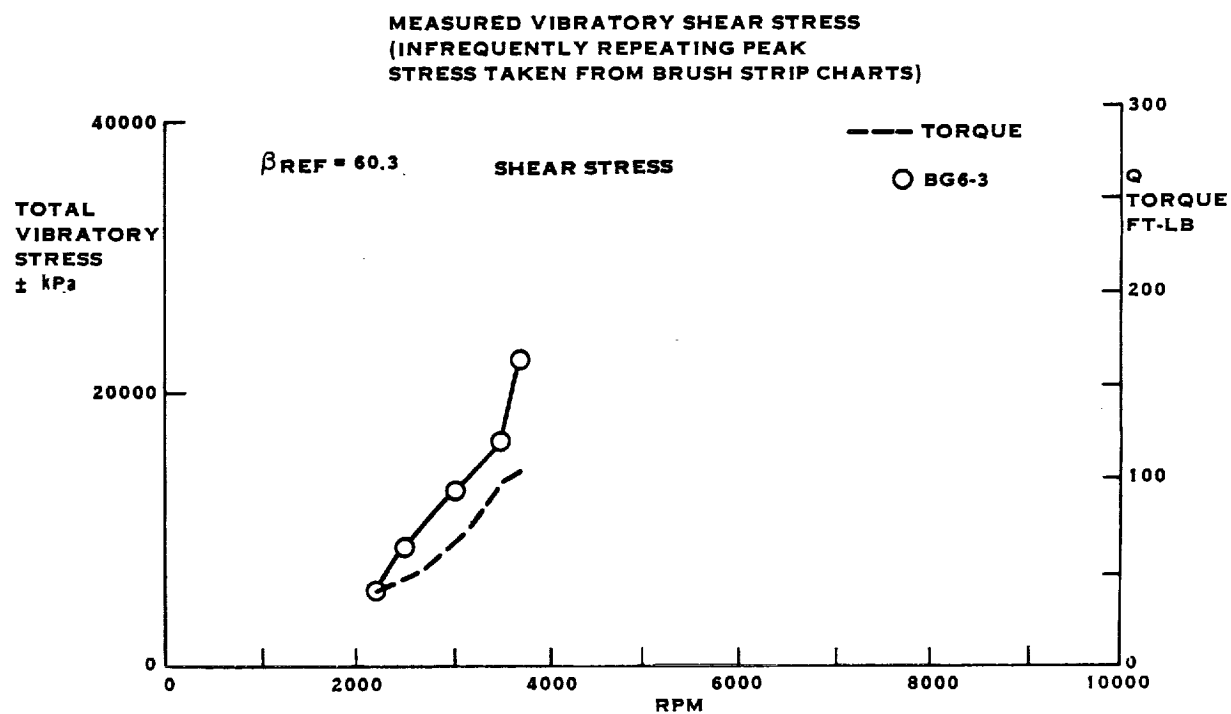


FIGURE A-6. SR-2 8 WAY STATIC PROP-FAN TESTS AT UTRC

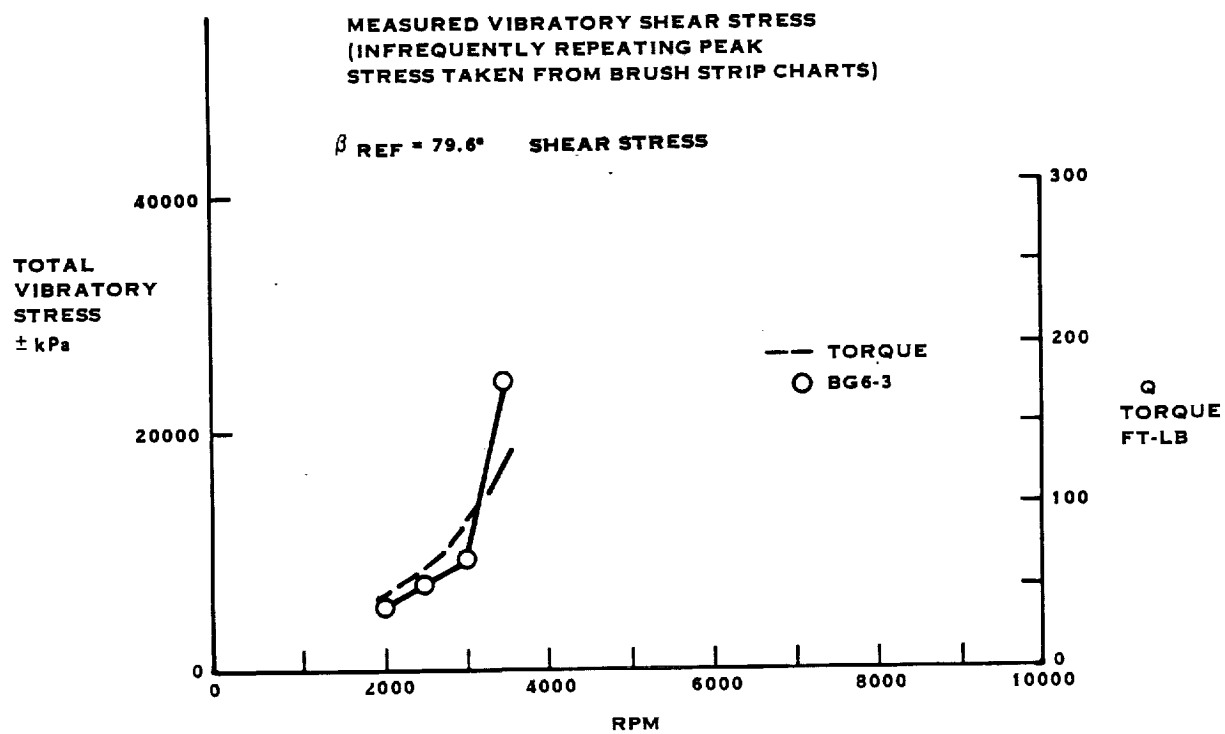


FIGURE A-7. SR-2 8 WAY STATIC PROP-FAN TESTS AT UTRC

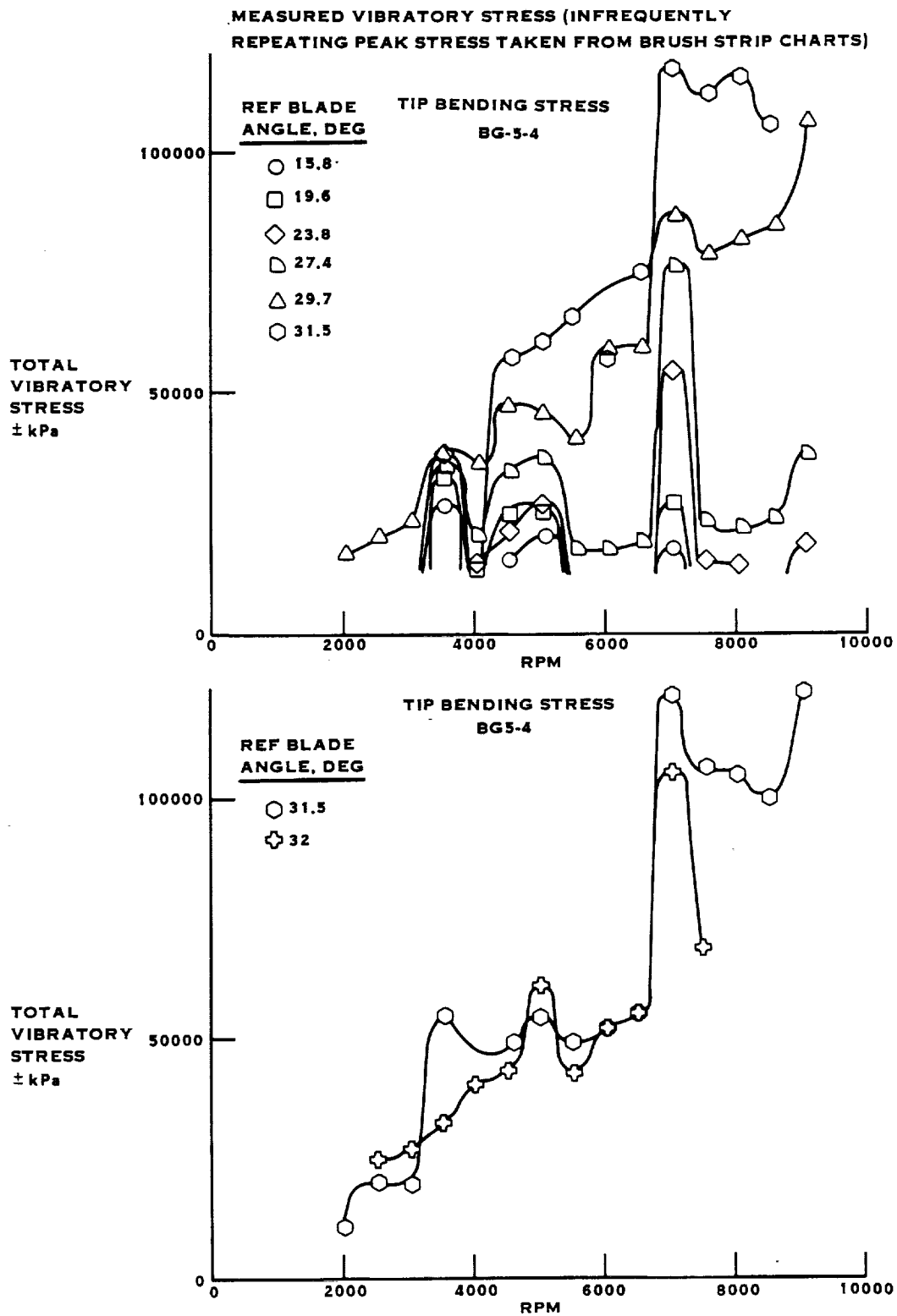


FIGURE A-8. SR-2 MODEL PROP-FAN TEST AT UTRC

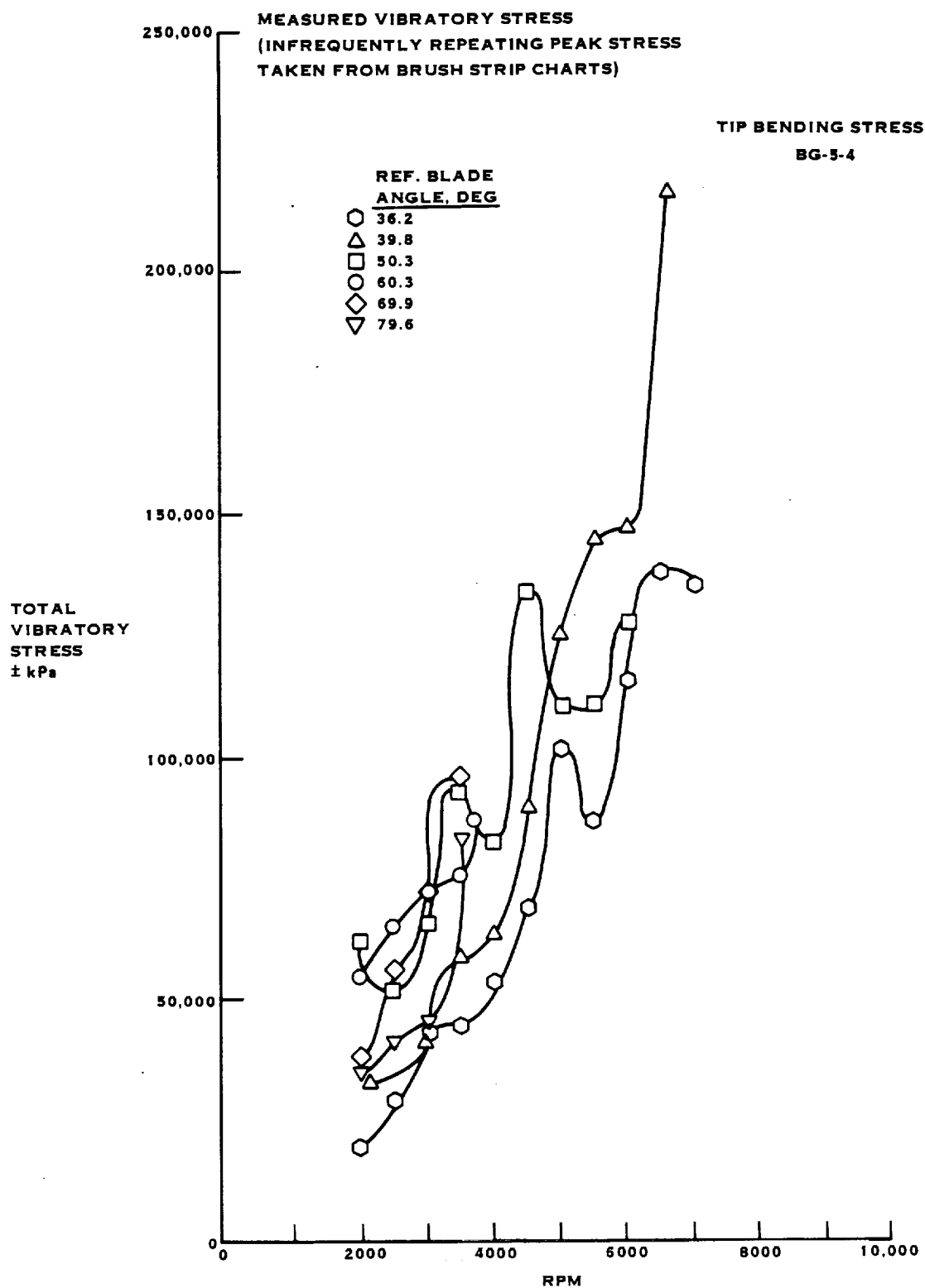


FIGURE A-9. SR-2 MODEL PROP-FAN TESTS AT UTRC

**MEASURED VIBRATORY STRESS
(INFREQUENTLY REPEATING PEAK STRESS
TAKEN FROM BRUSH STRIP CHARTS)**

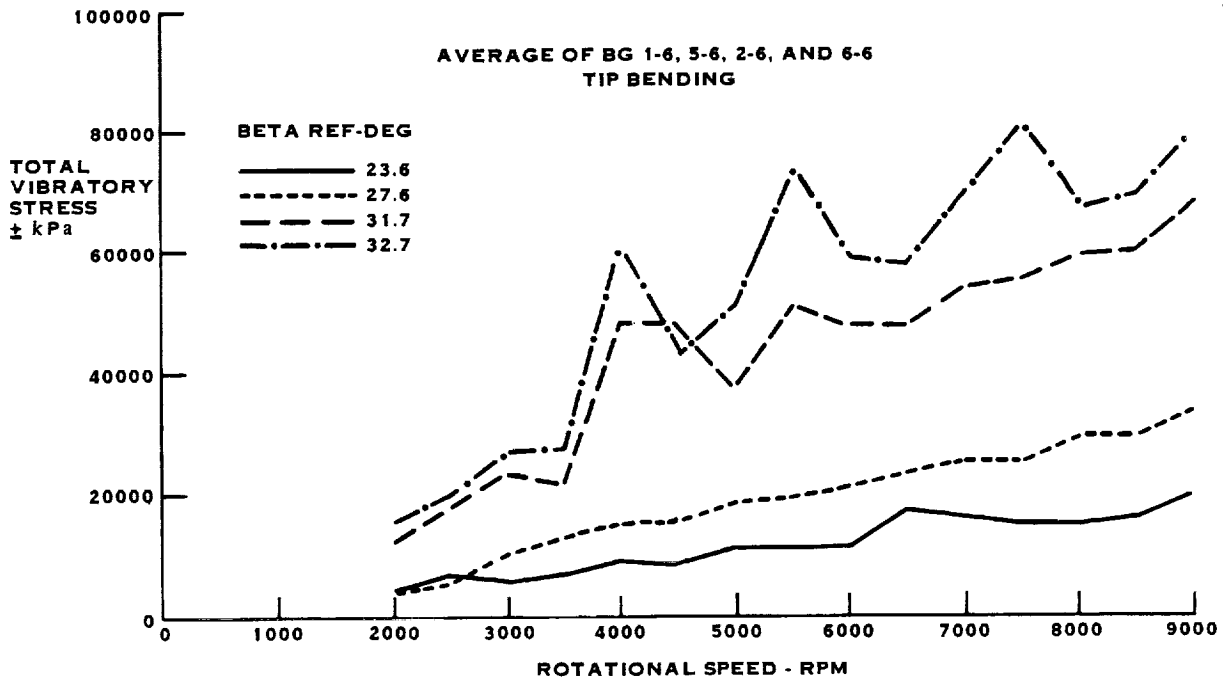
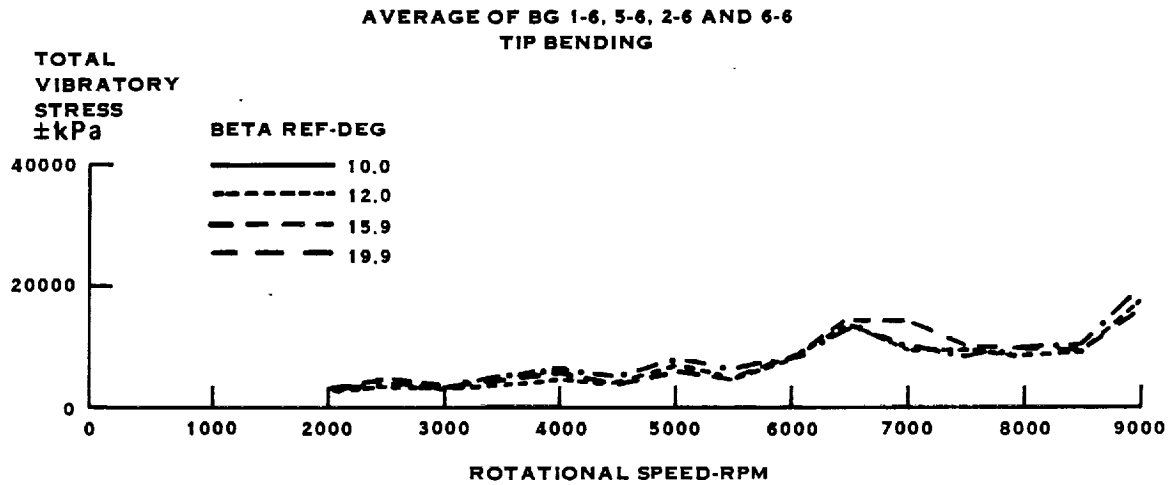


FIGURE A-10. SR-3 MODEL STATIC TESTS AT UTRC

MEASURED VIBRATORY STRESS
(INFREQUENTLY REPEATING PEAK STRESS
TAKEN FROM BRUSH STRIP CHARTS

AVERAGE OF BG 1-6, 5-6, 2-6, AND 6-6
TIP BENDING

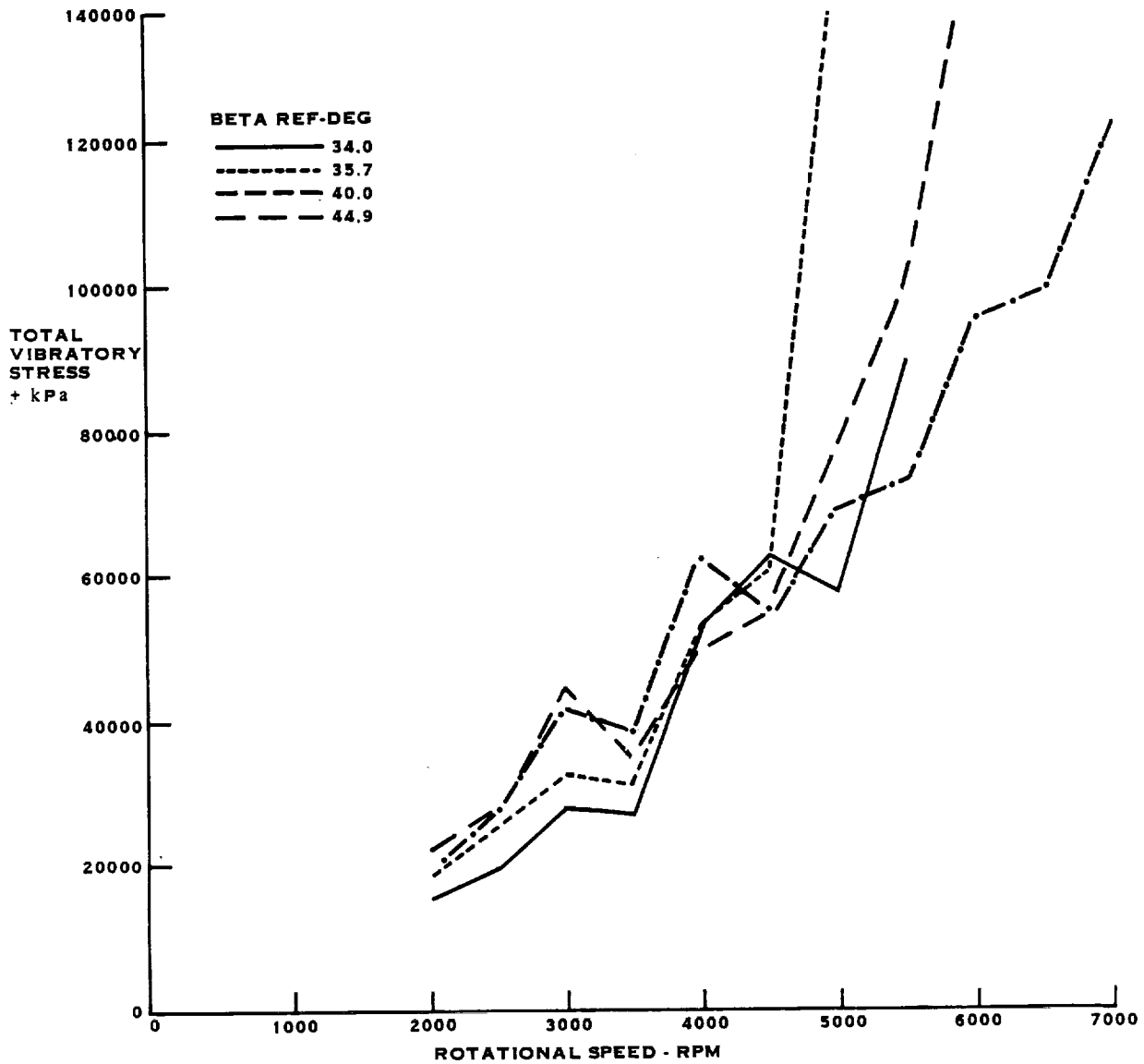


FIGURE A-11. SR-3 MODEL STATIC TESTS AT UTRC

MEASURED VIBRATORY STRESS
(INFREQUENTLY REPEATING PEAK STRESS
TAKEN FROM BRUSH STRIP CHARTS)

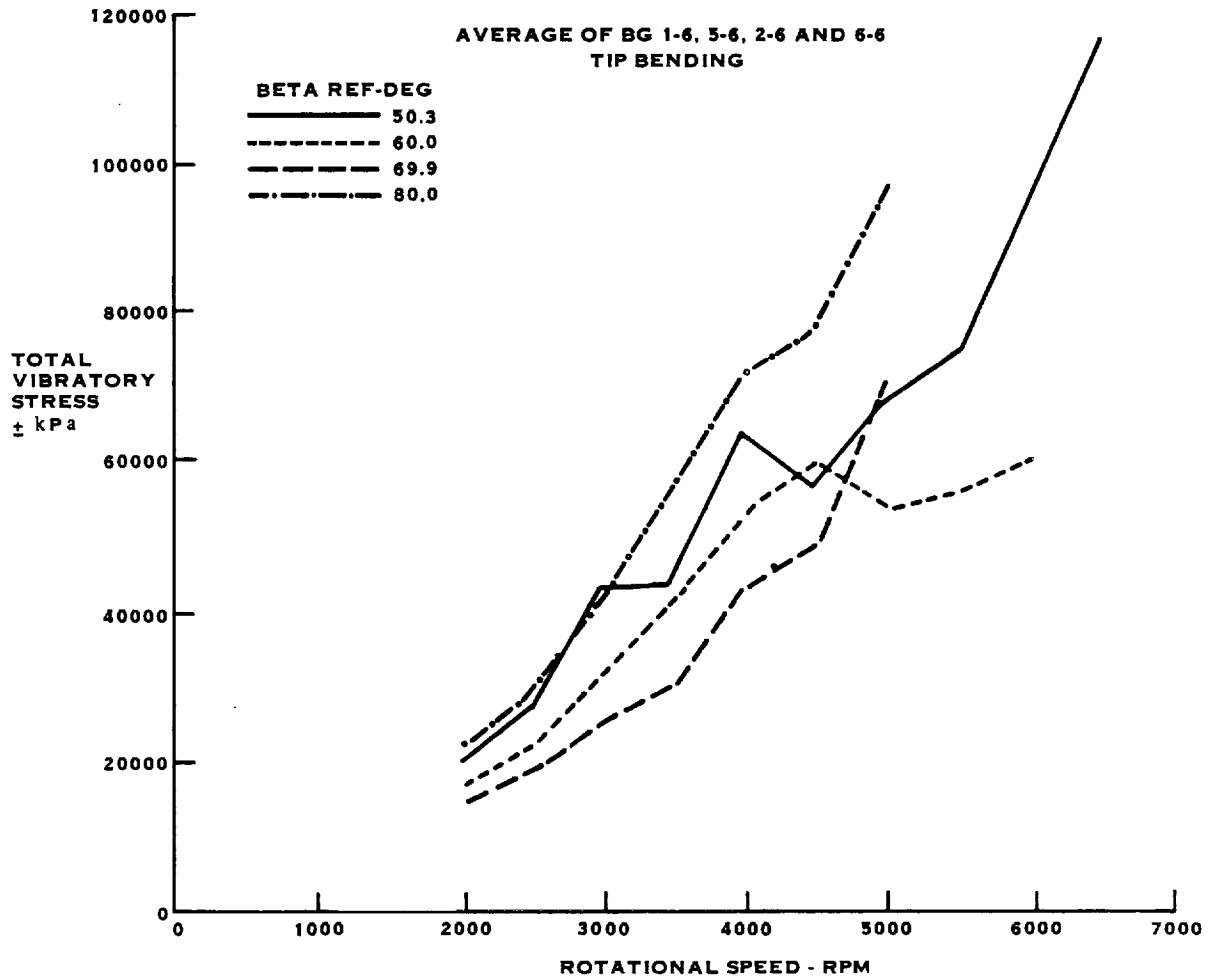


FIGURE A-12. SR-3 MODEL STATIC TESTS AT UTRC

MEASURED VIBRATORY STRESS
(INFREQUENTLY REPEATING PEAK STRESS
TAKEN FROM BRUSH STRIP CHARTS)

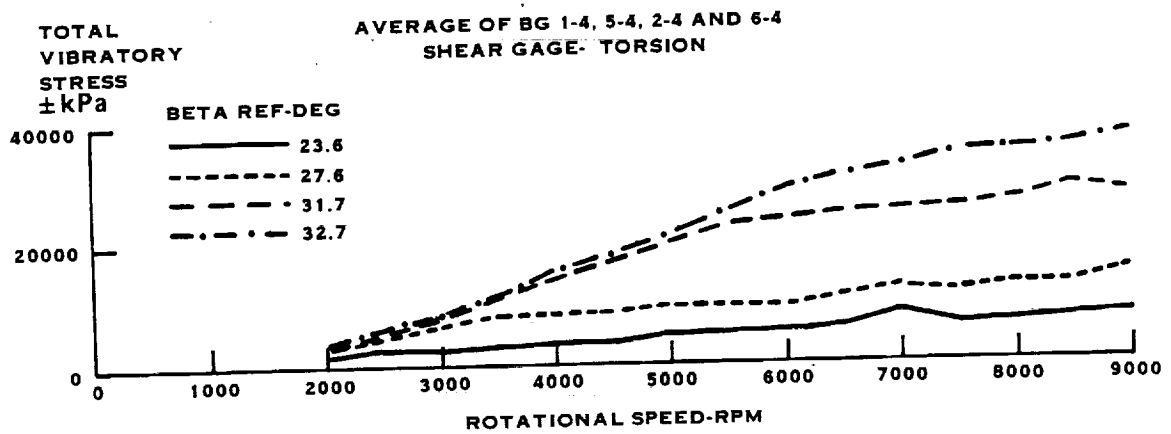
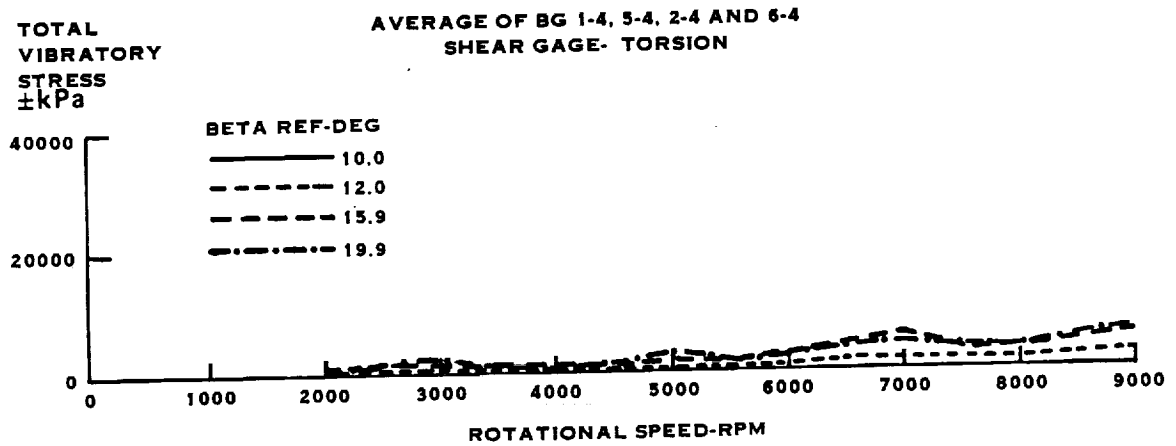


FIGURE A-13. SR-3 MODEL STATIC TESTS AT UTRC

MEASURED VIBRATORY STRESS
(INFREQUENTLY REPEATING PEAK STRESS
TAKEN FROM BRUSH STRIP CHARTS

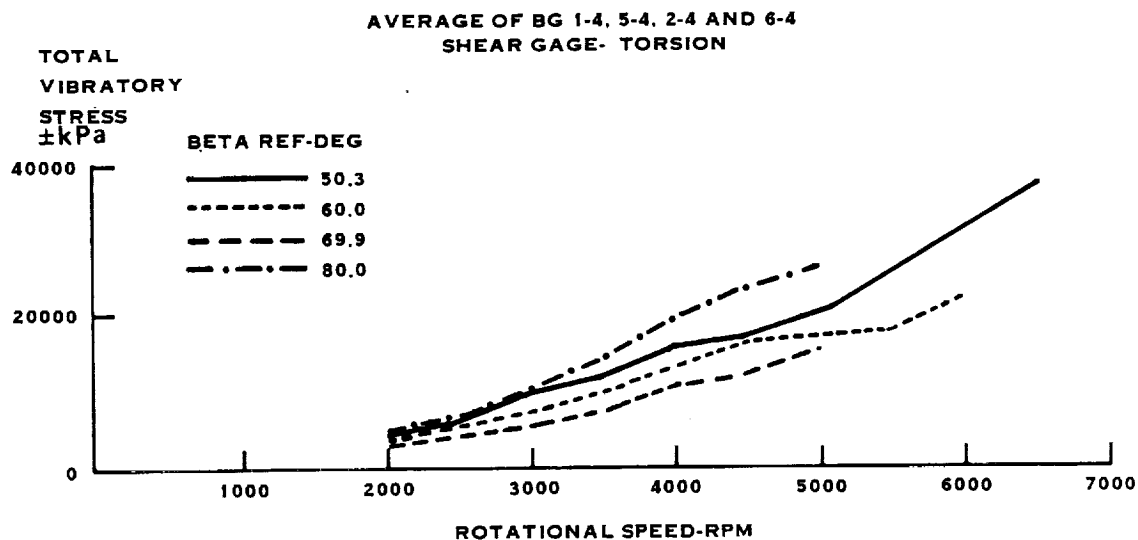
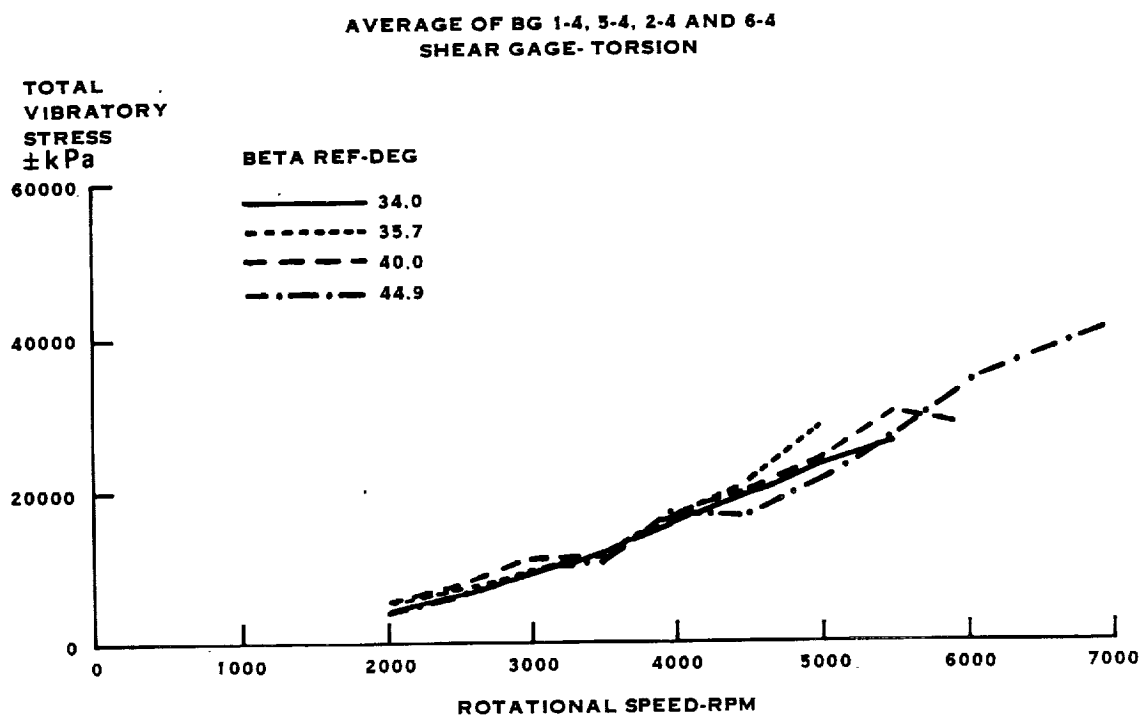


FIGURE A-14. SR-3 MODEL STATIC TESTS AT UTRC

MEASURED VIBRATORY STRESS
(INFREQUENTLY REPEATING PEAK STRESS
TAKEN FROM BRUSH STRIP CHARTS)

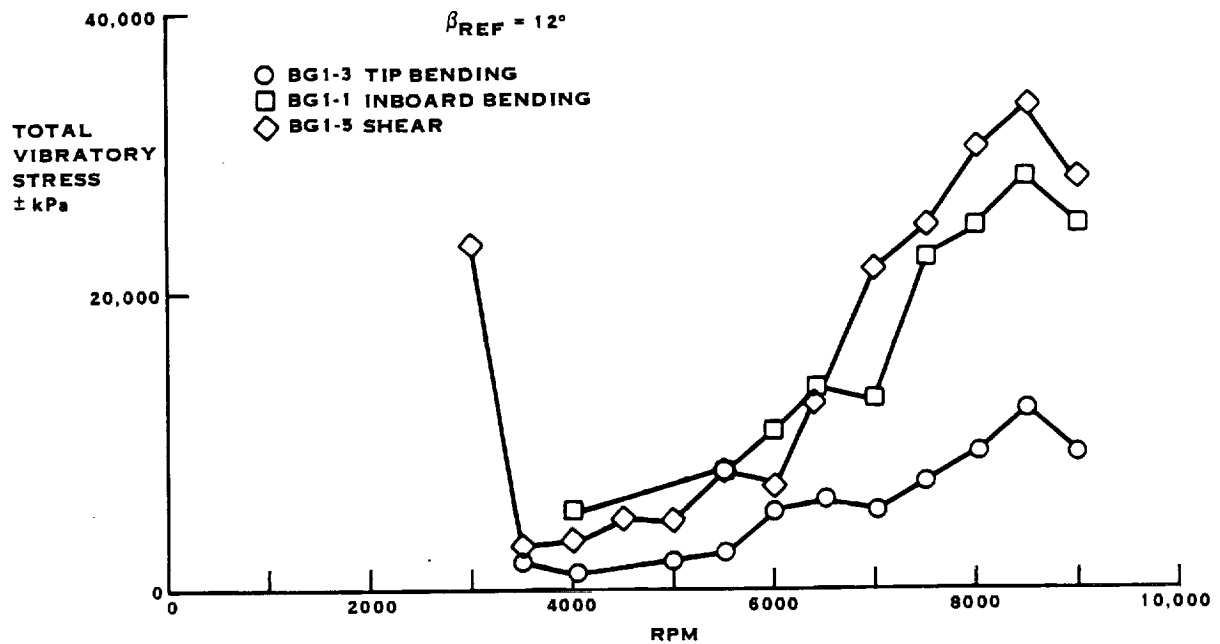
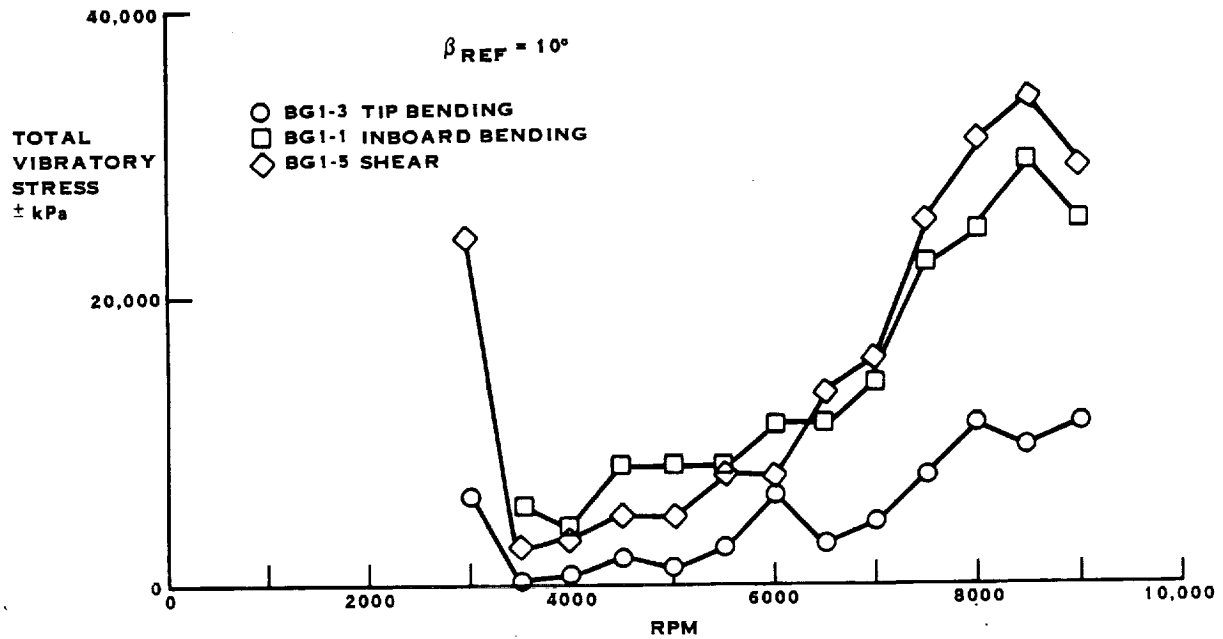


FIGURE A-15. SR-5 10 WAY STATIC PROP-FAN TESTS AT UTRC

MEASURED VIBRATORY STRESS
(INFREQUENTLY REPEATING PEAK STRESS
TAKEN FROM BRUSH STRIP CHARTS)

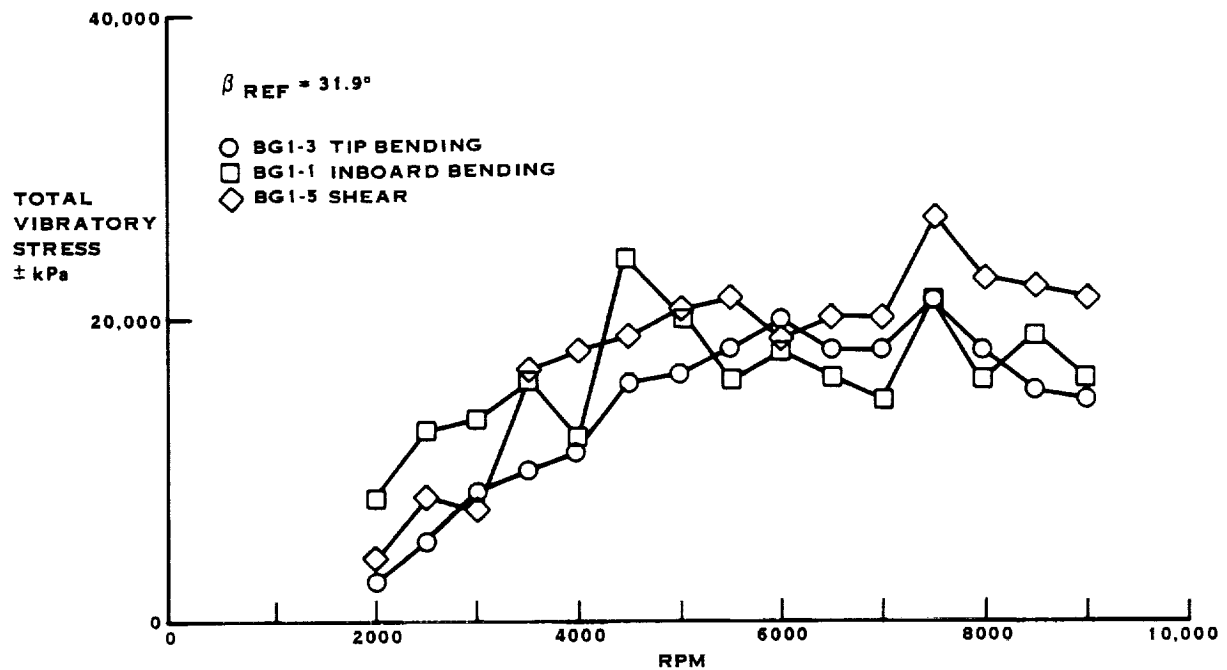
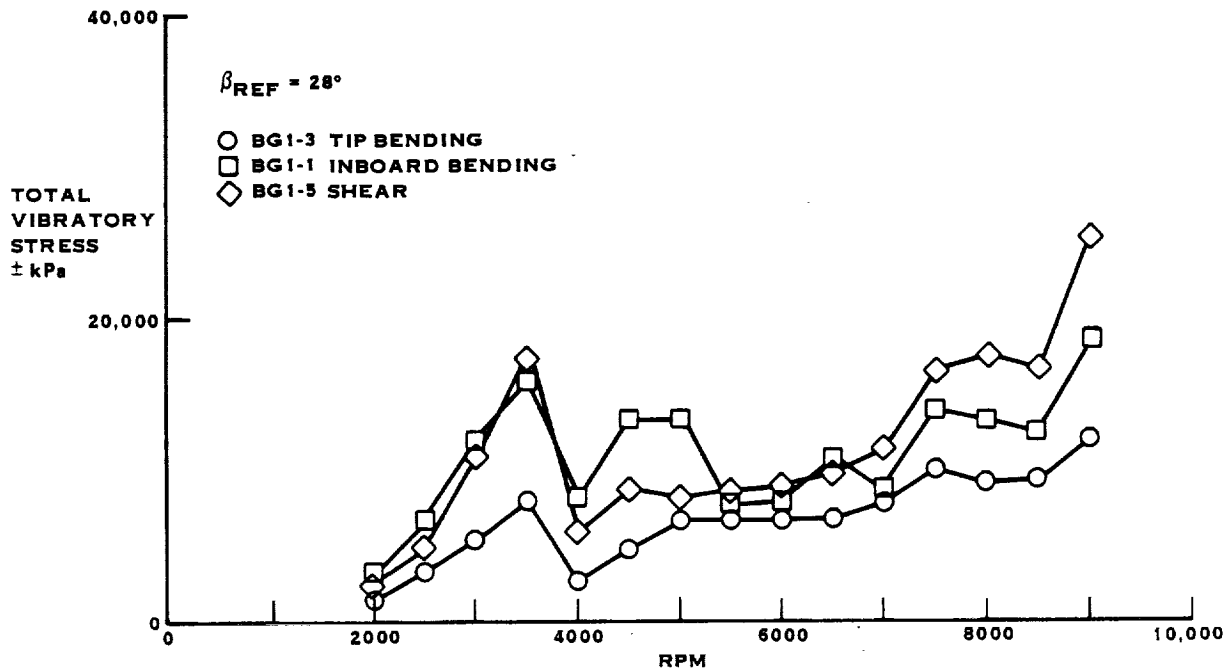


FIGURE A-16. SR-5 10 WAY STATIC PROP-FAN TESTS AT UTRC

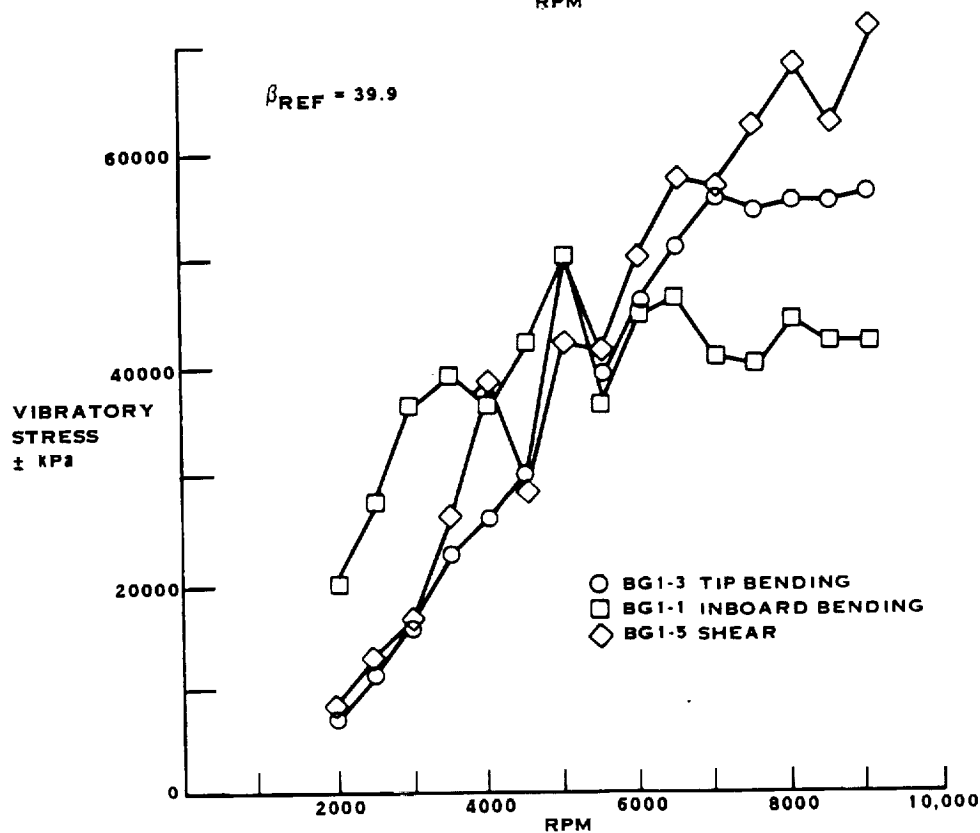
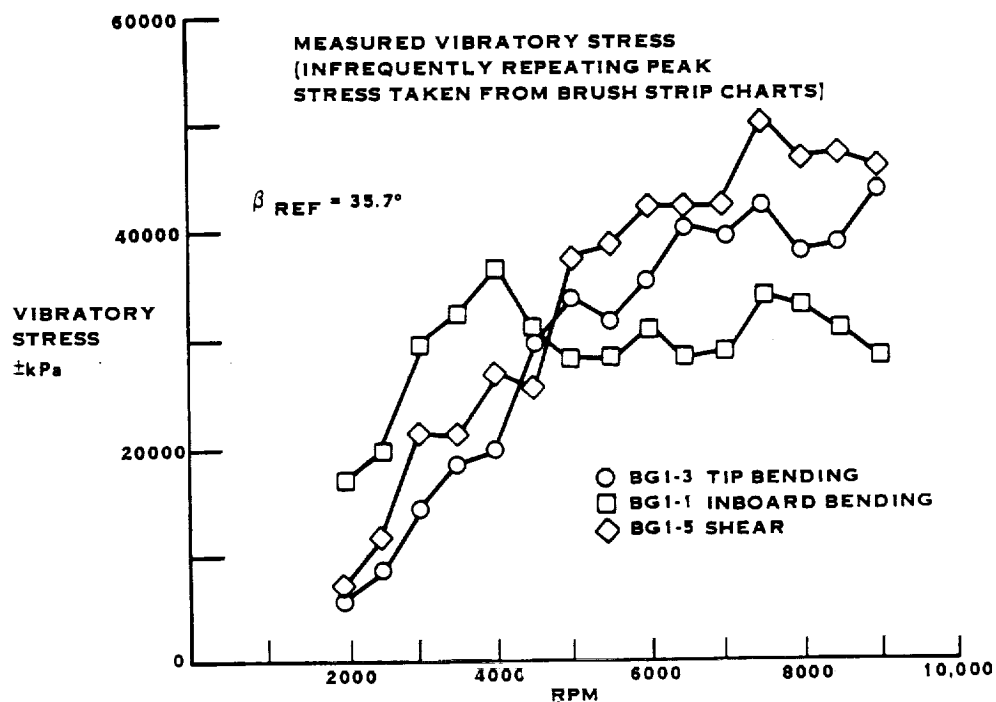


FIGURE A-17. SR-5 10 WAY STATIC PROP-FAN TESTS AT UTRC.

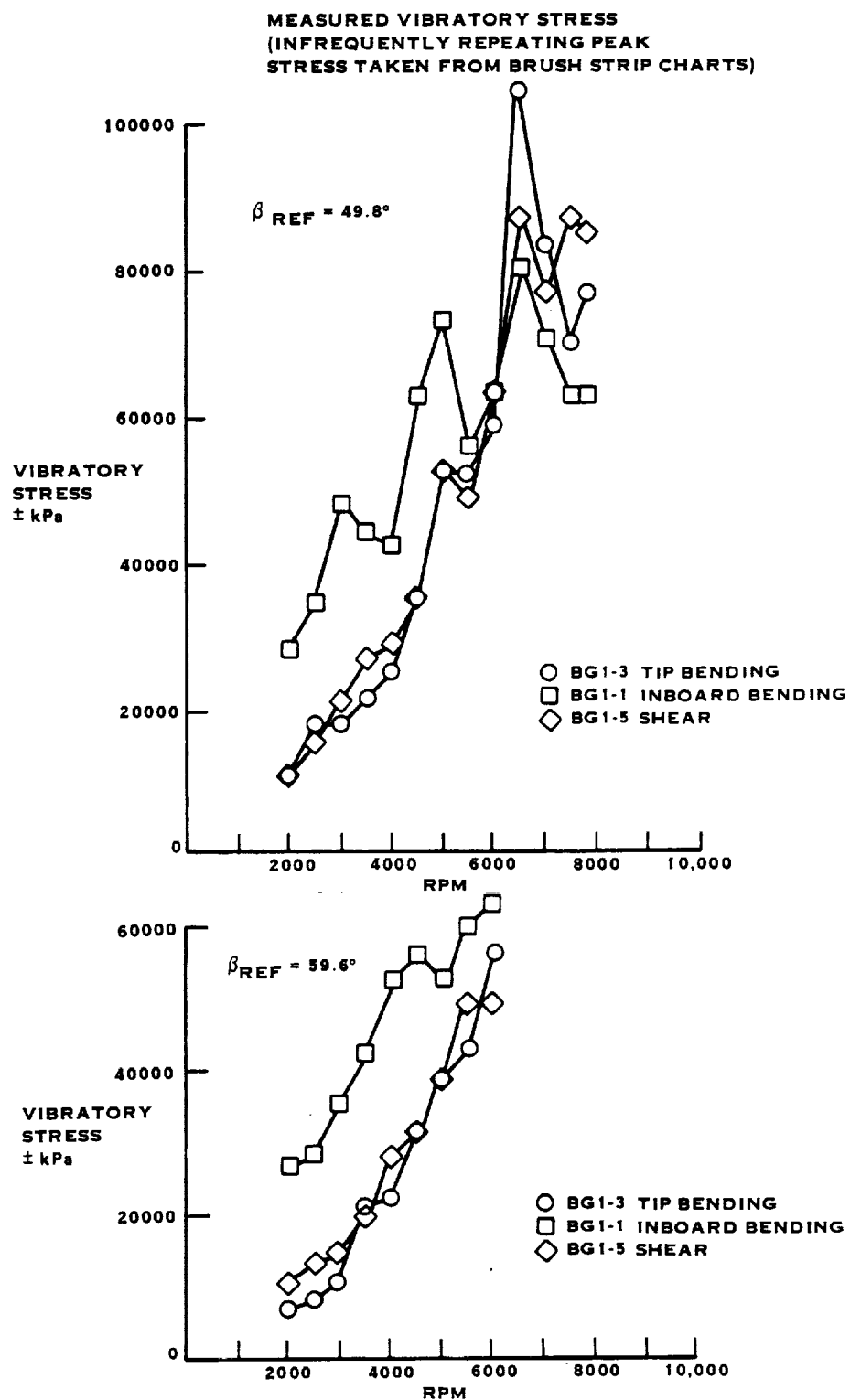


FIGURE A-18. SR-5 10 WAY STATIC PROP-FAN TESTS AT UTRC

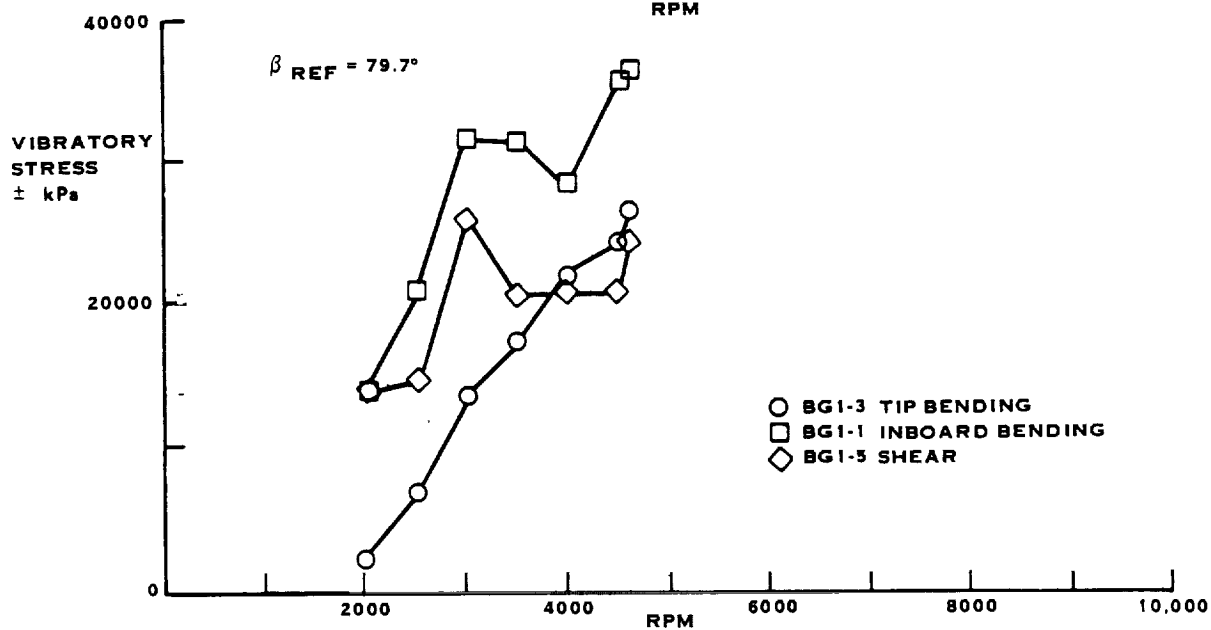
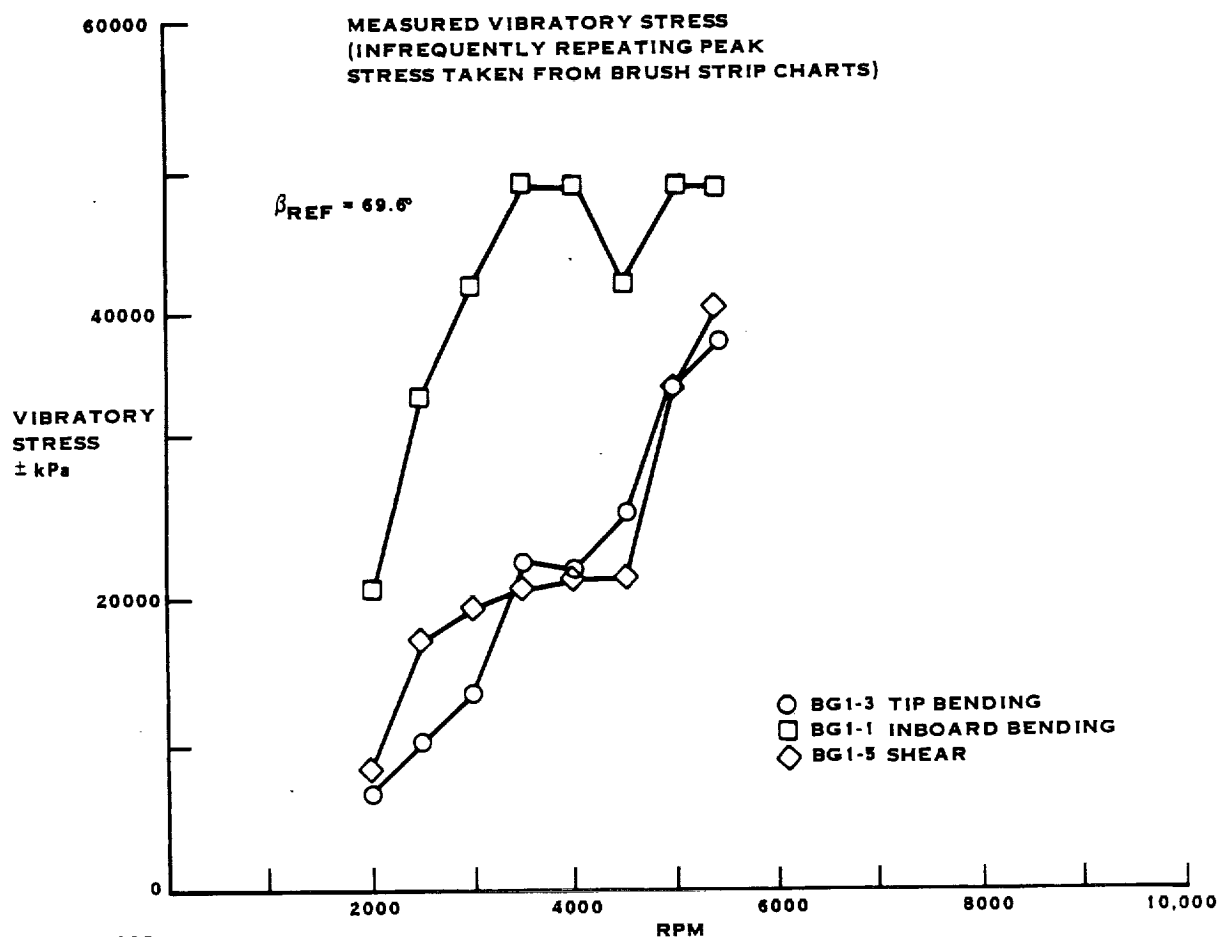


FIGURE A-19. SR-5 10 WAY STATIC PROP-FAN TESTS AT UTRC

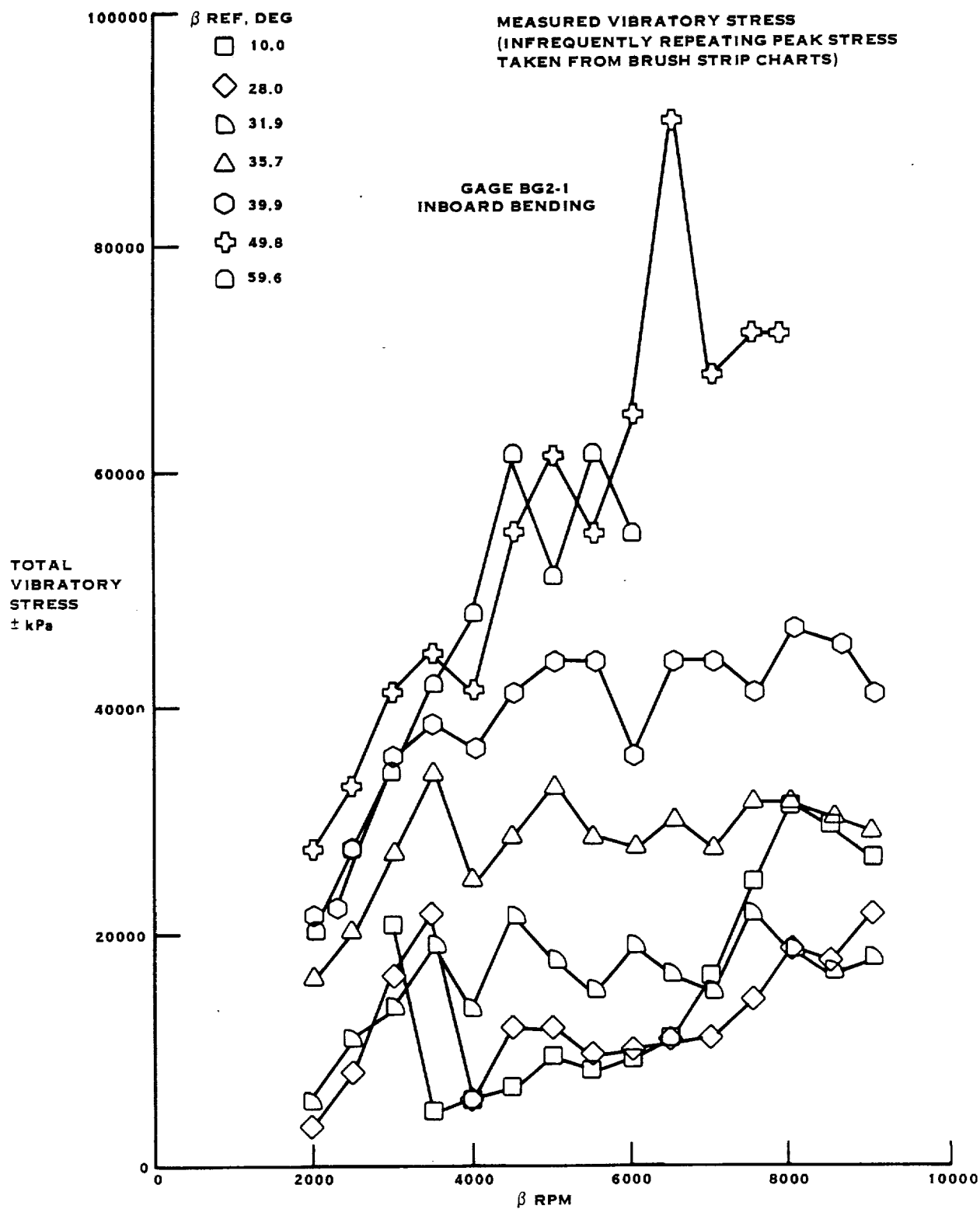


FIGURE A-20. SR-5 10 WAY STATIC PROP-FAN TESTS AT UTRC

MEASURED VIBRATORY STRESS
(INFREQUENTLY REPEATING PEAK
STRESS TAKEN FROM BRUSH STRIP CHARTS)

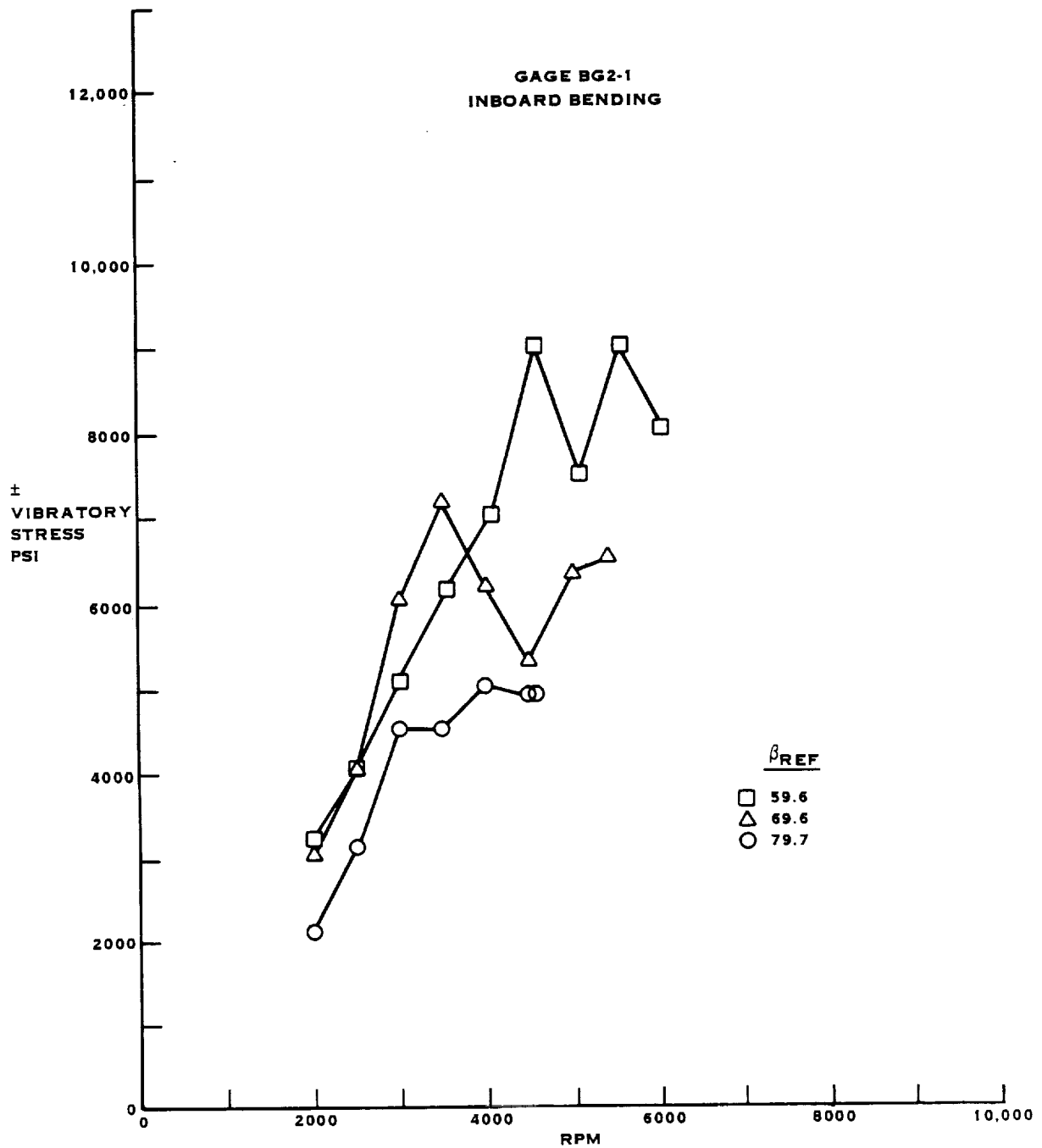


FIGURE A-21. SR-5 10 WAY STATIC PROP-FAN TESTS AT UTRC

APPENDIX B

STRESS PEAK TABULATION FOR THE SR-3 MODEL PROP-FAN

This table contains data obtained from spectral analyses using the computerized peak picking routines developed by Hamilton Standard. Listed are the predominant frequencies measured for each strain gage signal, followed by the stress amplitude. These are listed for each operating condition defined by:

REF. BLADE ANGLE
RPM
TORQUE
POWER COEFFICIENT

ORIGINAL PAGE IS
OF POOR QUALITY

TABLE B-1. SR-3 PROP-FAN MODEL STATIC TESTS AT UTRC
SPECTRAL STRESS PEAKS AND FREQUENCIES

Run No.	Ref. Blade Angle Deg.	RPM	Torque	Power Coeff	Gage No.	No. of Peaks	Spectral Frequencies(HZ)/Vibratory Stress (psi)
2	12	9050	80	.2617	BG1-4	0	
3	12	8630	70	.2518	BG1-4	0	
4	12	8025	65	.2704	BG1-4	0	
5	12	7500	55	.262	BG1-4	0	
6	12	7025	48	.2606	BG1-4	0	
7	12	6500	42	.2663	BG1-4	0	
8	12	6025	35	.2583	BG1-4	0	
9	12	5500	30	.2657	BG1-4	0	
10	12	5000	25	.2679	BG1-4	0	
11	12	4490	20	.2658	BG1-4	0	
12	12	3990	18	.3029	BG1-4	0	
13	12	3525	12	.2587	BG1-4	0	
14	12	3000	10	.2977	BG1-4	0	
15	12	2550	9	.3708	BG1-4	0	
16	12	2140	7	.4095	BG1-4	0	
2	12	9050	80	.2617	BG1-1	0	
3	12	8630	70	.2518	BG1-1	0	
4	12	8025	65	.2704	BG1-1	0	
5	12	7500	55	.262	BG1-1	0	
6	12	7025	48	.2606	BG1-1	1	234 1128
7	12	6500	42	.2663	BG1-1	1	108 677
8	12	6025	35	.2583	BG1-1	0	
9	12	5500	30	.2657	BG1-1	0	
10	12	5000	25	.2679	BG1-1	0	
11	12	4490	20	.2658	BG1-1	0	
12	12	3990	18	.3029	BG1-1	0	
13	12	3525	12	.2587	BG1-1	0	
14	12	3000	10	.2977	BG1-1	0	
15	12	2550	9	.3708	BG1-1	0	
16	12	2140	7	.4095	BG1-1	0	
2	12	9050	80	.2617	BG1-6	1	454 1011
3	12	8630	70	.2518	BG1-6	0	
4	12	8025	65	.2704	BG1-6	1	134 502
5	12	7500	55	.262	BG1-6	0	
6	12	7025	48	.2606	BG1-6	0	
7	12	6500	42	.2663	BG1-6	1	108 583
8	12	6025	35	.2583	BG1-6	0	
9	12	5500	30	.2657	BG1-6	0	
10	12	5000	25	.2679	BG1-6	0	
11	12	4490	20	.2658	BG1-6	0	
12	12	3990	18	.3029	BG1-6	0	
13	12	3525	12	.2587	BG1-6	0	
14	12	3000	10	.2977	BG1-6	0	
15	12	2550	9	.3708	BG1-6	0	
16	12	2140	7	.4095	BG1-6	0	
18	15.9	9030	115	.3778	BG1-4	0	
19	15.9	8540	105	.3857	BG1-4	0	
20	15.9	8015	95	.3962	BG1-4	0	
21	15.9	7540	80	.377	BG1-4	0	
22	15.9	7040	70	.3784	BG1-4	0	
23	15.9	6520	62	.3907	BG1-4	0	
24	15.9	6012	55	.4077	BG1-4	0	
25	15.9	5520	45	.3957	BG1-4	0	
26	15.9	5030	40	.4236	BG1-4	0	
27	15.9	4515	32	.4206	BG1-4	0	
28	15.9	4005	25	.4176	BG1-4	0	
29	15.9	3510	20	.4349	BG1-4	0	
30	15.9	3023	15	.4398	BG1-4	0	
31	15.9	2505	10	.4269	BG1-4	0	
32	15.9	2140	8	.468	BG1-4	0	
18	15.9	9030	115	.3778	BG1-4	0	
19	15.9	8540	105	.3857	BG1-4	0	
20	15.9	8015	95	.3962	BG1-4	0	

ORIGINAL PAGE IS
OF POOR QUALITY

TABLE B-1 (CONTINUED)

Run No.	Ref. Blade Angle Deg.	RPM	Torque	Power Coeff	Gage No.	No. of Peaks	Spectral Frequencies(HZ)/Vibratory Stress (psi)		
18	15.9	9030	115	.3778	BG1-1	1	148	521	
19	15.9	8540	105	.3857	BG1-1	0			
20	15.9	8015	95	.3962	BG1-1	0			
21	15.9	7540	80	.377	BG1-1	2	126	558	252 568
22	15.9	7040	70	.3784	BG1-1	2	118	812	234 1243
23	15.9	6520	62	.3907	BG1-1	2	108	786	218 982
24	15.9	6012	55	.4077	BG1-1	0			
25	15.9	5520	45	.3957	BG1-1	0			
26	15.9	5030	40	.4236	BG1-1	0			
27	15.9	4515	32	.4206	BG1-1	0			
28	15.9	4005	25	.4176	BG1-1	0			
29	15.9	3510	20	.4349	BG1-1	0			
30	15.9	3023	15	.4398	BG1-1	0			
31	15.9	2505	10	.4249	BG1-1	0			
32	15.9	2140	8	.468	BG1-1	0			
18	15.9	9030	115	.3778	BG1-6	2	148	749	448 682
19	15.9	8540	105	.3857	BG1-6	1	142	520	
20	15.9	8015	95	.3962	BG1-6	1	134	560	
21	15.9	7540	80	.377	BG1-6	1	126	619	
22	15.9	7040	70	.3784	BG1-6	1	118	894	
23	15.9	6520	62	.3907	BG1-6	2	108	690	218 588
24	15.9	6012	55	.4077	BG1-6	0			
25	15.9	5520	45	.3957	BG1-6	0			
26	15.9	5030	40	.4236	BG1-6	0			
27	15.9	4515	32	.4206	BG1-6	0			
28	15.9	4005	25	.4176	BG1-6	0			
29	15.9	3510	20	.4349	BG1-6	0			
30	15.9	3023	15	.4398	BG1-6	0			
31	15.9	2505	10	.4249	BG1-6	0			
32	15.9	2140	8	.468	BG1-6	0			
33	19.9	9020	165	.5433	BG1-4	0			
34	19.9	8500	150	.5562	BG1-4	0			
35	19.9	8000	135	.5651	BG1-4	0			
36	19.9	7542	120	.5652	BG1-4	0			
37	19.9	7030	100	.5421	BG1-4	0			
38	19.9	6525	92	.5789	BG1-4	0			
39	19.9	6010	75	.5563	BG1-4	0			
40	19.9	5520	60	.5276	BG1-4	0			
41	19.9	5025	50	.5305	BG1-4	0			
42	19.9	4510	42	.5532	BG1-4	0			
43	19.9	4010	35	.5831	BG1-4	0			
44	19.9	3510	29	.6306	BG1-4	0			
45	19.9	3000	21	.6251	BG1-4	0			
46	19.9	2500	15	.643	BG1-4	0			
47	19.9	2140	11	.6435	BG1-4	0			
33	19.9	9020	165	.5433	BG1-1	1	452	659	
34	19.9	8500	150	.5562	BG1-1	2	142	552	284 521
35	19.9	8000	135	.5651	BG1-1	1	266	529	
36	19.9	7542	120	.5652	BG1-1	0			
37	19.9	7030	100	.5421	BG1-1	2	118	657	234 862
38	19.9	6525	92	.5789	BG1-1	2	108	759	218 688
39	19.9	6010	75	.5563	BG1-1	1	200	509	
40	19.9	5520	60	.5276	BG1-1	0			
41	19.9	5025	50	.5305	BG1-1	0			
42	19.9	4510	42	.5532	BG1-1	0			
43	19.9	4010	35	.5831	BG1-1	0			
44	19.9	3510	29	.6306	BG1-1	0			
33	19.9	9020	165	.5433	BG1-6	2	150	582	452 860
34	19.9	8500	150	.5562	BG1-6	1	142	532	
35	19.9	8000	135	.5651	BG1-6	0			
36	19.9	7542	120	.5652	BG1-6	0			
37	19.9	7030	100	.5421	BG1-6	1	118	600	
38	19.9	6525	92	.5789	BG1-6	1	108	678	
39	19.9	6010	75	.5563	BG1-6	0			
40	19.9	5520	60	.5276	BG1-6	0			
41	19.9	5025	50	.5305	BG1-6	0			

ORIGINAL PAGE IS
OF POOR QUALITY

TABLE B-1 (CONTINUED)

Run No.	Ref. Blade Angle Deg.	RPM	Torque	Power Coeff	Gage No.	No. of Peaks	Spectral Frequencies(HZ)/Vibratory Stress (psi)	
42	19.9	4510	42	.5532	BG1-4	0		
43	19.9	4010	35	.5831	BG1-4	0		
44	19.9	3510	29	.6304	BG1-4	0		
53	23.6	9035	230	.7549	BG1-4	0		
54	23.6	8570	205	.7478	BG1-4	0		
55	23.6	8025	180	.7488	BG1-4	0		
56	23.6	7520	155	.7343	BG1-4	0		
57	23.6	7010	130	.7088	BG1-4	0		
58	23.6	6540	120	.7517	BG1-4	0		
59	23.6	5970	100	.7517	BG1-4	0		
60	23.6	5535	85	.7433	BG1-4	0		
61	23.6	5000	70	.7502	BG1-4	0		
62	23.6	4500	55	.7277	BG1-4	0		
63	23.6	4025	45	.7442	BG1-4	0		
53	23.6	9035	230	.7549	BG1-1	1	452 553	
54	23.6	8570	205	.7478	BG1-1	1	142 542	
55	23.6	8025	180	.7488	BG1-1	0		
56	23.6	7520	155	.7343	BG1-1	0		
57	23.6	7010	130	.7088	BG1-1	2	118 647 234 819	
58	23.6	6540	120	.7517	BG1-1	2	108 767 218 900	
59	23.6	5970	100	.7517	BG1-1	1	200 551	
60	23.6	5535	85	.7433	BG1-1	0		
61	23.6	5000	70	.7502	BG1-1	0		
62	23.6	4500	55	.7277	BG1-1	0		
63	23.6	4025	45	.7442	BG1-1	0		
64	23.6	3510	35	.7611	BG1-1	0		
65	23.6	2995	25	.7467	BG1-1	0		
66	23.6	2510	18	.7654	BG1-1	0		
67	23.6	2080	10	.6192	BG1-1	0		
53	23.6	9035	230	.7549	BG1-6	2	150 527 452 983	
54	23.6	8570	205	.7478	BG1-6	1	142 580	
55	23.6	8025	180	.7488	BG1-6	0		
56	23.6	7520	155	.7343	BG1-6	0		
57	23.6	7010	130	.7088	BG1-6	1	118 612	
58	23.6	6540	120	.7517	BG1-6	1	108 707	
59	23.6	5970	100	.7517	BG1-6	0		
60	23.6	5535	85	.7433	BG1-6	0		
61	23.6	5000	70	.7502	BG1-6	0		
62	23.6	4500	55	.7277	BG1-6	0		
63	23.6	4025	45	.7442	BG1-6	0		
64	23.6	3510	35	.7611	BG1-6	0		
53	23.6	9035	230	.7549	BG1-1	0		
54	23.6	8570	205	.7478	BG1-1	0		
55	23.6	8025	180	.7488	BG1-1	1	134 688	
56	23.6	7520	155	.7343	BG1-1	1	126 833	
57	23.6	7010	130	.7088	BG1-1	1	118 1134	
58	23.6	6540	120	.7517	BG1-1	2	110 792 218 1469	
59	23.6	5970	100	.7517	BG1-1	2	100 659 200 528	
60	23.6	5535	85	.7433	BG1-1	1	92 540	
61	23.6	5000	70	.7502	BG1-1	0		
62	23.6	4500	55	.7277	BG1-1	0		
63	23.6	4025	45	.7442	BG1-1	0		
64	23.6	3510	35	.7611	BG1-1	0		
65	23.6	2995	25	.7467	BG1-1	0		
66	23.6	2510	18	.7654	BG1-1	0		
67	23.6	2080	10	.6192	BG1-1	0		
53	23.6	9035	230	.7549	BG1-6	2	150 578 454 811	
54	23.6	8570	205	.7478	BG1-6	1	144 682	
55	23.6	8025	180	.7488	BG1-6	1	134 860	
56	23.6	7520	155	.7343	BG1-6	1	126 970	
57	23.6	7010	130	.7088	BG1-6	1	118 1031	
58	23.6	6540	120	.7517	BG1-6	1	110 621	
59	23.6	5970	100	.7517	BG1-6	1	100 552	
60	23.6	5535	85	.7433	BG1-6	1	92 516	
61	23.6	5000	70	.7502	BG1-6	0		
62	23.6	4500	55	.7277	BG1-6	0		

ORIGINAL PAGE IS
OF POOR QUALITY

TABLE B-1 CONTINUED

Run No.	Ref. Blade Angle Deg.	RPM	Torque	Power Coeff	Gage No.	No. of Peaks	Spectral Frequencies(HZ)/Vibratory Stress (psi)	
63	23.6	4025	45	.7442	BG1-6	0		
64	23.6	3510	35	.7611	BG1-6	0		
65	23.6	2995	25	.7467	BG1-6	0		
66	23.6	2510	18	.7654	BG1-6	0		
67	23.6	2080	10	.6192	BG1-6	0		
68	27.6	9000	275	.9096	BG1-4	0		
69	27.6	8555	250	.9151	BG1-4	0		
70	27.6	8050	220	.9095	BG1-4	0		
71	27.6	7585	190	.8848	BG1-4	0		
72	27.6	6960	165	.9126	BG1-4	0		
73	27.6	6570	145	.9195	BG1-4	0		
74	27.6	6015	125	.9256	BG1-4	0		
75	27.6	5520	105	.9232	BG1-4	0		
76	27.6	4980	90	.9722	BG1-4	0		
77	27.6	4530	72	.94	BG1-4	0		
78	27.6	4040	55	.9028	BG1-4	0		
79	27.6	3505	45	.9814	BG1-4	0		
80	27.6	3020	30	.8812	BG1-4	0		
81	27.6	2570	25	1.0141	BG1-4	0		
82	27.6	2145	15	.8734	BG1-4	0		
68	27.6	9000	275	.9096	BG1-1	0		
69	27.6	8555	250	.9151	BG1-1	2	142 849	286 701
70	27.6	8050	220	.9095	BG1-1	2	134 561	268 504
71	27.6	7585	190	.8848	BG1-1	1	126 659	
72	27.6	6960	165	.9126	BG1-1	2	116 709	232 711
73	27.6	6570	145	.9195	BG1-1	2	110 744	220 1644
74	27.6	6015	125	.9256	BG1-1	0		
75	27.6	5520	105	.9232	BG1-1	1	184 596	
76	27.6	4980	90	.9722	BG1-1	1	166 633	
77	27.6	4530	72	.94	BG1-1	0		
78	27.6	4040	55	.9028	BG1-1	0		
79	27.6	3505	45	.9814	BG1-1	0		
80	27.6	3020	30	.8812	BG1-1	0		
81	27.6	2570	25	1.0141	BG1-1	0		
82	27.6	2145	15	.8734	BG1-1	0		
68	27.6	9000	275	.9096	BG1-6	2	150 890	452 1028
69	27.6	8555	250	.9151	BG1-6	2	142 1096	428 957
70	27.6	8050	220	.9095	BG1-6	1	134 778	
71	27.6	7585	190	.8848	BG1-6	1	134 661	
72	27.6	6960	165	.9126	BG1-6	1	116 751	
73	27.6	6570	145	.9195	BG1-6	2	110 518	220 618
74	27.6	6015	125	.9256	BG1-6	0		
75	27.6	5520	105	.9232	BG1-6	0		
76	27.6	4980	90	.9722	BG1-6	0		
77	27.6	4530	72	.94	BG1-6	0		
78	27.6	4040	55	.9028	BG1-6	0		
79	27.6	3505	45	.9814	BG1-6	0		
80	27.6	3020	30	.8812	BG1-6	0		
81	27.6	2570	25	1.0141	BG1-6	0		
82	27.6	2145	15	.8734	BG1-6	0		
83	31.7	9050	290	.9486	BG1-4	0		
84	31.7	8570	260	.9484	BG1-4	0		
84	31.7	8570	260	.9484	BG1-4	1	740 680	
83	31.7	9050	290	.9486	BG1-4	1	752 737	
85	31.7	8055	240	.991	BG1-4	1	734 738	
86	31.7	7535	210	.9909	BG1-4	1	722 643	
87	31.7	7030	180	.9758	BG1-4	1	716 625	
88	31.7	6505	155	.9814	BG1-4	1	704 736	
89	31.7	6010	135	1.0013	BG1-4	1	694 760	
90	31.7	5505	115	1.0167	BG1-4	1	686 612	
91	31.7	5005	95	1.016	BG1-4	2	680 571	684 554
92	31.7	4520	75	.9835	BG1-4	0		
93	31.7	4055	65	1.0591	BG1-4	0		
94	31.7	3550	45	.9566	BG1-4	0		
95	31.7	3065	35	.9982	BG1-4	0		

TABLE B-1 (CONTINUED)

Run No.	Ref. Blade Angle Deg.	RPM	Torque	Power Coeff	Gage No.	No. of Peaks	Spectral Frequencies(HZ)/Vibratory Stress (psi)			
96	31.7	2525	25	1.0505	B01-4	0				
97	31.7	2130	15	.8858	B01-4	0				
-83	31.7	9050	290	.9484	B01-1	3	152 570	252 472	454 718	
84	31.7	8570	260	.9484	B01-1	3	238 585	244 582	286 536	
85	31.7	8055	240	.991	B01-1	3	134 922	238 493	268 502	
86	31.7	7535	210	.9909	B01-1	1	126 550			
-87	31.7	7030	180	.9758	B01-1	3	118 372	220 444	234 612	
88	31.7	6505	155	.9814	B01-1	2	108 937	216 1877		
89	31.7	6010	135	1.0013	B01-1	2	100 549	200 853		
90	31.7	5505	115	1.0167	B01-1	2	184 725	408 549		
91	31.7	5005	95	1.016	B01-1	0				
92	31.7	4520	75	.9835	B01-1	2	190 534	394 705		
93	31.7	4055	45	1.0591	B01-1	2	398 947	442 501		
94	31.7	3550	45	.9566	B01-1	0				
95	31.7	3065	35	.9982	B01-1	1	386 594			
96	31.7	2525	25	1.0505	B01-1	0				
97	31.7	2130	15	.8858	B01-1	0				
-83	31.7	9050	290	.9484	B01-6	5	440 863	454 2004	630 766	888 708 898 920
84	31.7	8570	260	.9484	B01-6	3	428 1050	626 859	890 870	
85	31.7	8055	240	.991	B01-6	4	134 910	434 931	624 651	878 831
86	31.7	7535	210	.9909	B01-6	6	126 672	426 871	432 806	438 883 624 1016 872 873
87	31.7	7030	180	.9758	B01-6	5	116 948	424 910	430 922	432 569 874 623
87	31.7	7030	180	.9758	B01-6	4	118 806	424 903	618 606	862 607
88	31.7	6505	155	.9814	B01-6	6	108 819	216 879	418 694	620 521 848 522 854 603
89	31.7	6010	135	1.0013	B01-6	3	202 548	414 868	846 818	
90	31.7	5505	115	1.0167	B01-6	5	184 601	408 1387	412 999	838 610 842 649
91	31.7	5005	95	1.016	B01-6	4	400 718	406 678	416 838	832 607
92	31.7	4520	75	.9835	B01-6	1	396 1485			
93	31.7	4055	45	1.0591	B01-6	2	398 1821	444 890		
94	31.7	3550	45	.9566	B01-6	1	390 573			
95	31.7	3065	35	.9982	B01-6	1	388 1073			
96	31.7	2525	25	1.0505	B01-6	1	382 529			
97	31.7	2130	15	.8858	B01-6	0				
x 101 100	35.7	4750	105	1.2468	B01-4	2	410 974	484 649		
101	35.7	4750	105	1.2468	B01-4	2	676 777	680 855		
102	35.7	4505	90	1.1881	B01-4	1	680 830			
103	35.7	4010	70	1.1663	B01-4	1	672 599			
104	35.7	3515	50	1.0842	B01-4	0				
105	35.7	3005	40	1.1868	B01-4	0				
106	35.7	2500	30	1.286	B01-4	0				
107	35.7	2170	18	1.0241	B01-4	0				
x 100	35.7	5790	145	.3596	B01-1	4	192 1140	204 1482	400 676	412 5418
101	35.7	4750	105	1.2468	B01-1	2	192 1105	400 3252		
102	35.7	4505	90	1.1881	B01-1	4	190 1082	384 572	390 550	398 553
103	35.7	4010	70	1.1663	B01-1	2	184 891	392 689		
104	35.7	3515	50	1.0842	B01-1	1	178 845			
105	35.7	3005	40	1.1868	B01-1	1	174 1338			
106	35.7	2500	30	1.286	B01-1	2	170 1162	178 773		
107	35.7	2170	18	1.0241	B01-1	1	170 509			
x 100	35.7	5790	145	.3596	B01-6	4	6 485	412 12170	824 1615	836 643
101	35.7	4750	105	1.2468	B01-6	4	192 680	388 604	400 8247	826 435
102	35.7	4505	90	1.1881	B01-6	5	188 757	384 1414	390 1453	426 525 826 512
103	35.7	4010	70	1.1663	B01-6	2	392 1041	400 517		
104	35.7	3515	50	1.0842	B01-6	3	388 602	394 670	816 504	
105	35.7	3005	40	1.1868	B01-6	2	176 712	384 707		
106	35.7	2500	30	1.286	B01-6	3	172 565	176 561	380 512	
107	35.7	2170	18	1.0241	B01-6	0				
108	40	5670	170	1.4167	B01-4	4	404 597	684 617	690 742	698 712
109	40	5510	160	1.4119	B01-4	3	684 776	692 618	700 596	
110	40	5010	130	1.3874	B01-4	2	680 536	686 697		
111	40	4510	110	1.4489	B01-4	2	676 615	680 709		
112	40	4000	85	1.4233	B01-4	0				
113	40	3520	65	1.4055	B01-4	0				
114	40	3015	45	1.3263	B01-4	1	174 530			
115	40	2530	35	1.4649	B01-4	0				
116	40	2160	25	1.4356	B01-4	0				

TABLE B-1 (CONTINUED)

Run No.	Ref. Blade Angle Deg.	RPM	Torque	Power Coeff	Gage No.	No. of Peaks	Spectral Frequencies(HZ)/Vibratory Stress (psf)				
108	40	5670	170	1.4167	BG1-1	5	94 620	188 527	202 1934	402 2309	406 2215
109	40	5510	160	1.4119	BG1-1	4	188 724	198 1034	398 1812	406 1132	
110	40	5010	130	1.3876	BG1-1	2	190 1184	402 1068			
111	40	4510	110	1.4489	BG1-1	3	190 1282	202 675	394 811		
112	40	4000	85	1.4233	BG1-1	2	180 2003	184 2435			
113	40	3520	65	1.4055	BG1-1	2	140 515	180 1090			
114	40	3015	45	1.3263	BG1-1	1	176 2839				
115	40	2530	35	1.4649	BG1-1	1	170 981				
116	40	2160	25	1.4356	BG1-1	1	168 993				
118	40	5670	170	1.4167	BG1-6	6	94 599	202 656	402 7650	420 534	836 649
109	40	5510	160	1.4119	BG1-6	7	92 566	200 811	396 4004	406 2919	834 791
							842 902				
110	40	5010	130	1.3876	BG1-6	6	84 606	194 663	386 558	402 2968	418 560
111	40	4510	110	1.4489	BG1-6	5	188 978	382 511	392 1115	398 1136	826 746
112	40	4000	85	1.4233	BG1-6	2	182 1945	392 727			
113	40	3520	65	1.4055	BG1-6	3	176 705	182 547	390 615		
114	40	3015	45	1.3263	BG1-6	3	176 1955	378 519	384 782		
115	40	2530	35	1.4649	BG1-6	3	170 693	378 510	386 625		
116	40	2160	25	1.4356	BG1-6	1	168 663				
117	50.3	6225	280	1.9358	BG1-4	2	702 1012	710 810			
118	50.3	6030	260	1.9157	BG1-4	2	690 749	704 1051			
119	50.3	5520	230	2.0223	BG1-4	2	690 542	696 800			
-120	50.3	5010	190	2.028	BG1-4	2	682 576	688 738			
121	50.3	4505	155	2.0461	BG1-4	0					
122	50.3	4015	125	2.0775	BG1-4	2	182 929	676 557			
123	50.3	3520	95	2.0541	BG1-4	0					
124	50.3	3025	70	2.0495	BG1-4	0					
125	50.3	2520	50	2.1094	BG1-4	0					
126	50.3	2136	35	2.0552	BG1-4	0					
117	50.3	6225	280	1.9358	BG1-1	4	104 1383	184 660	202 4431	208 2753	404 858
118	50.3	6030	260	1.9157	BG1-1	4	100 1273	182 676	188 918	202 5513	212 767
119	50.3	5520	230	2.0223	BG1-1	4	92 1432	184 1569	196 2464	212 533	402 607
-120	50.3	5010	190	2.028	BG1-1	8	84 908	158 512	162 590	168 926	192 2782
							230 743	398 598			200 596
121	50.3	4505	155	2.0461	BG1-1	6	74 773	186 2145	194 776	200 771	206 839
122	50.3	4015	125	2.0775	BG1-1	3	180 3949	184 3686	392 617		394 537
123	50.3	3520	95	2.0541	BG1-1	4	162 1066	174 1448	178 1840	388 541	
124	50.3	3025	70	2.0495	BG1-1	1	174 1836				
125	50.3	2520	50	2.1094	BG1-1	2	168 738	172 787			
126	50.3	2136	35	2.0552	BG1-1	1	168 820				
117	50.3	6225	280	1.9358	BG1-6	7	202 2784	384 511	404 2026	430 516	618 727
							848 747				840 650
118	50.3	6030	260	1.9157	BG1-6	7	100 536	202 2333	388 641	406 2135	616 825
							846 897				838 744
119	50.3	5520	230	2.0223	BG1-6	11	174 506	184 827	194 934	200 737	386 524
							404 1333	410 706	616 627	834 925	400 1368
-120	50.3	5010	190	2.028	BG1-6	6	192 994	390 888	394 1032	404 722	828 686
121	50.3	4505	155	2.0461	BG1-6	3	186 672	394 1122	826 563		832 658
122	50.3	4015	125	2.0775	BG1-6	2	182 3305	390 1232			
123	50.3	3520	95	2.0541	BG1-6	4	162 635	176 790	388 754	816 546	
124	50.3	3025	70	2.0495	BG1-6	2	172 824	384 839			
125	50.3	2520	50	2.1094	BG1-6	1	170 913				
126	50.3	2136	35	2.0552	BG1-6	1	170 549				
127	60	5280	290	2.7869	BG1-4	1	684 502				
128	60	5215	280	2.7583	BG1-4	1	686 520				
129	60	5000	260	2.7863	BG1-4	1	684 565				
130	60	4510	220	2.8978	BG1-4	1	678 570				
131	60	4025	180	2.9767	BG1-4	0					
132	60	3500	135	2.9525	BG1-4	0					
133	60	3045	100	2.8895	BG1-4	0					
134	60	2510	65	2.7641	BG1-4	0					
135	60	2150	50	2.8979	BG1-4	0					
127	60	5280	290	2.7869	BG1-4	3	176 901	190 1253	194 972		
128	60	5215	280	2.7583	BG1-4	2	174 512	190 1317			
129	60	5000	260	2.7863	BG1-4	1	188 1340				
130	60	4510	220	2.8978	BG1-4	1	184 2268				

ORIGINAL PAGE IS
OF POOR QUALITY

ORIGINAL PAGE IS
OF POOR QUALITY

TABLE B-1 (CONTINUED)

Run No.	Ref. Blade Angle Deg.	RPM	Torque	Power Coeff	Gage No.	No. of Peaks	Spectral Frequencies(HZ)/Vibratory Stress (psi)							
131	60	4025	180	2.9767	BG1-4	1	180	1535						
132	60	3500	135	2.9525	BG1-4	1	174	2022						
133	60	3045	100	2.8895	BG1-4	1	174	1289						
134	60	2510	65	2.7641	BG1-4	1	168	818						
135	60	2150	50	2.8979	BG1-4	1	168	1139						
127	60	5280	290	2.7869	BG1-6	6	194	792	394	843	402	579	616	418
128	60	5215	280	2.7583	BG1-6	4	190	823	394	725	614	564	830	401
129	60	5000	240	2.7863	BG1-6	4	188	1135	394	941	612	494	826	678
130	60	4510	220	2.8978	BG1-6	3	184	1614	390	1019	452	510		
131	60	4025	180	2.9767	BG1-6	2	180	1378	384	974				
132	60	3500	135	2.9525	BG1-6	2	174	1374	384	942				
133	60	3045	100	2.8895	BG1-6	2	172	724	382	735				
134	60	2510	65	2.7641	BG1-6	1	170	518						
135	60	2150	50	2.8979	BG1-6	1	168	624						
135	60	2150	50	2.8979	BG1-4	1	674	510						
137	69.9	4500	240	3.4399	BG1-4	0								
138	69.9	4000	205	3.4326	BG1-4	0								
139	69.9	3510	140	3.4793	BG1-4	0								
140	69.9	3025	118	3.4548	BG1-4	0								
141	69.9	2510	83	3.5296	BG1-4	0								
142	69.9	2130	58	3.425	BG1-4	0								
136	69.9	4785	290	3.3933	BG1-1	1	184	1640						
137	69.9	4500	240	3.4399	BG1-1	1	182	1630						
138	69.9	4000	205	3.4326	BG1-1	1	180	1022						
139	69.9	3510	140	3.4793	BG1-1	1	176	1331						
140	69.9	3025	118	3.4548	BG1-1	1	170	869						
141	69.9	2510	83	3.5296	BG1-1	1	170	686						
142	69.9	2130	58	3.425	BG1-1	1	168	571						
136	69.9	4785	290	3.3933	BG1-6	4	184	887	394	1203	444	571	824	550
137	69.9	4500	240	3.4399	BG1-6	4	180	891	390	981	394	917	820	570
138	69.9	4000	205	3.4326	BG1-6	2	174	591	388	1125				
139	69.9	3510	140	3.4793	BG1-6	2	174	885	384	851				
140	69.9	3025	118	3.4548	BG1-6	2	172	590	382	912				
141	69.9	2510	83	3.5296	BG1-6	1	374	532						
142	69.9	2130	58	3.425	BG1-6	0								
143	80	5000	280	3.0006	BG1-4	1	672	740						
144	80	4520	230	3.0161	BG1-4	1	664	544						
145	80	4020	185	3.067	BG1-4	0								
146	80	3530	140	3.01	BG1-4	0								
147	80	3025	100	2.9278	BG1-4	0								
148	80	2510	70	2.9767	BG1-4	0								
149	80	2150	48	2.782	BG1-4	0								
143	80	5000	280	3.0006	BG1-1	4	166	1576	184	3451	200	670	392	947
144	80	4520	230	3.0161	BG1-1	3	150	701	182	3280	392	620		
145	80	4020	185	3.067	BG1-1	3	134	587	176	3306	386	820		
146	80	3530	140	3.01	BG1-1	3	118	548	172	2355	384	524		
147	80	3025	100	2.9278	BG1-1	1	170	1472						
148	80	2510	70	2.9767	BG1-1	2	166	1104	172	1057				
149	80	2150	48	2.782	BG1-1	1	168	911						
143	80	5000	280	3.0006	BG1-6	9	166	1066	182	2046	372	539	392	2299
144	80	4520	230	3.0161	BG1-6	5	436	710	610	702	822	945	414	511
145	80	4020	185	3.067	BG1-6	2	148	500	180	2341	390	1652	398	766
146	80	3530	140	3.01	BG1-6	2	174	2054	384	1433			820	706
147	80	3025	100	2.9278	BG1-6	2	172	1274	384	1120				
148	80	2510	70	2.9767	BG1-6	1	168	1033	378	730				
149	80	2150	48	2.782	BG1-6	1	166	810						
150	34	5700	115	.9483	BG1-4	2	166	971						
151	34	5010	100	1.0674	BG1-4	2	410	1013	684	954				
152	34	4525	78	1.0206	BG1-4	1	682	805	686	794				
153	34	4015	62	1.0304	BG1-4	1	678	640						
154	34	3515	45	.9758	BG1-4	0	672	524						
155	34	3015	32	.9431	BG1-4	0								
156	34	2520	22	.9281	BG1-4	0								
157	34	2167	15	.8558	BG1-4	0								
150	34	5700	115	.9483	BG1-1	3	204	1064	400	561	410	4352		

TABLE B-1 (CONTINUED)

Run No.	Ref. Blade Angle Deg.	RPM	Torque	Power Coeff	Gage No.	No. of Peaks	Spectral Frequencies(HZ)/Vibratory Stress(psi)					
151	34	5010	100	1.0674	BG1-1	2	196 564	408 578				
152	34	4525	78	1.0204	BG1-1	3	190 724	388 789	396 524			
153	34	4015	62	1.0304	BG1-1	4	178 583	188 744	392 1084	398 543		
154	34	3515	45	.9758	BG1-1	1	180 664					
155	34	3015	32	.9431	BG1-1	2	174 655	178 614				
156	34	2520	22	.9281	BG1-1	1	170 949					
157	34	2167	15	.8558	BG1-1	1	148 499					
150	34	5700	115	.9483	BG1-6	4	410 12449	822 694	834 672	840 570		
151	34	5010	100	1.0674	BG1-6	3	404 1532	420 553	834 708			
152	34	4525	78	1.0204	BG1-6	3	390 2932	400 1026	824 705			
153	34	4015	62	1.0304	BG1-6	1	392 2655					
154	34	3515	45	.9758	BG1-6	1	388 875					
155	34	3015	32	.9431	BG1-6	1	386 700					
156	34	2520	22	.9281	BG1-6	1	172 578					
157	34	2167	15	.8558	BG1-6	0						
158	32.7	9025	280	.921	BG1-4	4	628 516	632 507	746 867	754 762		
159	32.7	8517	265	.9787	BG1-4	2	740 1252	746 817				
160	32.7	8030	230	.9556	BG1-4	2	728 770	732 805				
161	32.7	7530	210	.9922	BG1-4	2	720 636	726 629				
162	32.7	7020	175	.9514	BG1-4	2	696 514	714 959				
163	32.7	6585	155	.9577	BG1-4	1	706 765					
164	32.7	6025	135	.9963	BG1-4	2	690 661	696 772				
165	32.7	5530	110	.9637	BG1-4	2	684 547	690 753				
166	32.7	5040	100	1.0547	BG1-4	2	680 573	688 537				
167	32.7	4510	75	.9879	BG1-4	1	674 648					
168	32.7	3990	60	1.0097	BG1-4	1	672 673					
169	32.7	3470	45	1.0013	BG1-4	0						
170	32.7	3055	35	1.0047	BG1-4	0						
171	32.7	2485	20	.8677	BG1-4	0						
172	32.7	2110	15	.9026	BG1-4	0						
158	32.7	9025	280	.921	BG1-1	4	150 802	246 541	250 573	442 510		
159	32.7	8517	265	.9787	BG1-1	5	142 581	236 644	240 754	248 813	284 500	
160	32.7	8030	230	.9556	BG1-1	4	134 655	222 568	232 616	238 790		
161	32.7	7530	210	.9922	BG1-1	3	230 827	252 736	426 538			
162	32.7	7020	175	.9514	BG1-1	5	220 540	226 569	234 712	416 529	420 514	
163	32.7	6585	155	.9577	BG1-1	3	110 738	214 1003	220 1051			
164	32.7	6025	135	.9963	BG1-1	4	100 703	202 1201	208 850	410 505		
165	32.7	5530	110	.9637	BG1-1	3	184 996	204 747	404 1147			
166	32.7	5040	100	1.0547	BG1-1	2	194 775	404 509				
167	32.7	4510	75	.9879	BG1-1	2	192 665	196 637				
168	32.7	3990	60	1.0097	BG1-1	3	182 688	396 1338	440 518			
169	32.7	3470	45	1.0013	BG1-1	0						
170	32.7	3055	35	1.0047	BG1-1	2	176 870	384 521				
171	32.7	2485	20	.8677	BG1-1	1	174 623					
172	32.7	2110	15	.9026	BG1-1	1	170 691					
158	32.7	9025	280	.921	BG1-6	9	150 618	300 527	430 553	438 764	448 944	628 1437
159	32.7	8517	265	.9787	BG1-6	7	892 1064	896 948	908 615			
160	32.7	8030	230	.9556	BG1-6	9	142 656	428 1160	438 859	626 833	742 754	882 945
161	32.7	7530	210	.9922	BG1-6	7	888 748					
162	32.7	7020	175	.9514	BG1-6	5	414 1396	430 792	440 617	446 512	452 518	622 772
163	32.7	6585	155	.9577	BG1-6	6	870 484	878 1105	888 718			
164	32.7	6025	135	.9963	BG1-6	6	416 507	426 1124	440 920	622 1115	856 550	864 762
165	32.7	5530	110	.9637	BG1-6	4	872 716					
166	32.7	5040	100	1.0547	BG1-6	2	414 1396	420 1579	434 550	620 942	858 942	
167	32.7	4510	75	.9879	BG1-6	3	110 753	220 764	414 911	612 630	620 750	852 565
168	32.7	3990	60	1.0097	BG1-6	2	200 612	408 1080	416 1313	422 793	614 607	842 818
169	32.7	3470	45	1.0013	BG1-6	1	184 647	406 2063	610 519	836 618		
170	32.7	3055	35	1.0047	BG1-6	2	404 1022	830 610				
171	32.7	2485	20	.8677	BG1-6	0	384 839	394 1060	402 641			
172	32.7	2110	15	.9026	BG1-6	0	396 3191	442 1490				
176	44.9	6800	280	1.6223	BG1-4	4	392 678					
177	44.9	6520	270	1.7014	BG1-4	3	386 836	392 552				
							704 720	710 690	716 1537	732 503		
							706 690	710 926	720 626			

ORIGINAL PAGE IS
OF POOR QUALITY

ORIGINAL PAGE IS
OF POOR QUALITY

TABLE B-1 (CONTINUED)

Run No.	Ref. Blade Angle Deg.	RPM	Torque	Power Coeff	Gage No.	No. of Peaks	Spectral Frequencies(HZ)/Vibratory Stress (psi)							
178	44.9	6045	235	1.7229	BG1-4	2	700 1032	710 645						
179	44.9	5500	195	1.727	BG1-4	3	688 664	696 754	706 535					
180	44.9	5000	165	1.7682	BG1-4	1	688 991							
181	44.9	4500	135	1.7861	BG1-4	1	682 709							
182	44.9	4000	105	1.7582	BG1-4	1	184 670							
183	44.9	3495	80	1.7546	BG1-4	0								
184	44.9	3018	60	1.7648	BG1-4	0								
185	44.9	2505	40	1.7078	BG1-4	0								
186	44.9	2157	28	1.6123	BG1-4	0								
176	44.9	6800	280	1.6223	BG1-1	12	114 1349	194 677	198 749	210 5158	226 912	318 582		
							396 610	404 1001	412 994	420 632	428 511	718 533		
177	44.9	6520	270	1.7016	BG1-1	8	110 971	190 682	204 3497	208 3883	218 1804	390 629		
							412 1369	422 513						
178	44.9	6045	235	1.7229	BG1-1	6	100 1668	190 1609	202 2028	208 1458	220 511	410 1173		
179	44.9	5500	195	1.727	BG1-1	9	92 915	170 502	176 570	184 897	194 1945	204 1031		
							254 542	396 584	406 761					
180	44.9	5000	165	1.7682	BG1-1	7	166 607	182 546	190 1593	200 669	234 800	394 903		
							402 727							
181	44.9	4500	135	1.7861	BG1-1	5	74 685	188 1062	200 759	206 1055	394 599			
182	44.9	4000	105	1.7582	BG1-1	2	66 680	182 7468						
183	44.9	3495	80	1.7546	BG1-1	3	160 1106	170 534	180 914					
184	44.9	3018	60	1.7648	BG1-1	1	174 2515							
185	44.9	2505	40	1.7078	BG1-1	1	170 1549							
186	44.9	2157	28	1.6123	BG1-1	1	168 1402							
176	44.9	6800	280	1.6223	BG1-6	13	212 1933	220 619	384 509	390 725	400 2340	406 1662		
							414 2519	420 2121	432 512	624 1640	696 525	716 617		
							856 1042							
177	44.9	6520	270	1.7016	BG1-6	14	204 3036	216 839	368 551	382 896	402 997	408 1640		
							416 1568	424 715	434 640	616 1109	624 1001	690 649		
							844 661	850 1100						
178	44.9	6045	235	1.7229	BG1-6	10	100 538	188 770	196 517	202 1058	392 598	404 1809		
							412 2464	620 745	838 628	848 897				
179	44.9	5500	195	1.727	BG1-6	9	196 1046	202 565	388 727	398 1474	406 1407	414 1125		
							422 525	616 660	838 907					
180	44.9	5000	165	1.7682	BG1-6	7	194 581	388 549	396 1906	406 664	456 543	830 541		
							834 617							
181	44.9	4500	135	1.7861	BG1-6	5	184 817	206 517	386 523	396 1444	828 652			
182	44.9	4000	105	1.7582	BG1-6	3	184 3059	390 665	394 712					
183	44.9	3495	80	1.7546	BG1-6	2	178 866	390 689						
184	44.9	3018	60	1.7648	BG1-6	3	172 1330	380 832	386 1418					
185	44.9	2505	40	1.7078	BG1-6	2	170 757	380 725						
186	44.9	2157	28	1.6123	BG1-6	1	168 856							
189	38	5725	165	1.3487	BG1-4	4	408 672	690 913	694 717	698 573				
190	38	5520	150	1.3189	BG1-4	2	690 708	698 599						
191	38	5020	125	1.3289	BG1-4	2	682 867	690 667						
192	38	4518	100	1.3125	BG1-4	2	676 655	682 644						
193	38	3995	80	1.3429	BG1-4	1	676 743							
194	38	3520	60	1.2974	BG1-4	1	670 610							
195	38	3000	45	1.3396	BG1-4	0								
196	38	2510	33	1.3922	BG1-4	0								
197	38	2180	21	1.1839	BG1-4	0								
189	38	5725	165	1.3487	BG1-1	5	190 606	196 762	204 785	210 582	408 3816			
190	38	5520	150	1.3189	BG1-1	4	184 613	198 1185	394 757	402 2583				
191	38	5020	125	1.3289	BG1-1	3	84 551	194 1336	402 748					
192	38	4518	100	1.3125	BG1-1	2	188 1346	398 702						
193	38	3995	80	1.3429	BG1-1	1	180 1728							
194	38	3520	60	1.2974	BG1-1	1	178 933							
195	38	3000	45	1.3396	BG1-1	1	174 2263							
196	38	2510	33	1.3922	BG1-1	1	172 1049							
197	38	2180	21	1.1839	BG1-1	1	168 746							
189	38	5725	165	1.3487	BG1-6	4	190 532	400 1996	408 9162	840 774				
190	38	5520	150	1.3189	BG1-6	3	200 640	400 7823	838 840					
191	38	5020	125	1.3289	BG1-6	7	84 546	194 650	392 598	402 2091	414 999	610 507		
							832 1068							
192	38	4518	100	1.3125	BG1-6	6	190 744	384 850	390 971	396 1096	446 515	826 593		
193	38	3995	80	1.3429	BG1-6	4	180 1153	184 906	390 951	396 912				

ORIGINAL PAGE IS
OF POOR QUALITY

TABLE B-1 (CONTINUED)

Run No.	Ref. Blade Angle Deg.	RPM	Torque	Power Coeff	Gage No.	No. of Peaks	Spectral Frequencies(HZ)/Vibratory Stress (psi)		
194	38	3520	40	1.2974	BG1-6	2	178 632	390 840	
195	38	3000	45	1.3396	BG1-6	2	174 1312	386 738	
196	38	2510	33	1.3922	BG1-6	2	172 780	382 527	
197	38	2180	21	1.1839	BG1-6	1	170 606		
198	-10	9010	12	.0396	BG1-4	0			
199	-10	8560	11	.0402	BG1-4	0			
200	-10	8020	10	.0417	BG1-4	0			
201	-10	7525	9	.0426	BG1-4	0			
203	-10	6500	8	.0507	BG1-4	0			
204	-10	5985	7	.0524	BG1-4	0			
205	-10	5540	6	.0524	BG1-4	0			
206	-10	5010	5	.0534	BG1-4	0			
207	-10	4530	4	.0522	BG1-4	0			
208	-10	3990	3	.0505	BG1-4	0			
209	-10	3510	3	.0652	BG1-4	0			
210	-10	3005	2	.0593	BG1-4	0			
211	-10	2100	0	0	BG1-4	0			
198	-10	9010	12	.0396	BG1-1	1	150 668		
199	-10	8560	11	.0402	BG1-1	1	142 590		
200	-10	8020	10	.0417	BG1-1	1	134 520		
201	-10	7525	9	.0426	BG1-1	1	126 507		
203	-10	6500	8	.0507	BG1-1	0			
204	-10	5985	7	.0524	BG1-1	0			
205	-10	5540	6	.0524	BG1-1	0			
206	-10	5010	5	.0534	BG1-1	0			
207	-10	4530	4	.0522	BG1-1	0			
208	-10	3990	3	.0505	BG1-1	0			
209	-10	3510	3	.0652	BG1-1	0			
210	-10	3005	2	.0593	BG1-1	0			
211	-10	2100	0	0	BG1-1	0			
198	-10	9010	12	.0396	BG1-6	1	150 528		
199	-10	8560	11	.0402	BG1-6	1	144 517		
200	-10	8020	10	.0417	BG1-6	0			
201	-10	7525	9	.0426	BG1-6	0			
203	-10	6500	8	.0507	BG1-6	0			
204	-10	5985	7	.0524	BG1-6	0			
205	-10	5540	6	.0524	BG1-6	0			
206	-10	5010	5	.0534	BG1-6	0			
207	-10	4530	4	.0522	BG1-6	0			
208	-10	3990	3	.0505	BG1-6	0			
209	-10	3510	3	.0652	BG1-6	0			
210	-10	3005	2	.0593	BG1-6	0			
211	-10	2100	0	0	BG1-6	0			

APPENDIX C

SR-3 CAMPBELL DIAGRAMS

This appendix contains Campbell diagrams from the zero forward speed SR-3 model Prop-Fan tests conducted at UTRC, given in terms of response frequency vs. RPM for various blade angles. These Campbell diagrams were generated from the data obtained from the spectral analyses data using computerized peak-picking routines. These are the same data that are tabulated in Appendix B and were plotted automatically by computer. Shown are plots of frequency versus rotational speed. A plot is generated for each blade angle. Modal response frequencies are evident at the higher blade angles.

<u>FIGURE NO.</u>	<u>REFERENCE BLADES-ANGLES, DEG</u>
C-1	-10.0, 12.0
C-2	15.9, 19.9
C-3	23.6, 27.6
C-4	31.7, 32.7
C-5	34.0, 35.7
C-6	38.0, 40.0
C-7	60.0, 69.9
C-8	80.0

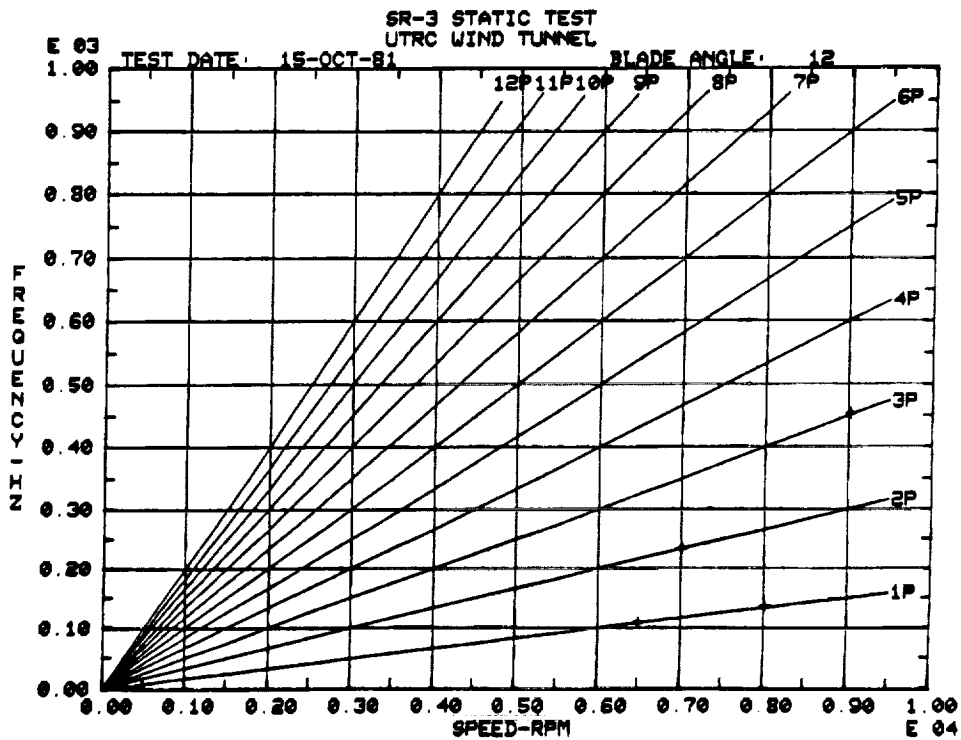
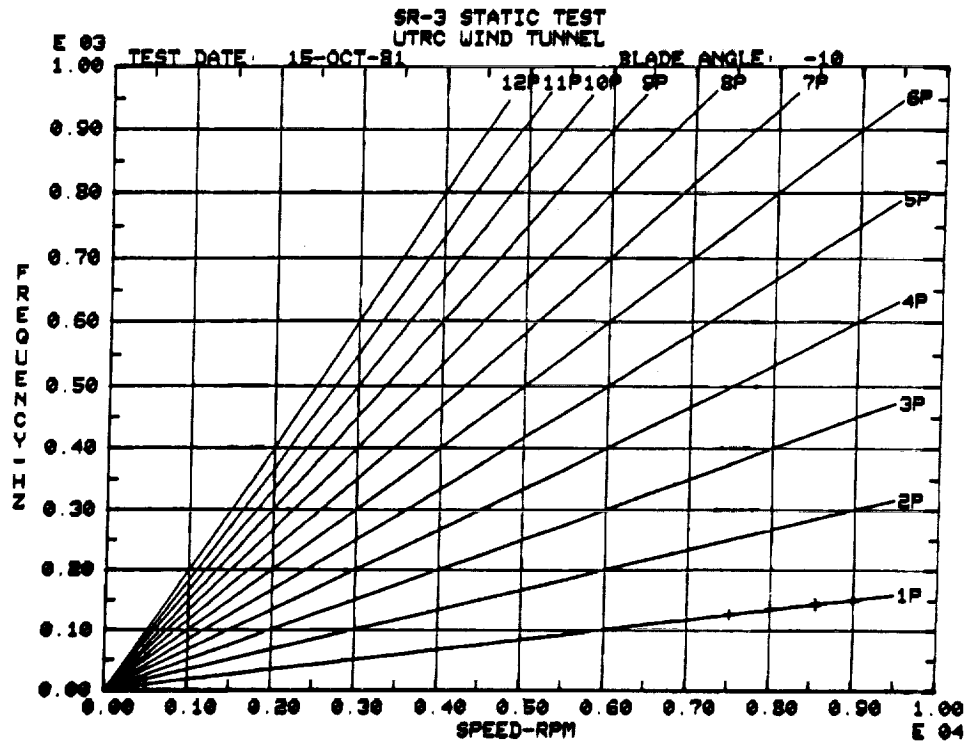


FIGURE C-1. SR-3 PROP-FAN STATIC TESTS. CAMPBELL DIAGRAMS FOR
REFERENCE BLADE ANGLES OF -10 DEG'S AND 12.0 DEG'S

ORIGINAL PAGE IS
OF POOR QUALITY

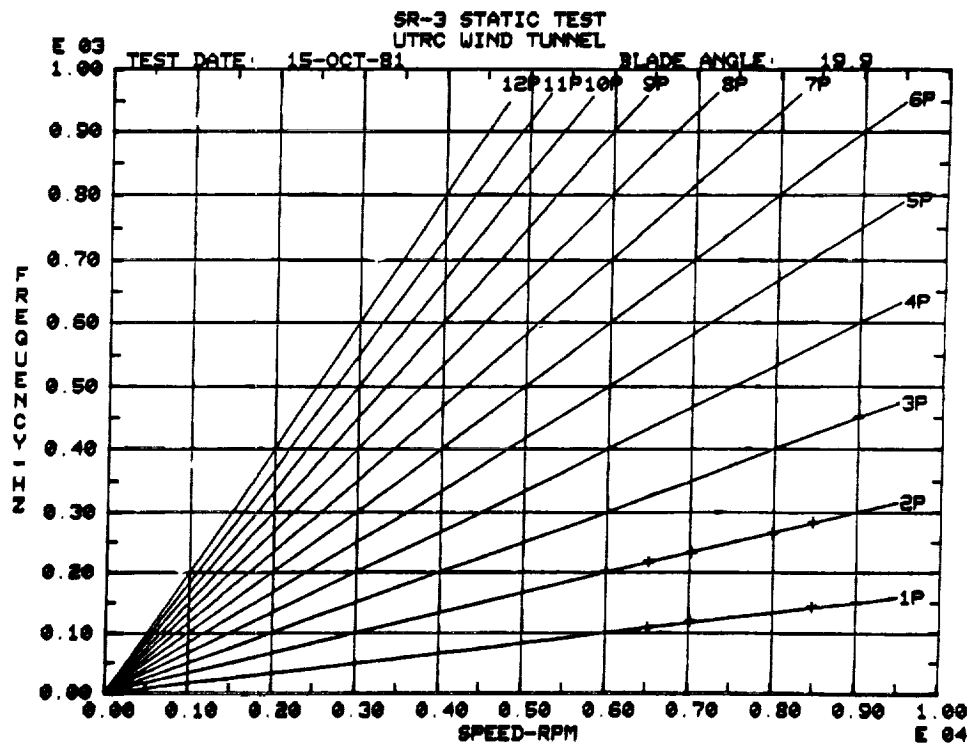
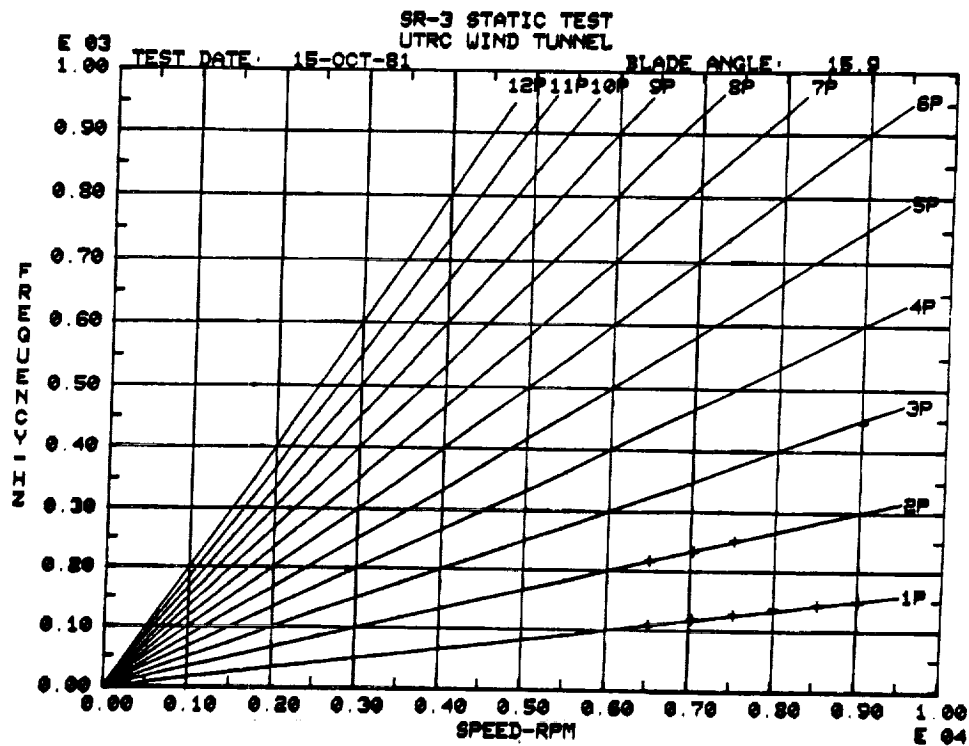


FIGURE C-2. SR-3 PROP-FAN STATIC TESTS, CAMPBELL DIAGRAMS FOR
REFERENCE BLADE ANGLES OF 15.9 DEG'S AND 19.9 DEG'S

ORIGINAL PAGE IS
OF POOR QUALITY

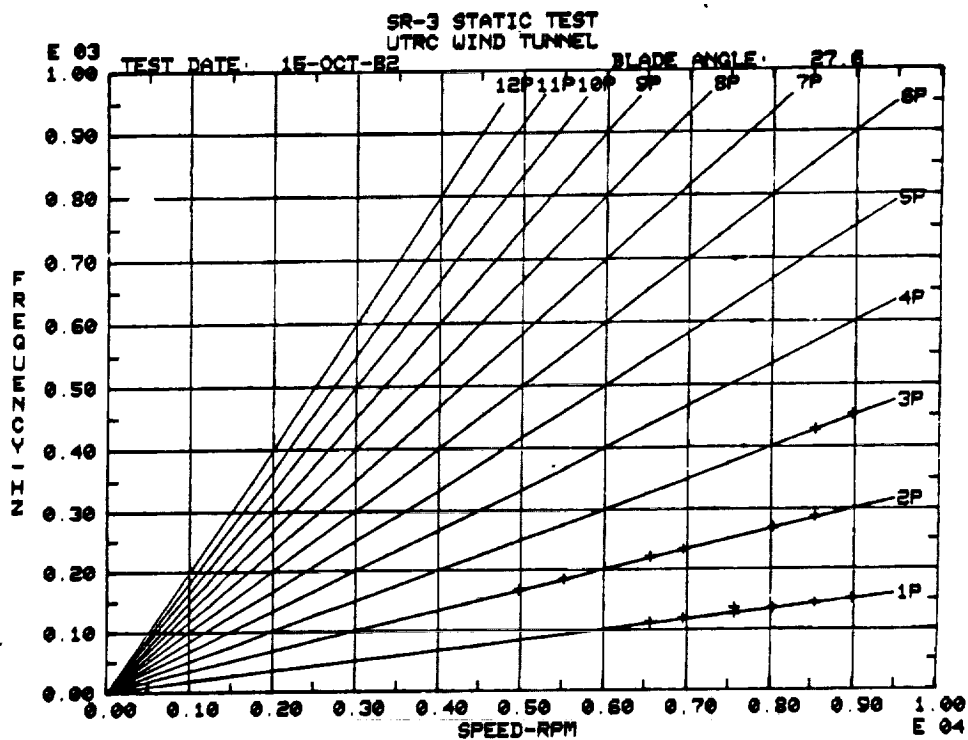
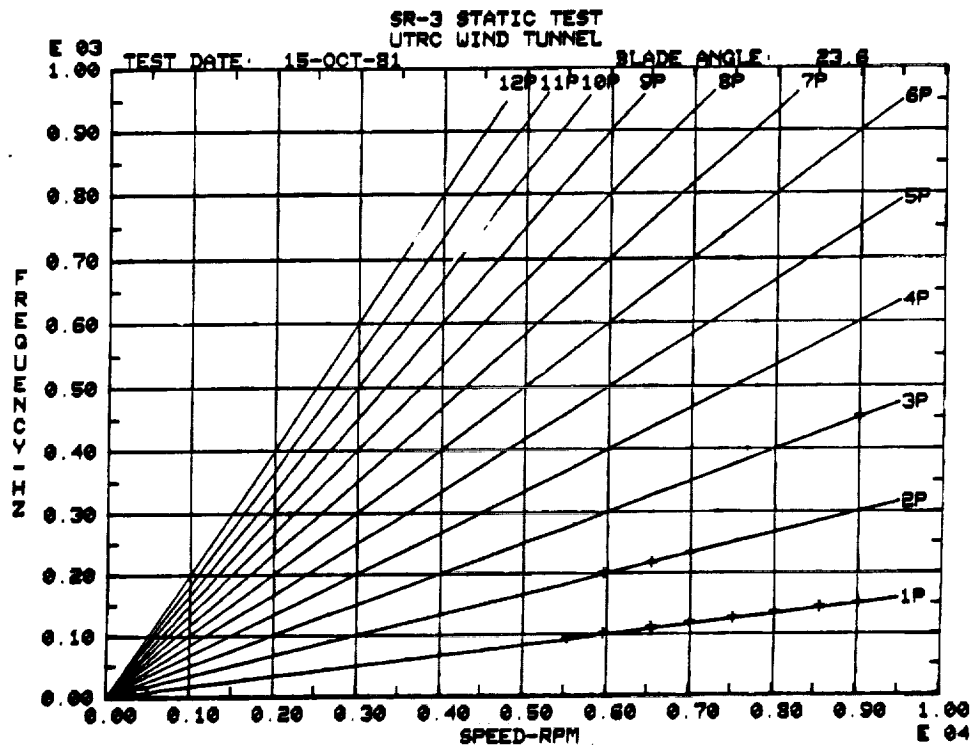


FIGURE C-3. SR-3 PROP-FAN STATIC TESTS, CAMPBELL DIAGRAMS FOR
REFERENCE BLADE ANGLES OF 23.6 DEG'S AND 27.6 DEG'S

ORIGINAL PAGE 13
OF POOR QUALITY

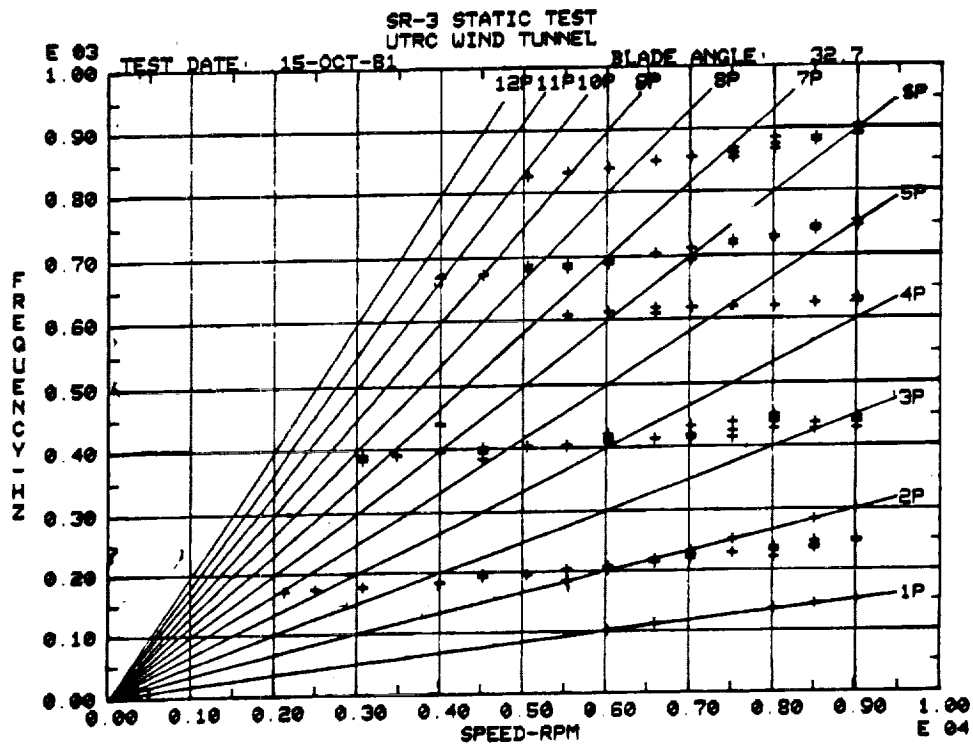
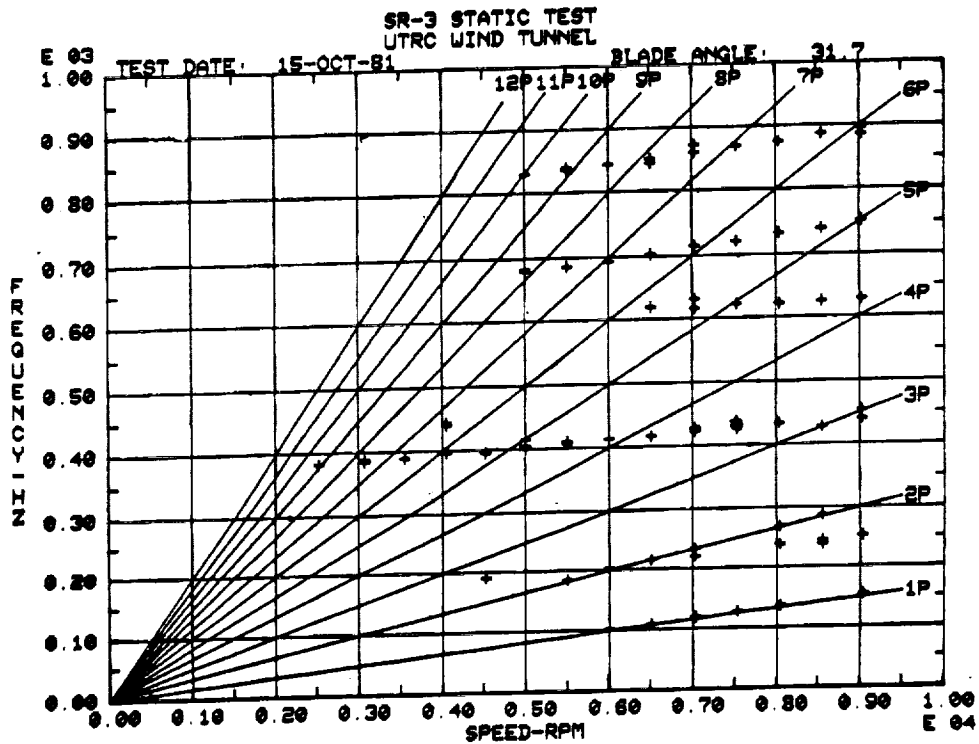


FIGURE C-4. SR-3 PROP-FAN STATIC TESTS, CAMPBELL DIAGRAMS FOR
REFERENCE BLADE ANGLES OF 31.7 DEG'S AND 32.7 DEG'S

ORIGINAL PAGE IS
OF POOR QUALITY

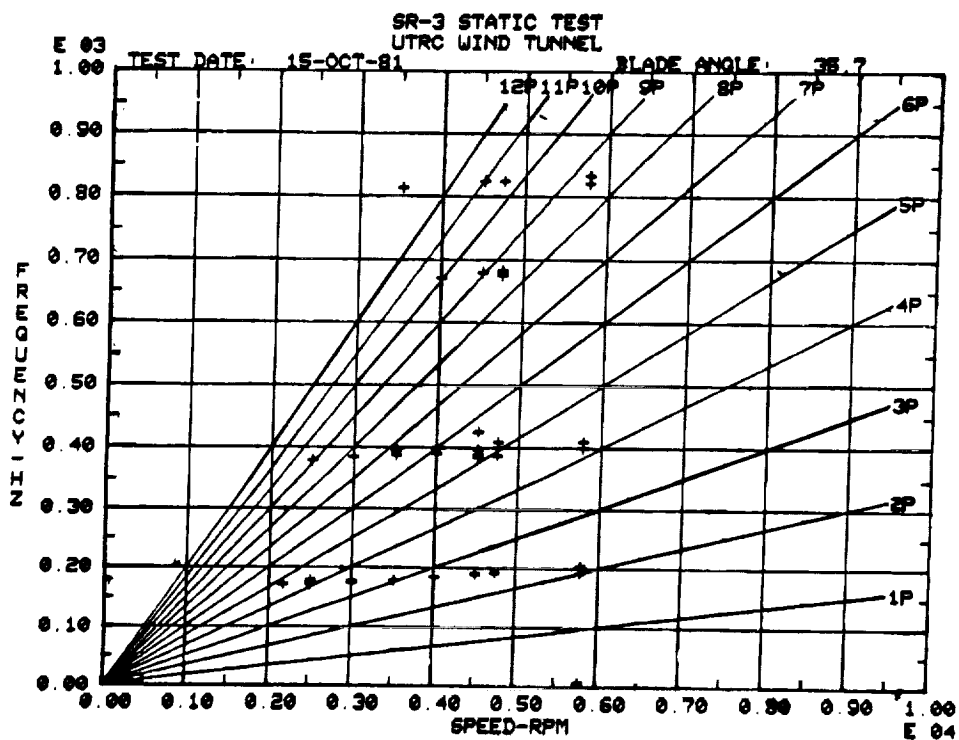
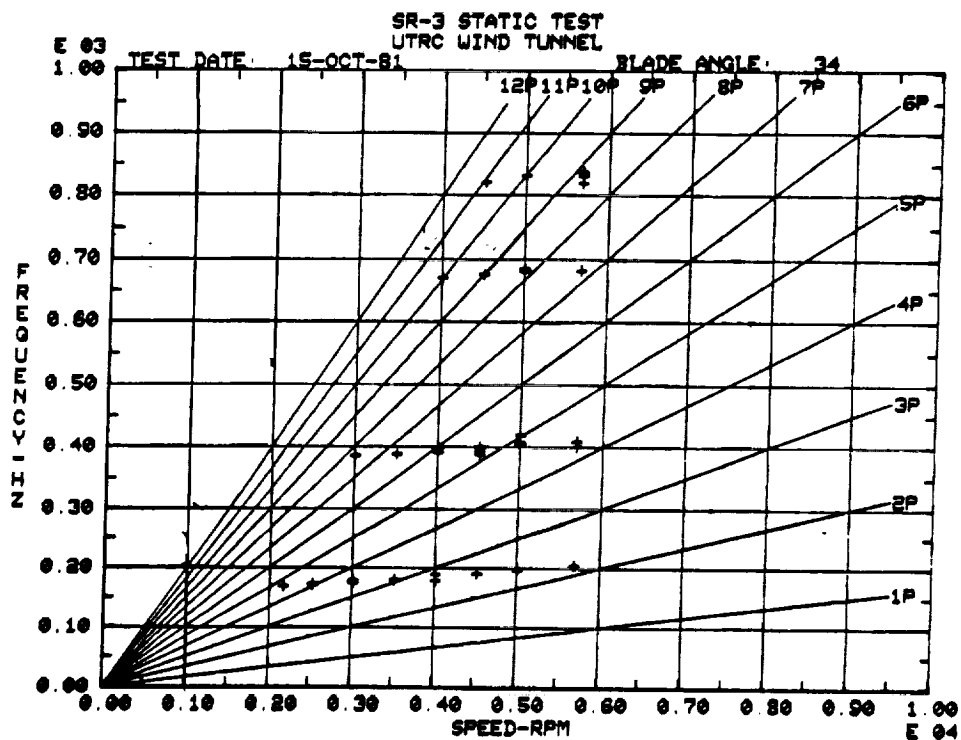


FIGURE C-5. SR-3 PROP-FAN STATIC TESTS, CAMPBELL DIAGRAMS FOR
REFERENCE BLADE ANGLES OF 34 DEG'S AND 35.7 DEG'S

ORIGINAL PAGE IS
OF POOR QUALITY

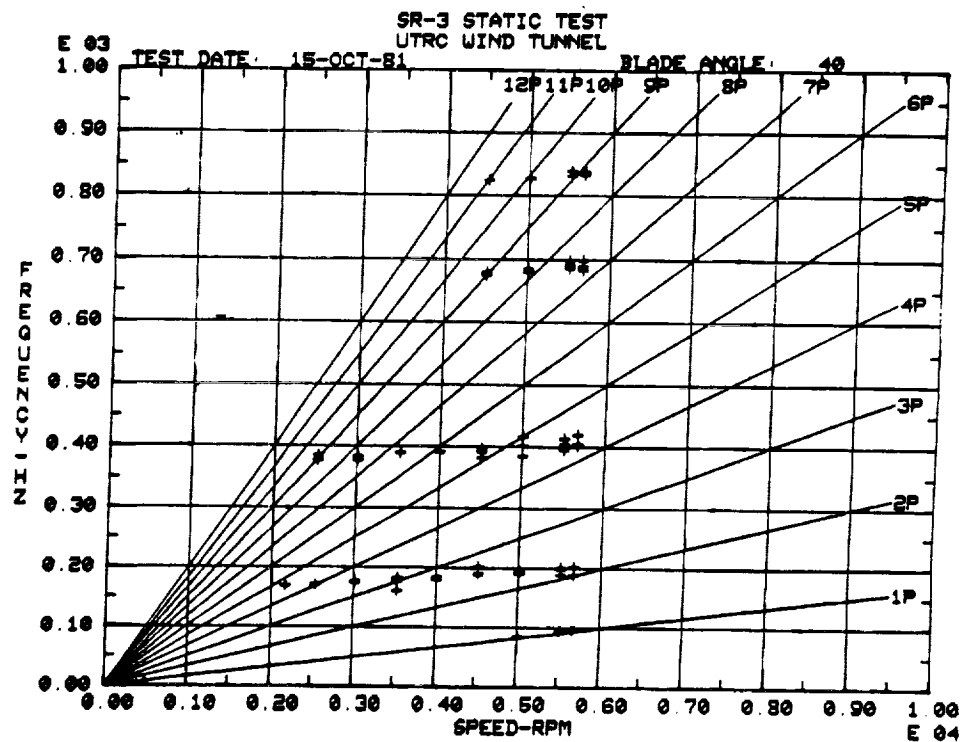
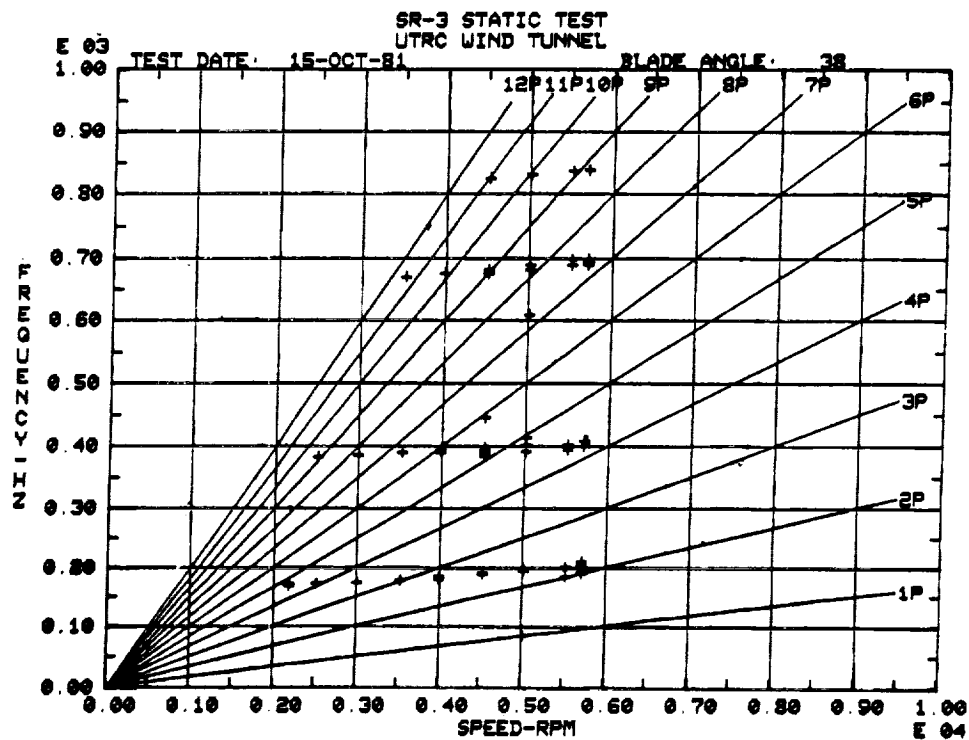


FIGURE C-6. SR-3 PROP-FAN STATIC TESTS, CAMPBELL DIAGRAMS FOR
REFERENCE BLADE ANGLES OF 38 DEG'S AND 40 DEG'S

ORIGINAL PAGE IS
OF POOR QUALITY

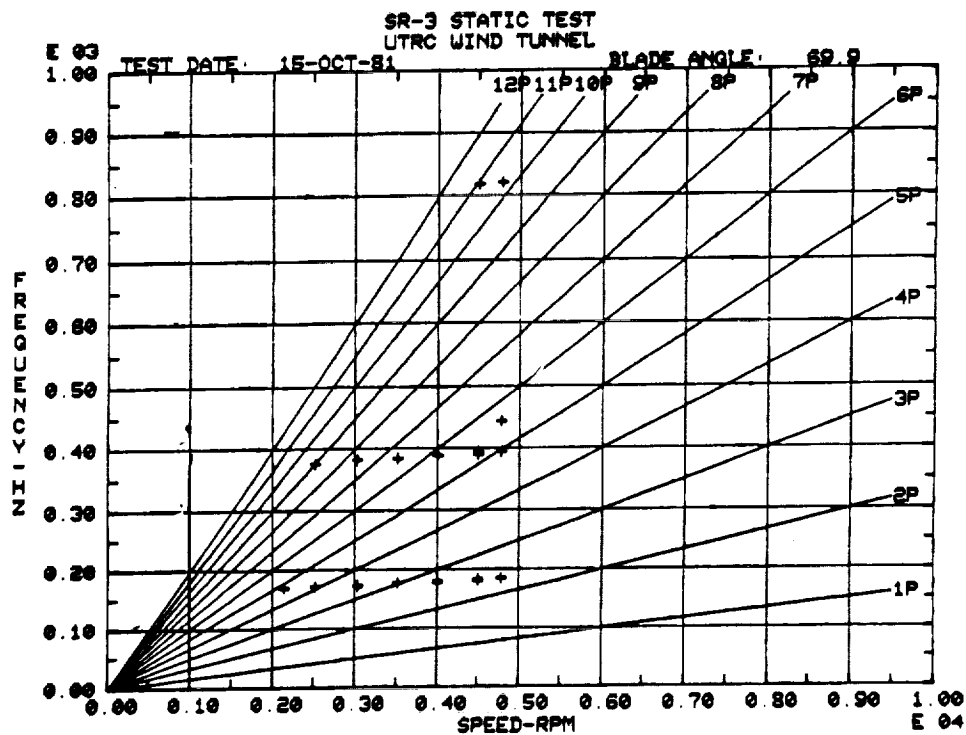
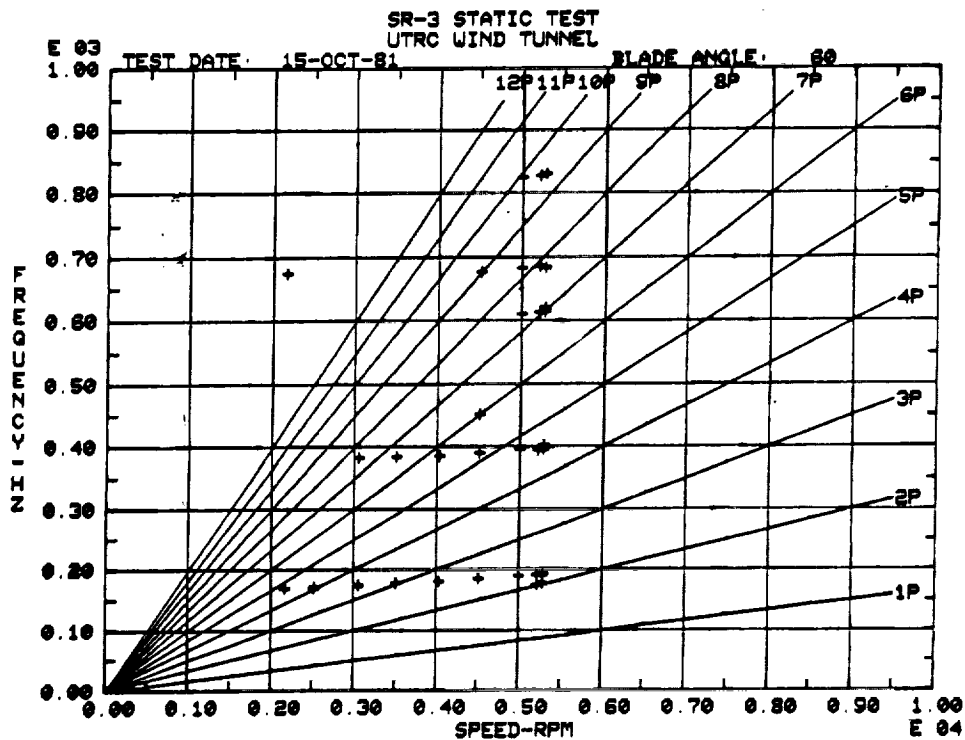


FIGURE C-7. SR-3 PROP-FAN STATIC TESTS, CAMPBELL DIAGRAMS FOR
REFERENCE BLADE ANGLES OF 60 DEG'S AND 69.9 DEG'S

ORIGINAL PAGE IS
OF POOR QUALITY

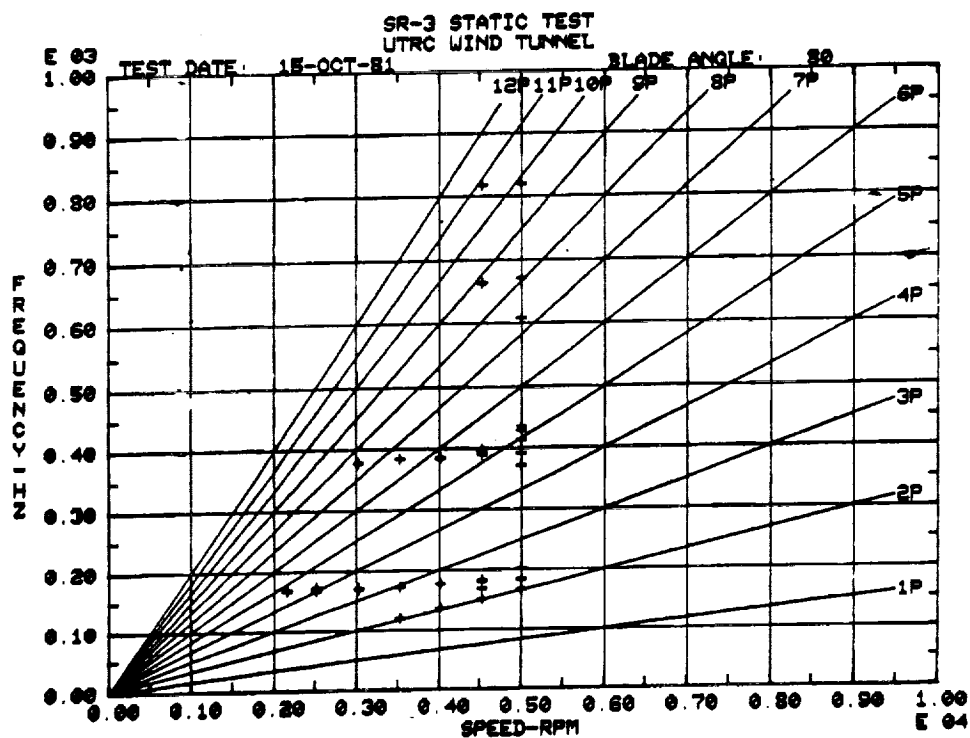


FIGURE C-8. SR-3 PROP-FAN STATIC TESTS, CAMPBELL DIAGRAMS FOR
REFERENCE BLADE ANGLES OF 80.0 DEG'S